NASA CONTRACTOR REPORT

NASA CR-66700

NASA CR-66700

FINAL REPORT
STUDY OF DIRECT VERSUS ORBITAL ENTRY FOR MARS MISSIONS

Volume VII - Supplementary Report

Prepared by
MARTIN MARIETTA CORPORATION
DENVER, COLORADO

for
Langley Research Center

NATIONAL AERONAUTICS AND SPACE ADMINISTRATION • WASHINGTON, D.C. • OCTOBER 1968

NASA CR-66700

FINAL REPORT

STUDY OF DIRECT VERSUS ORBITAL ENTRY FOR MARS MISSIONS

VOLUME VII: SUPPLEMENTARY REPORT

By Raymond S. Wiltshire, William J. Pragluski, Joe C. Pohlen, Theodore F. Morey, Dean A. Schneebeck, and Hugh E. Craig

Prepared under Contract No. NAS1-7976 by
MARTIN MARIETTA CORPORATION
Denver, Colorado

for

NATIONAL AERONAUTICS AND SPACE ADMINISTRATION

FOREWORD

This Final Report for the "Study of Direct Versus Orbital Entry for Mars Missions" (NASA Contract NAS1-7976) is provided in accordance with Part III A.4 of the contract schedule as amended. This report is in seven volumes as follows:

NASA CR-66659 - Volume I - Summary;

NASA CR-66660 - Volume II - Parametric Studies, Final Analyses, and Conceptual Designs;

NASA CR-66661 - Volume III - Appendix A - Launch Vehicle Performance and Flight Mechanics;

NASA CR-66662 - Volume IV - Appendix B - Entry and Terminal Phase Performance Analysis;

NASA CR-66663 - Volume V - Appendix C - Entry Configuration Analysis;

NASA CR-66664 - Volume VI - Appendix D - Subsystem Studies and Parametric Data;

NASA CR-66700 - Volume VII - Supplementary Report.

CONTENTS

FINAL REPORT

DIRECT VERSUS ORBITAL ENTRY FOR MARS MISSIONS

VOLUME VII - SUPPLEMENTARY REPORT

By Raymond S. Wiltshire, William J. Pragluski, Theodore F. Morey
Joe C. Pohlen, Dean A. Schneebeck, and Hugh E. Craig

SUMMARY

This report documents the results of the work accomplished in Modification 1 to the Direct Versus Orbital Entry for Mars Missions Study. The objective of this study was to determine and document any changes that the new Mars environmental model, "Mars Engineering Model Parameters for Mission and Design Studies," dated May 1968 by the Langley Research Center, would cause in the results of that study.

The mission analysis studies were conducted in two parts. First, all entry trajectories were rerun using the new Mars atmosphere data. Two differences of relatively minor significance were identified; the peak drag deceleration is less over almost the entire range of entry parameters, and the altitude at which Mach 2 is reached in the MEM 5/68-min atmosphere is higher than in VM-8 for the higher entry ballistic coefficient B_E, entry angle γ_E, region. These differences are apparent for both the direct and out-of-orbit entry modes.

The Mach 2 parachute/vernier terminal phase system performance was then analyzed using the initial conditions from the revised entry trajectories. The performance in the new atmospheres in all cases is improved over that in the VM atmospheres, primarily because of the higher density at low altitudes. This increased performance can be applied in a number of ways, i.e., to provide:

1) More useful landed weight for a given entry weight/aeroshell diameter;

2) Smaller entry weight/aeroshell diameter for a given useful landed weight;

3) Greater allowable dispersions in entry angle/entry velocity;

4) Capability to land at higher elevations.

A landing stability analysis was run combining statistical data on surface slope from the new environmental model with other pertinent data. The results show that the point designs described in Volume II of the basic study have a 99.82% probability of landing successfully on the surfaces defined by NASA-Langley Research Center.* The surface-bearing strength data in the new model confirmed that the original landing foot pads were sized correctly.

The thermal control analysis resulted in only a small (12.5%) reduction in the heater power required due to the reduced conductivity of the atmosphere.

The solar array results presented in the basic study are still valid, although the effect of the environmental parameters influencing the design are different. The previous design was based on 8% atmospheric attenuation and 17° maximum surface slopes. The new environmental model indicates that 1% of 22° should be used. The reduced efficiency due to increased slopes in compensated almost exactly by reduction in atmospheric attenuation.

The final task accomplished during this study was to determine the minimum aeroshell diameter required to meet the mission objectives using the out-of-orbit mode. A 7.3-ft-diameter aeroshell is sufficient to meet the performance requirements. However, this system has no performance or weight margin and, as was discussed in the basic report, packaging the system within an aeroshell this small presents significant problems. For these reasons, an aeroshell diameter of 9 to 9.5 ft would be recommended for the out-of-orbit mode.

The primary conclusions of the original study are still valid:

1) Either entry mode is feasible;
2) The out-of-orbit mode provides greater inflight mission flexibility;
3) The Titan IIIC/Centaur launch vehicle is required for either mission mode if orbiter science capability is desired.

---

*Mars Engineering Model Parameters for Mission and Design Studies, NASA-Langely Research Center, May 1968.

The one significant change concerns the bulbous shroud requirement. The direct entry mode still requires a bulbous shroud; however, it is highly probable that the out-of-orbit mission can be accommodated with a system that will fit within the standard Surveyor shroud.

INTRODUCTION

This study is an extension to the Mars Mission Mode Study recently completed for the Langley Research Center by Martin Marietta Corporation. The objective of this study was to determine and document any changes that the new Mars environmental model, reference 1, dated May 1968 by the Langley Research Center, would cause in the results of that study. The 10.5-ft-diameter aeroshell $\left(B_E = 0.35\right)$ out-of-orbit mode is the primary configuration used to determine any conceptual design impact.

Specifically, entry trajectories, both direct and out-of-orbit, were rerun; Mach 2 parachute/vernier terminal phase system analysis revised; and landing, stability, thermal control, and solar array analyses were reexamined. Finally, using these results, the impact on the Configuration 1B conceptual design was determined. All conclusions reached during the direct versus out-of-orbit entry mode study were reviewed and changes identified.

SYMBOLS AND ABBREVIATIONS

ACS	attitude control system
B_E	entry ballistic coefficient, $M/C_D A$, slugs/foot^2
c	surface heat capacity, Btu/pound-°F
$D_{A/S}$	diameter of aeroshell, feet
g	gravitational acceleration
G&C	guidance and control
k	surface thermal conductivity, Btu/hour-foot-°F
$\sqrt{kpc}$	surface thermal inertia, Btu/foot^2-°R-hour$^{\frac{1}{2}}$

M	Mach number
MEM	Mars environmental model
T_a	atmospheric temperature, °F
T_g	surface temperature, °F
W_E	entry weight, pounds
W_{LE}	landed equipment weight, pounds
α_s	surface solar absorptivity
γ_E	entry angle, degrees
ϵ	surface emissivity
ρ	surface density, pounds/foot^3
$\oplus$	Earth

ENTRY TRAJECTORY AND TERMINAL PHASE ANALYSIS

The entry trajectory defines performance from entry at 800 000 ft above the mean Martian surface to terminal phase initiation occurring typically from 10 000 to 20 000 ft above the terrain. The terminal phase parachute/vernier system decelerates the capsule from velocities at the end of the entry phase to zero velocity at the Martian surface. The objectives of this study are to: (1) determine the effect of the updated Martian atmosphere models (ref. 1) on entry trajectory characteristics and terminal phase system performance, and (2) determine changes, if any, to the conclusions of the Mission Mode Study resulting from the use of the new atmosphere models. Data are presented parametrically and a comparison of point designs made. Thus, results of this study may be directly related to the results presented in reference 2 (Volumes I, II, and IV).

Entry Trajectory Analysis

The entry trajectory analysis includes generation of entry trajectory time histories over the following range of entry parameters:

Orbital mode	Direct mode
$V_E = 16\ 000$ fps	$V_E = 21\ 000$ fps
$16 \leq -\gamma_E \leq 24°$	$20 \leq -\gamma_E \leq 40°$
$0.2 \leq B_E \leq 0.6$ slug/ft^2	$0.2 \leq B_E \leq 0.6$ slug/ft^2

Data are presented for the minimum, mean, and maximum atmosphere models defined in reference 1, herein designated as MEM 5/68-min, MEM 5/68-mean, and MEM 5/68-max. A brief description of the new atmosphere is given along with a comparison of significant characteristics of the new atmosphere and the VM atmospheres critical to the Mission Mode Study. Data presented are limited to the altitude at which Mach 2.0 occurs (for terminal phase parachute deployment) and peak drag acceleration characteristics. These dependent variables are presented as a function of the entry parameters described above. Vehicle drag characteristics, planetary constants, and computational methods are the same as presented in reference 2 (Volume IV).

Important characteristics of the new atmosphere model are given in table 1.

TABLE 1.- ATMOSPHERE MODEL CHARACTERISTICS

Characteristics	MEM 5/68 model		
	Min	Mean	Max
Surface pressure, mb	6	9	20
Surface density, slug/ft^3 x 10^5	4.10	3.70	5.40
Surface temperature, °R	270	414	504
Tropopause altitude, ft x 10^{-3}	354.35	337.943	----
Composition, % by mass			
CO_2	100	74.4	25
N_2	0	12.8	50
A	0	12.8	25
Molecular weight	44	40.5	33.6
Specific heat ratio	1.38	1.34	1.40

Density versus altitude for the three MEM 5/68 atmospheres is shown in figure 1. Ambient temperature and speed of sound are compared to the VM-8 data in figure 2. A comparison of the MEM 5/68-min density characteristics with VM-7 and VM-8 is shown in figure 3. The VM-7 and VM-8 models are the critical atmospheres used previously (ref. 2) from the standpoint of entry environment and terminal phase design conditions. The above data illustrate:

1) The MEM 5/68-min atmosphere has the lowest density at altitudes above 5 000 ft, indicating that it will be critical for velocity/flightpath angle characteristics during entry, terminal phase initiation, and the aero-decelerator portion of the terminal phase;

2) A higher minimum speed of sound and a higher minimum density than the critical VM atmospheres. This indicates less critical conditions for entry trajectory characteristics (i.e., peak drag deceleration) for terminal phase initiation and terminal phase performance.

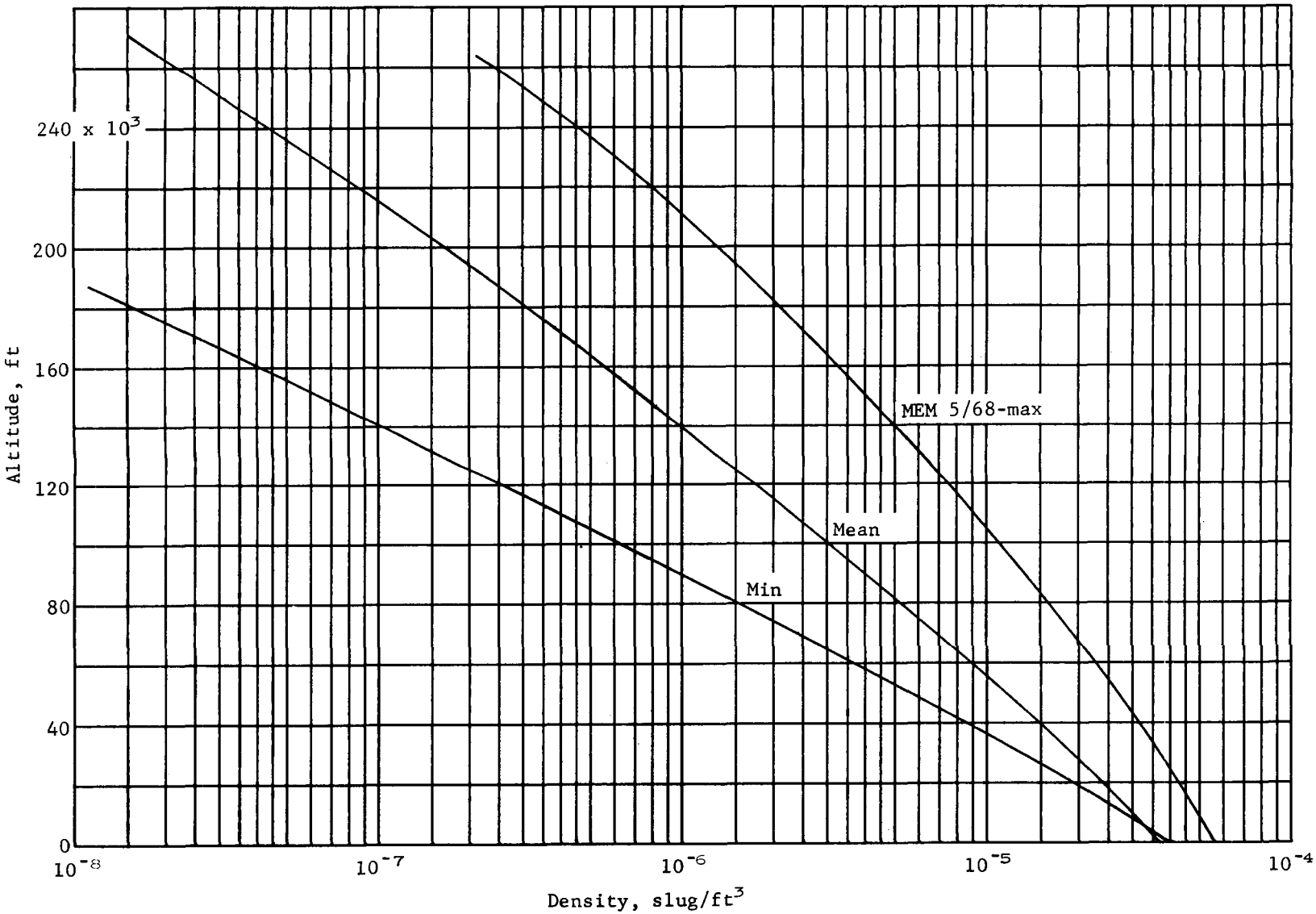

Figure 1.- MEM 5/68 Model Atmosphere Density Characteristics

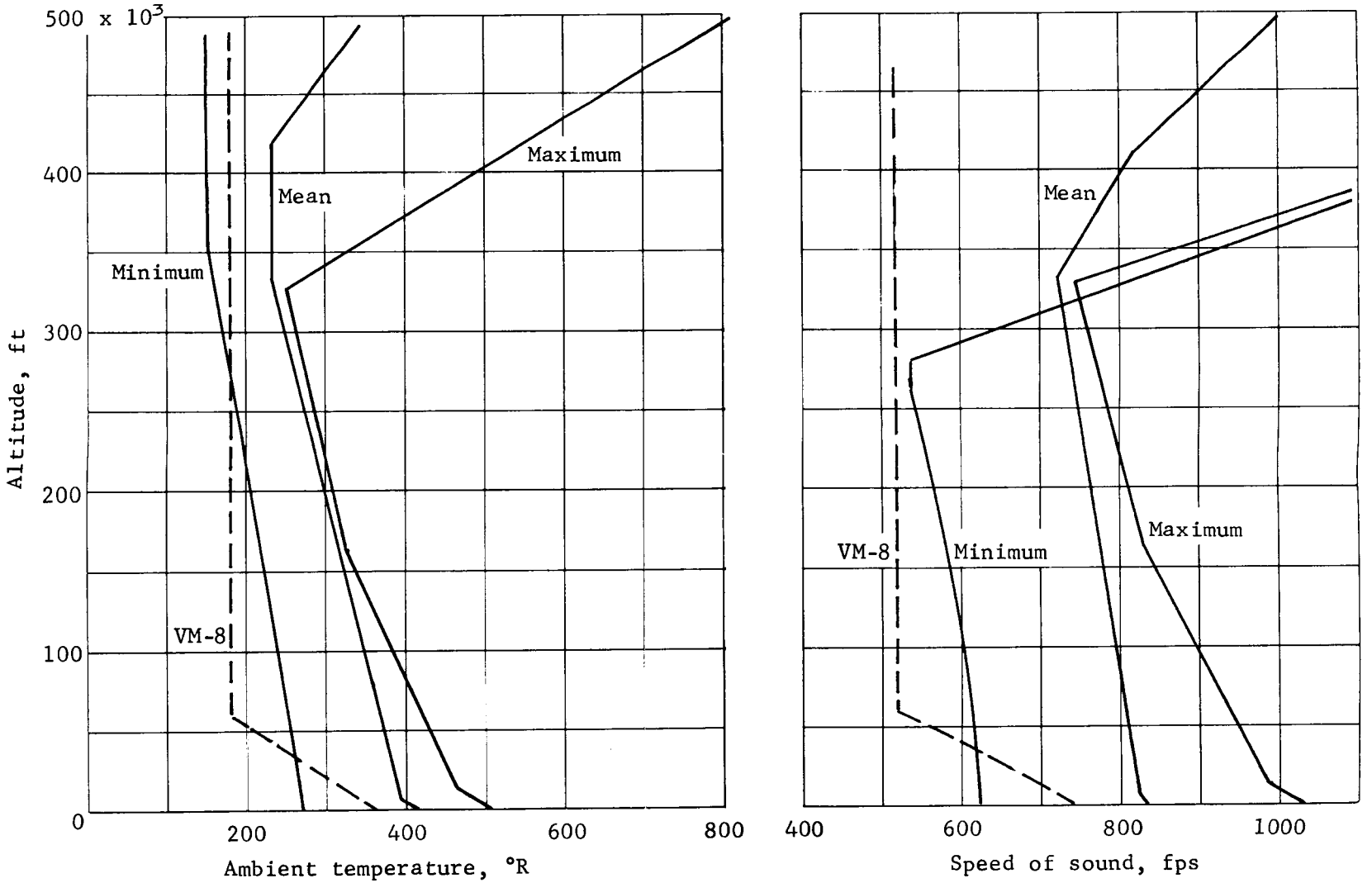

Figure 2.- MEM 5/68 Ambient Temperature and Speed of Sound

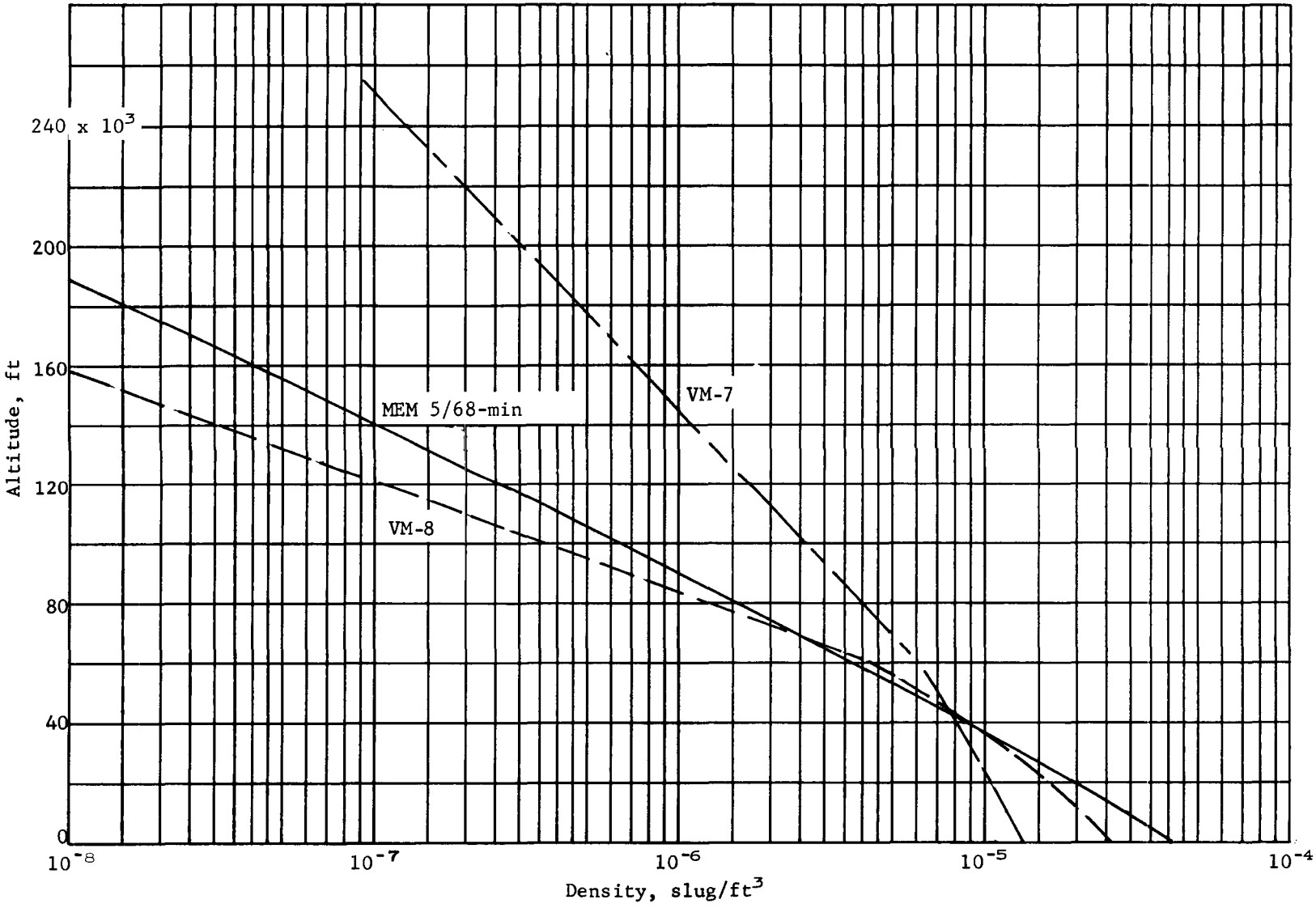

Figure 3.- Atmosphere Density Comparison

The altitude at which the entry capsule has decelerated to Mach 2.0 in the MEM 5/68-min atmosphere is shown in figure 4 for the orbit mode and figure 5 for the direct mode. The data are presented as a function of entry conditions. Data for VM-8, critical for Mach 2 among the VM models, is superimposed for reference. The altitude at which Mach 2 is reached in the MEM 5/68-min atmosphere is essentially the same as in VM-8 for the lower B_E, γ_E and higher than in VM-8 as B_E, γ_E increase. The altitude at Mach 2 for the MEM 5/68-min and mean atmospheres is shown for the orbit and direct modes in figures 6 and 7, respectively. The same data for the MEM 5/68-max atmosphere, orbit and direct modes are shown in figure 8. The MEM 5/68-min atmosphere shows the lowest altitude at Mach 2.

The altitude at $M = 2$ characteristics (figs. 4 and 5) show little difference between the old and new atmosphere models at low B_E and γ_E and increasing difference favoring the new atmospheres at higher B_E and γ_E. This trend appeared a little unusual, at first, when looking at the altitude/density relationships shown in figure 3. The trend is better understood by looking in detail at some of the entry trajectories. The data in figure 9 show the altitude/velocity relationship for two direct entry trajectories ($B_E = 0.2$ and 0.6 slug/ft^2). The data show that the higher density at altitude in the MEM 5/68-min atmosphere causes an earlier deceleration for both B_E, and the curves tend to merge in the 30 000- to 40 000-ft altitude range where the VM-8 and MEM 5/68-min atmosphere densities are about the same. The low altitude/velocity end of the curves are reproduced in figure 10 for more detail. Again, the altitude/velocity relationship in the 30 000- to 40 000-ft altitude region appears quite similar for the VM-8 and MEM 5/68-min atmosphere trajectories at constant B_E. However, the curves spread apart, again, at lower altitudes where the MEM 5/68-min atmosphere density is greater than that for VM-8. The $M = 2$ lines for both atmospheres are superimposed on the figure. It is shown that all the curves seem to cross at the place for the $B_E = 0.2$ slug/ft^2 example, leading to no difference between the atmosphere models. The altitude at $M = 2$ for higher B_E is below the 30 000-ft range where the MEM 5/68-min atmosphere density is higher. Here the altitude at $M = 2$ is clearly higher for the new atmospheres in spite of the fact that some of the potential gain is lost because of the lower speed of sound. The results are keyed to the fact that B_E, γ_E combinations that

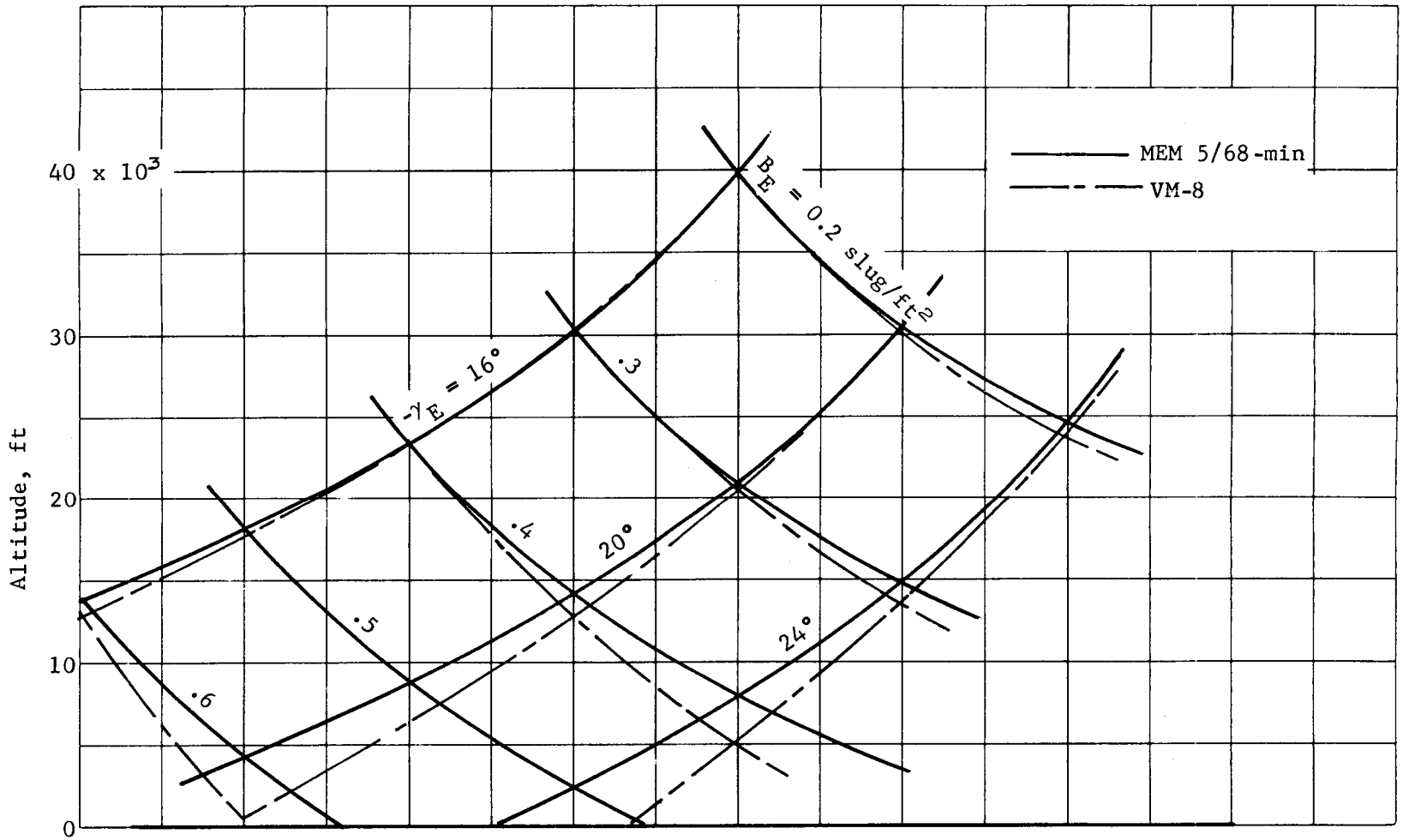

Figure 4.- Altitude at Mach 2.0, Orbit Mode

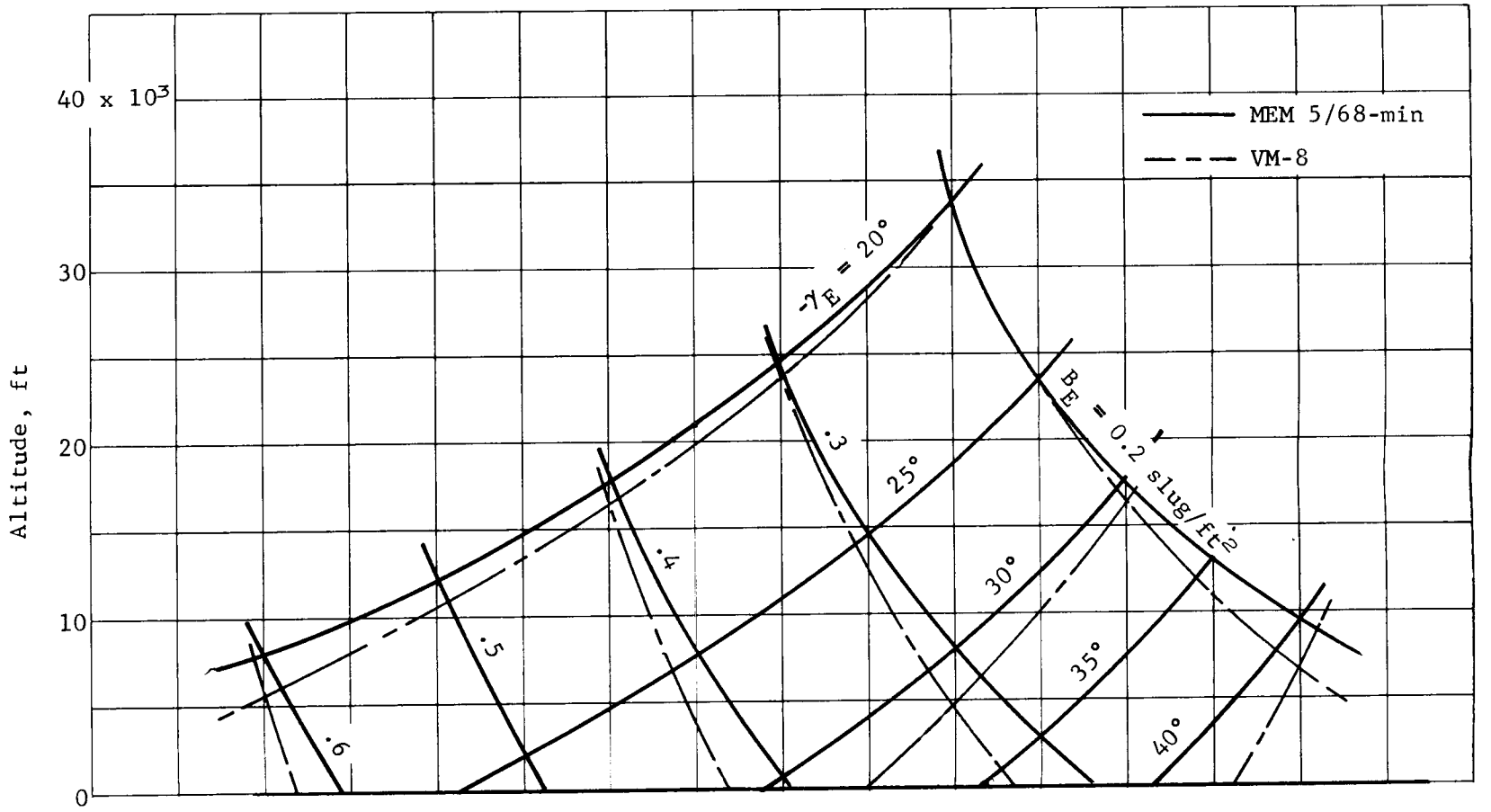

Figure 5.- Altitude at Mach 2.0, Direct Mode

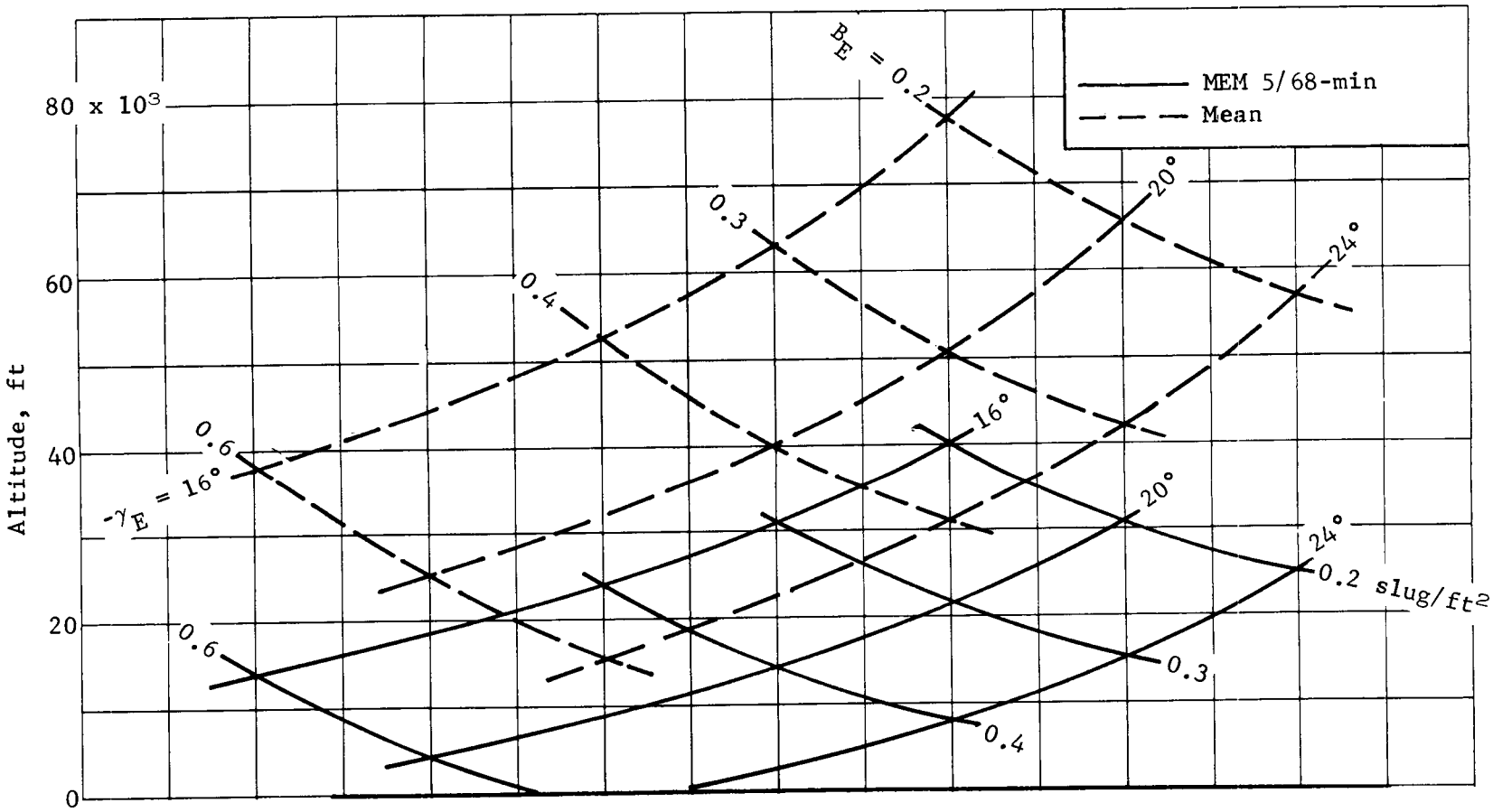

Figure 6.- Altitude at Mach 2.0, Orbit Mode

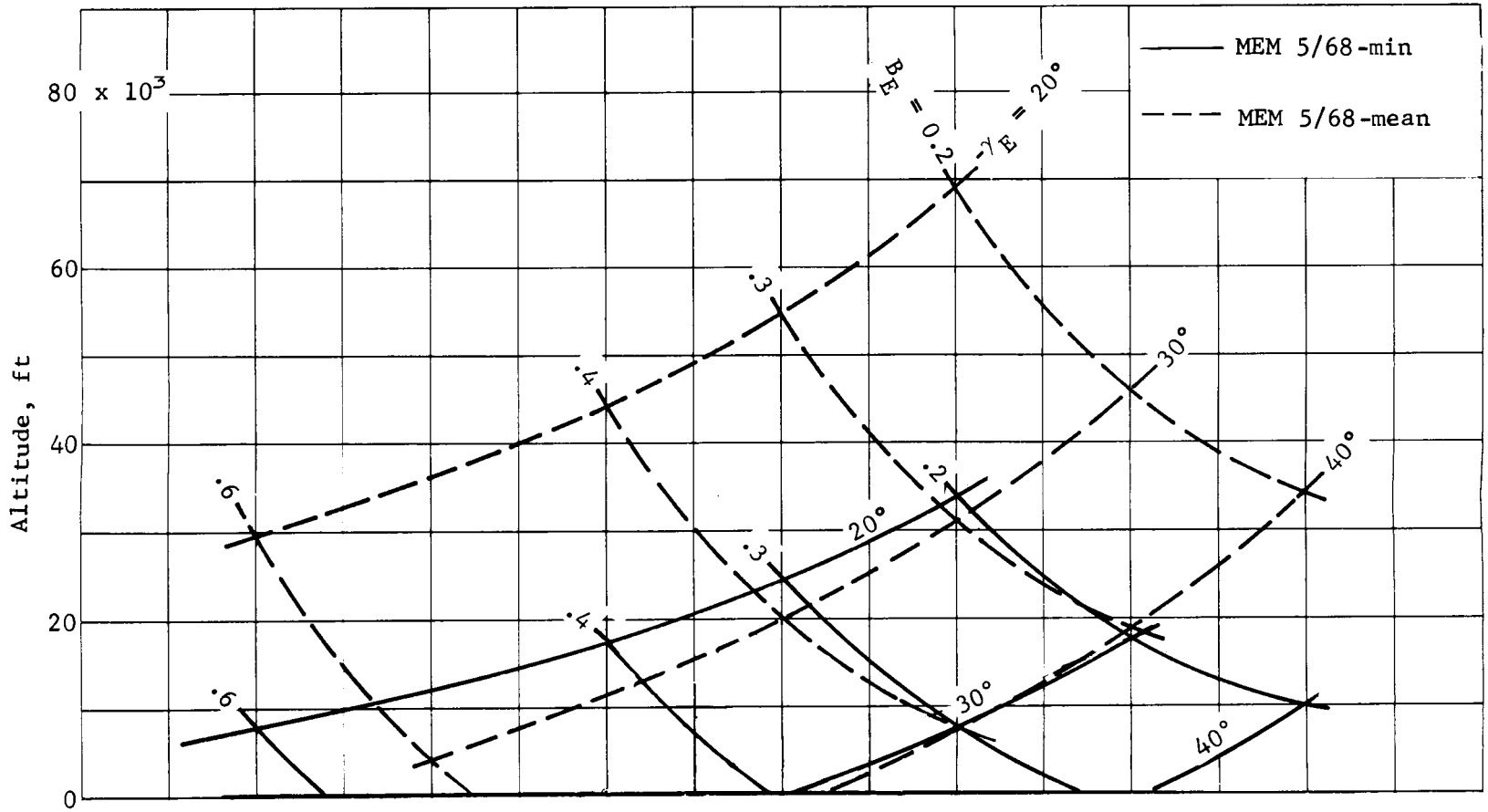

Figure 7.- Altitude at Mach 2.0, Direct Mode

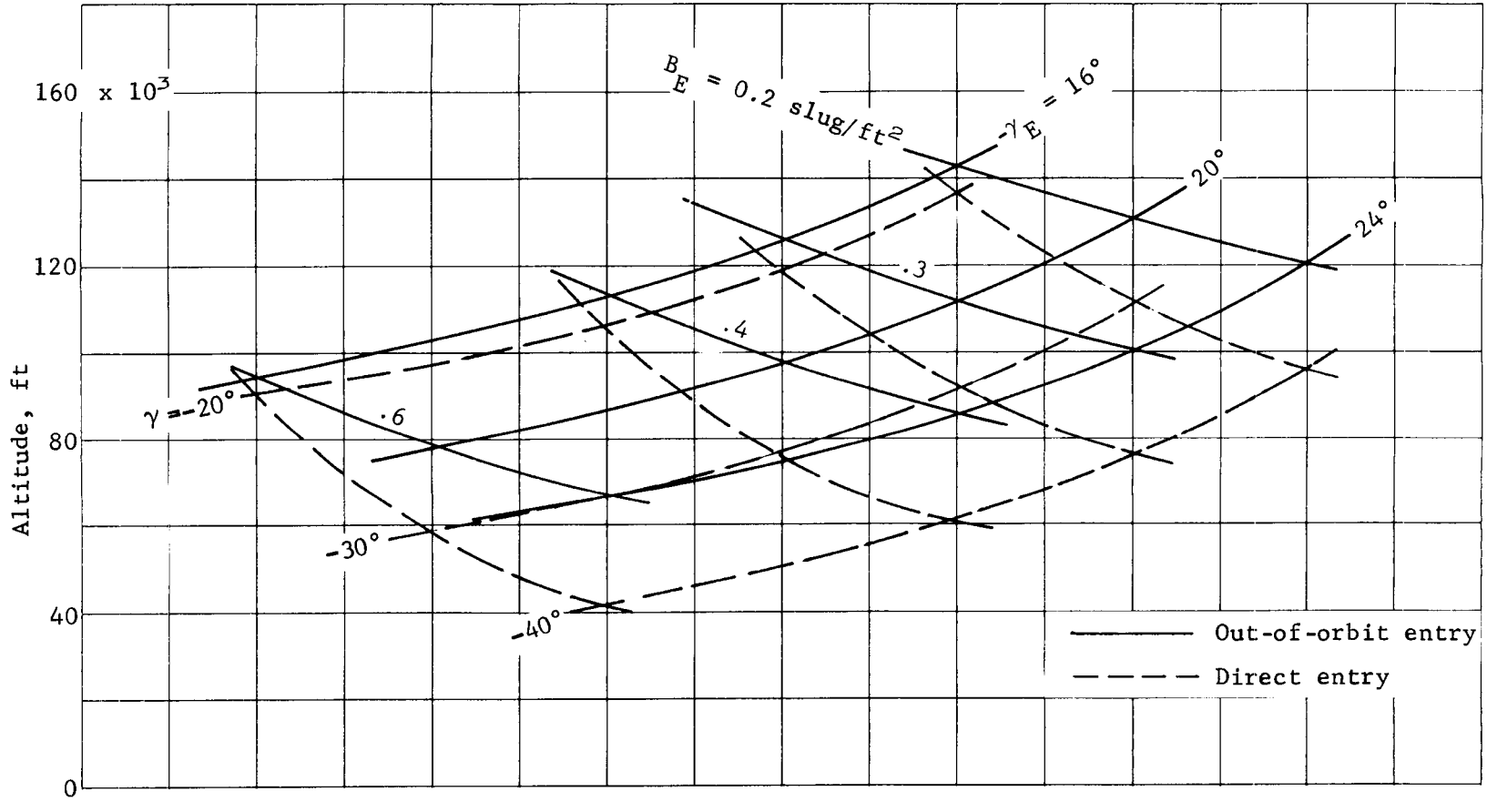

Figure 8.- Altitude at Mach 2.0, MEM 5/68-Maximum Atmosphere

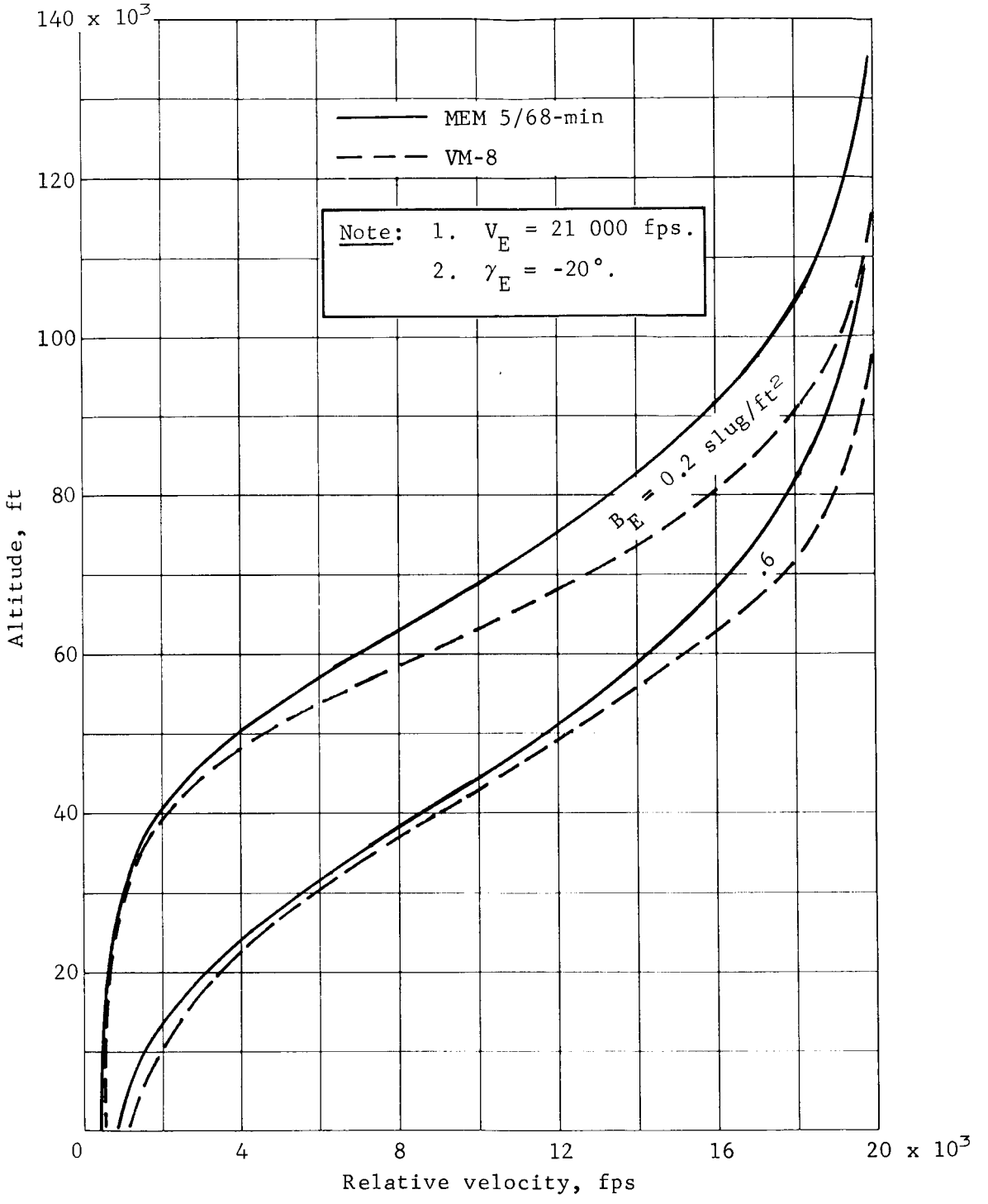

Figure 9.- High Altitude/Velocity Relationships

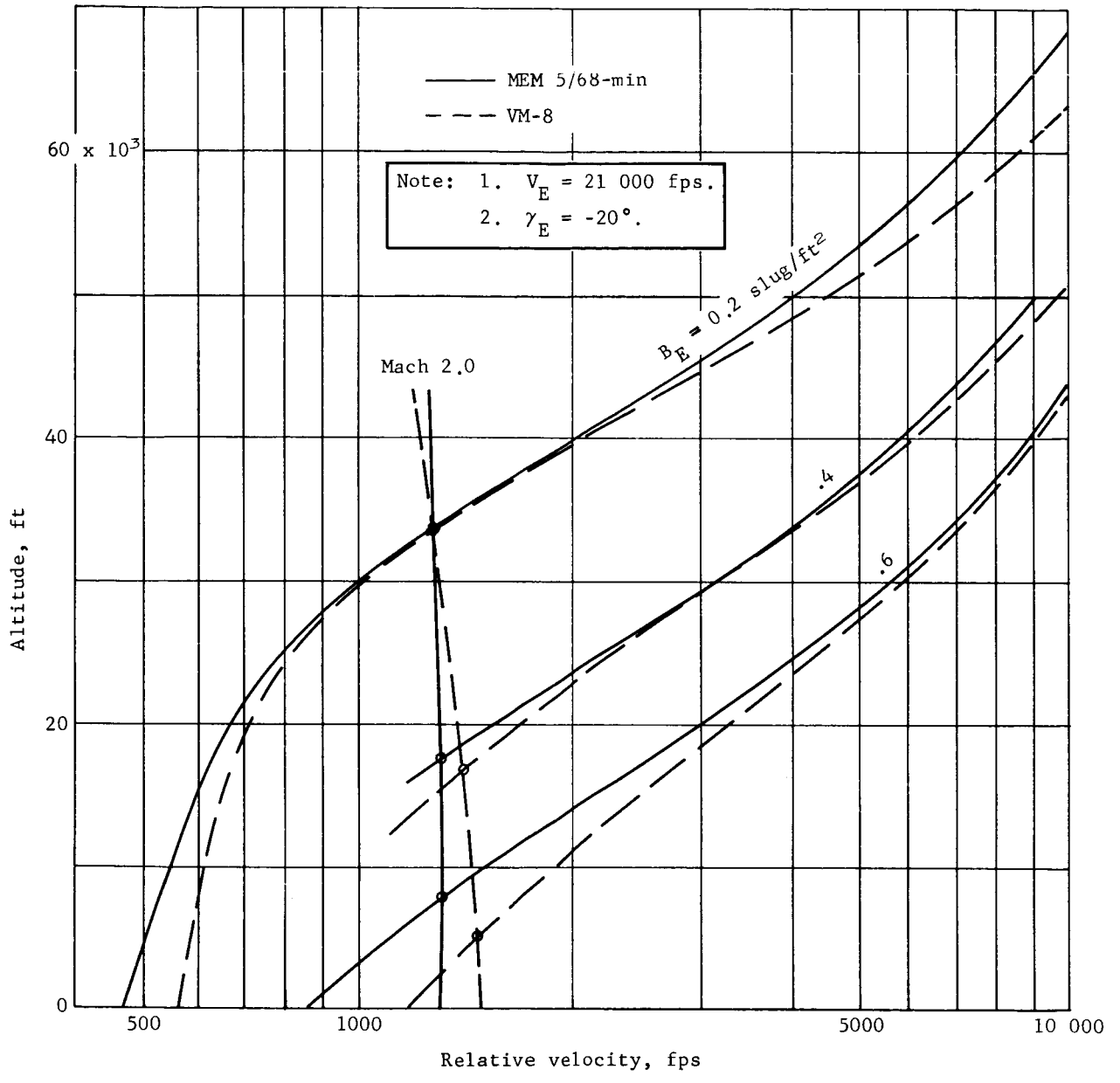

Figure 10.- Low Altitude/Velocity Relationships

result in $M = 2$ in the 30 000- to 40 000-ft altitude range where the old and new atmosphere densities are equivalent show no appreciable difference. Working at altitudes below 30 000 ft will show some advantage for the new atmospheres and this only happens for the higher B_E, γ_E combinations. The coincidence of the data for $B_E = 0.2$ and $M = 2$ is just that.

The data shown in figure 9 at high altitude implies an earlier buildup of entry load factor with the new atmospheres, while the peak load factor, inversely proportional to scale height, is lower if it occurs above 50 000 ft (fig. 3). The altitude at peak load factor for the MEM 5/68-min at VM-8 atmospheres are shown in the MEM 5/68-min and VM-8 atmospheres are shown in figures 11 and 12 for the orbital and direct modes, respectively. The crossover in the density curves between the MEM 5/68-min and VM-8 atmospheres is reflected in these data. The peak drag deceleration in MEM 5/68-min during entry is shown parametrically for the orbital and direct modes in figures 13a and 13b, respectively. Also shown for comparison is deceleration in VM-8 (critical for the VM models). The peak deceleration in the MEM 5/68-min atmosphere is less over the range of entry parameters than in VM-8, with the exception of the $B_E = 0.6$ slug/ft^2, $\gamma_E = -40°$ point, direct entry. Maximum peak values for the orbital mode are approximately 22 g (Earth) versus 31 g with the VM atmospheres. It is noted that peak deceleration is constant with varying B_E at a given γ_E in the MEM 5/68-min atmosphere. This is contrasted with a nonlinear variation with B_E in the VM-8 model. This occurs because of the difference in tropopause altitude between the two model atmospheres (fig. 2). Peak g occurs considerably below the tropopause altitude in the MEM 5/68-min atmosphere, thus eliminating the change in scale height in the region of peak g as experienced in VM-8. Thus, the nonlinear peak g effect in the MEM 5/68-min atmosphere is eliminated. Peak deceleration in the other MEM 5/68 atmosphere models is lower than in the MEM 5/68-min model as illustrated in table 2.

TABLE 2.- PEAK DRAG DECELERATION

Mode	B_E, slug/ft^2	$-\gamma_E$, deg	Peak $g_\oplus$ in			
			MEM 5/68			
			Min	Mean	Max	VM-8
Orbital	0.3	20	16.0	11.0	10.4	22.5
Direct	0.3	30	46.0	31.0	27.5	54.0

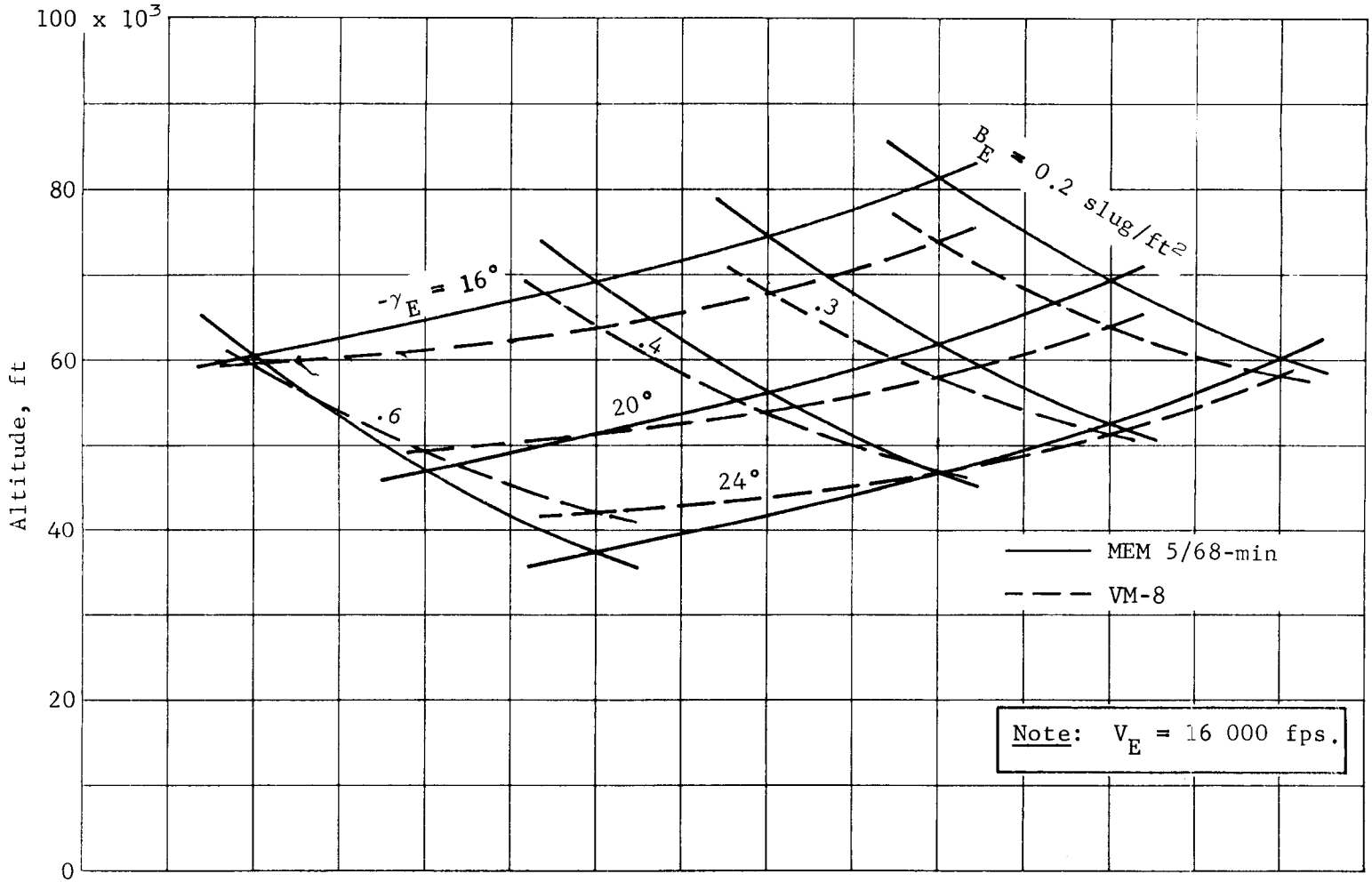

Figure 11.- Altitude at Peak Load Factor, Orbital Mode

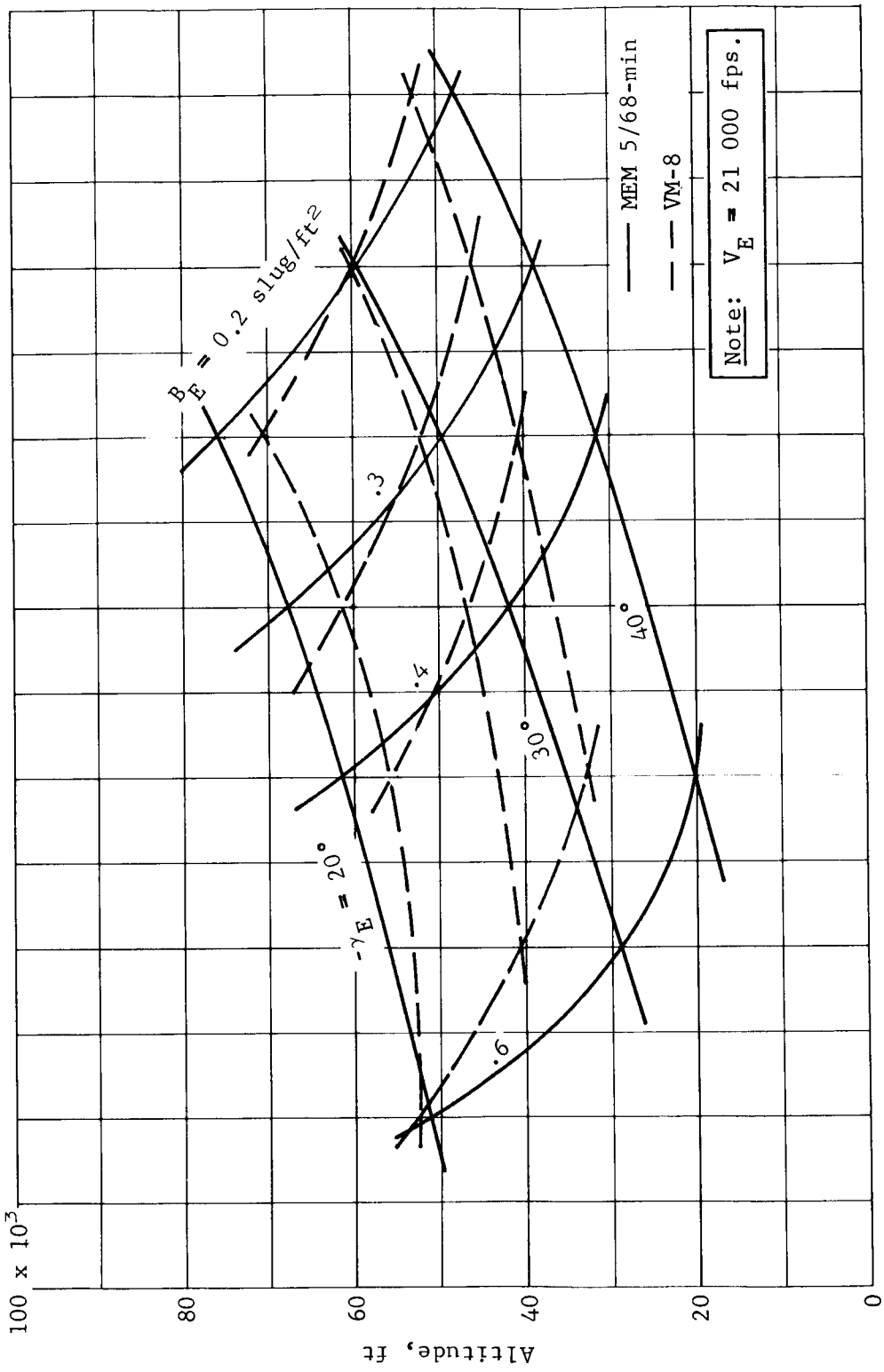

Figure 12.- Altitude at Peak Load Factor, Direct Mode

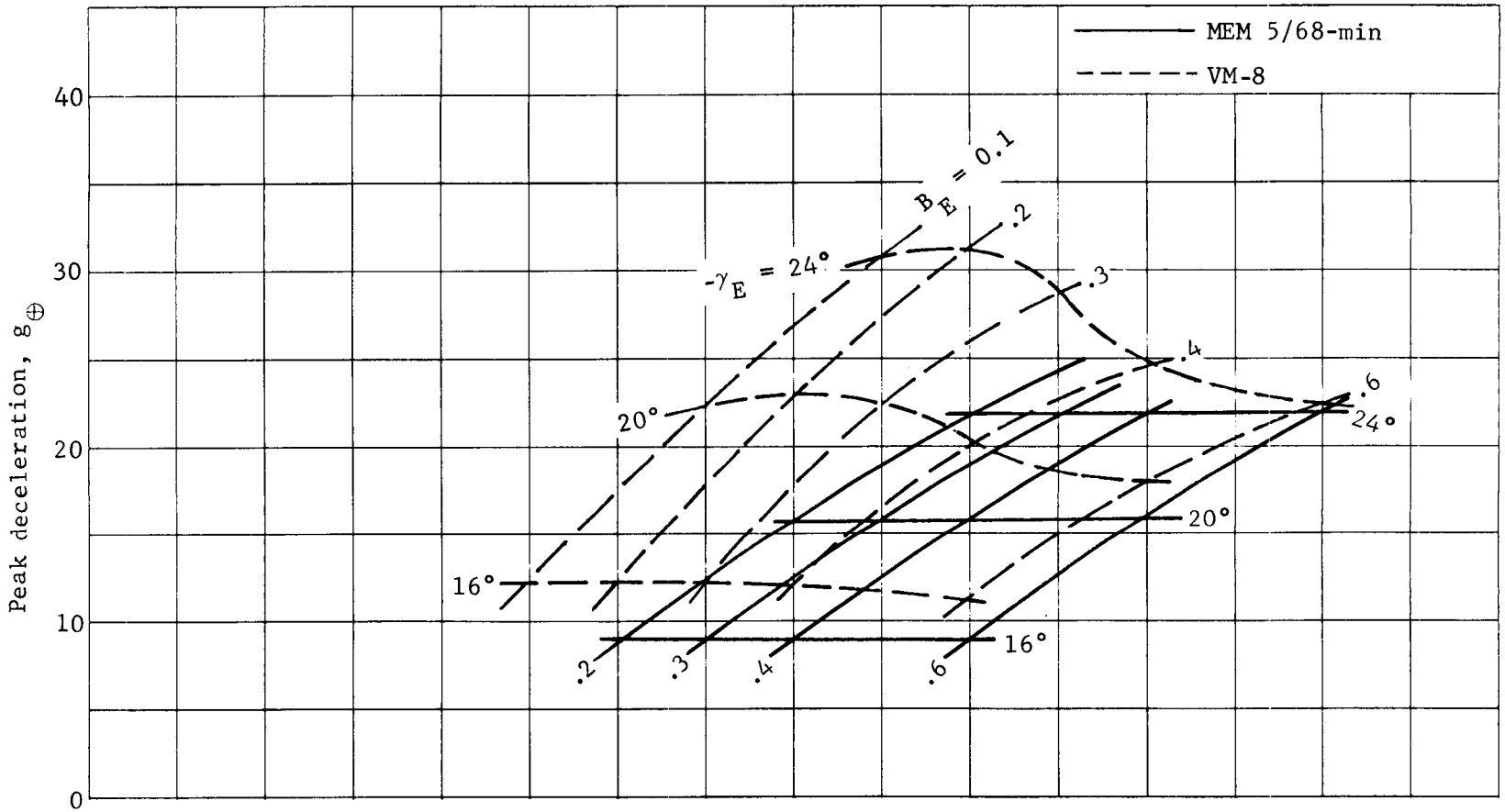

Figure 13a. - Peak Drag Deceleration, Orbit Mode

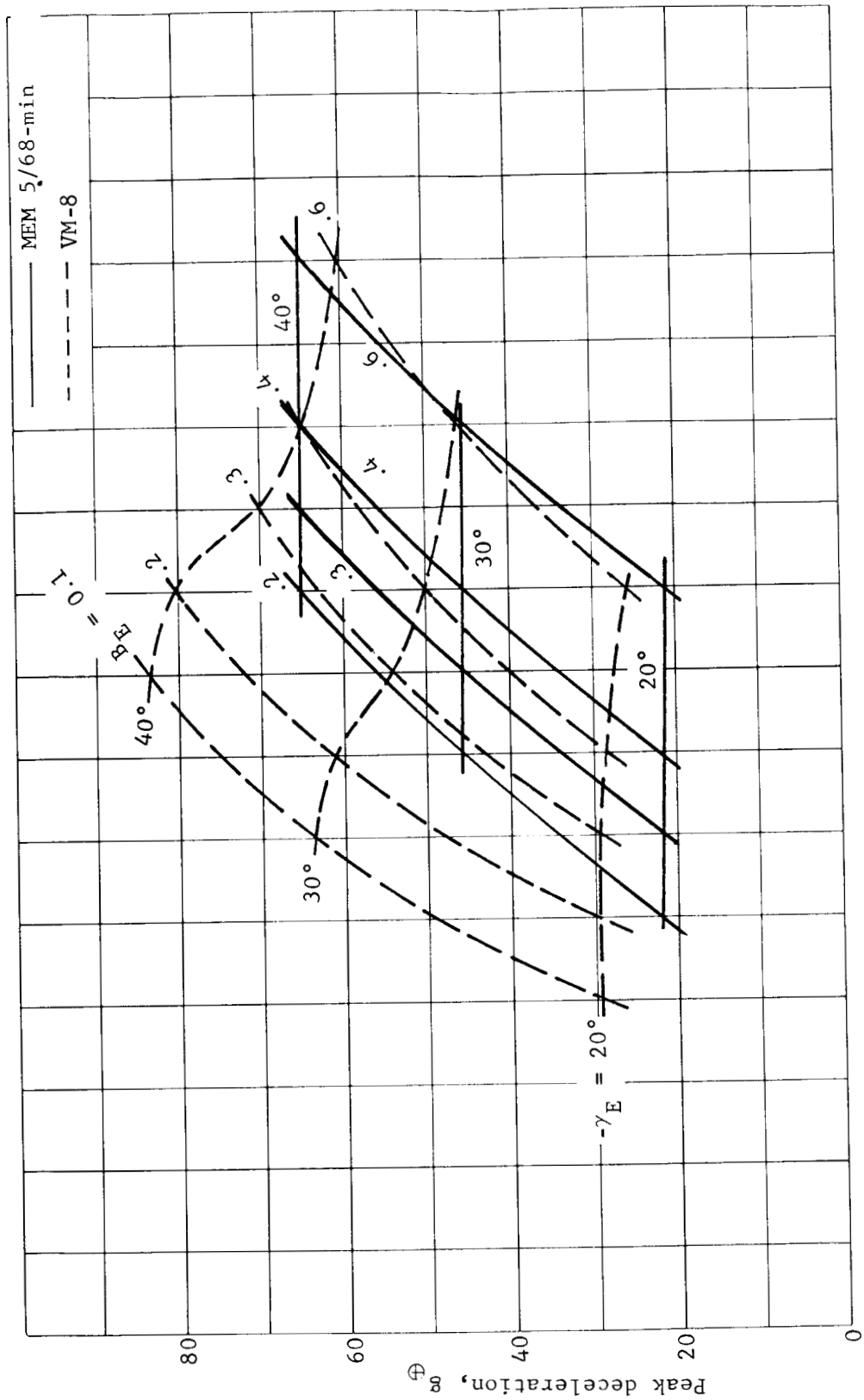

Figure 13b. - Peak Drag Deceleration, Direct Mode

Time from entry to 20 000-ft altitude in the MEM 5/68-min; mean and max atmospheres is shown as a function of entry flight path angle and ballistic coefficient for the orbital and direct modes in figures 14a and 14b. Superimposed on the time plots are limit plots for the VM-8, VM-7, and VM-3 model atmospheres. These VM atmospheres represent the limit and mean entry times from the previous study data (ref. 2).

For the orbit mode (fig. 14a), time to 20 000 ft is less in the VM atmosphere over the entire range of entry conditions investigated. For the direct mode, time to 20 000 ft is slightly greater at high ballistic coefficients in the VM-8 atmosphere than in the MEM 5/68-min model. The apparent inconsistency in time trend between orbit and direct mode can be understood by reference to the density vs altitude curve (fig. 3), and the altitude for peak drag deceleration (figs. 11 and 12). The peak deceleration during entry for the orbit mode occurs between 80 000- and 40 000-ft altitude. The higher density in the MEM 5/68-min in the altitude range from 35 000 ft down to 20 000 ft is the dominant factor in the larger descent times for this mode. In the direct entry mode, peak deceleration occurs between 35 000 ft and 20 000 ft. In that altitude range the slightly higher scale height in VM-8 and the reduced descent altitude increment to 20 000 ft result in relatively reduced time to 20 000 ft for the direct case.

A comparison was made of the time to 20 000-ft altitude between the VM-9 atmosphere (not a specified model in the Mars Mission Mode Study) and the MEM 5/68-max atmosphere. It was found that for the orbital mode (the only entry mode available with comparable parametric ranges), the time difference was 10 sec or less.

Downrange angle covered from entry to 20 000-ft altitude is shown for the three MEM 5/68 atmospheres for the orbital and direct modes in figures 14c and 14d. These downrange angles were compared to those in the corresponding VM atmospheres and were found to differ less than 0.5°.

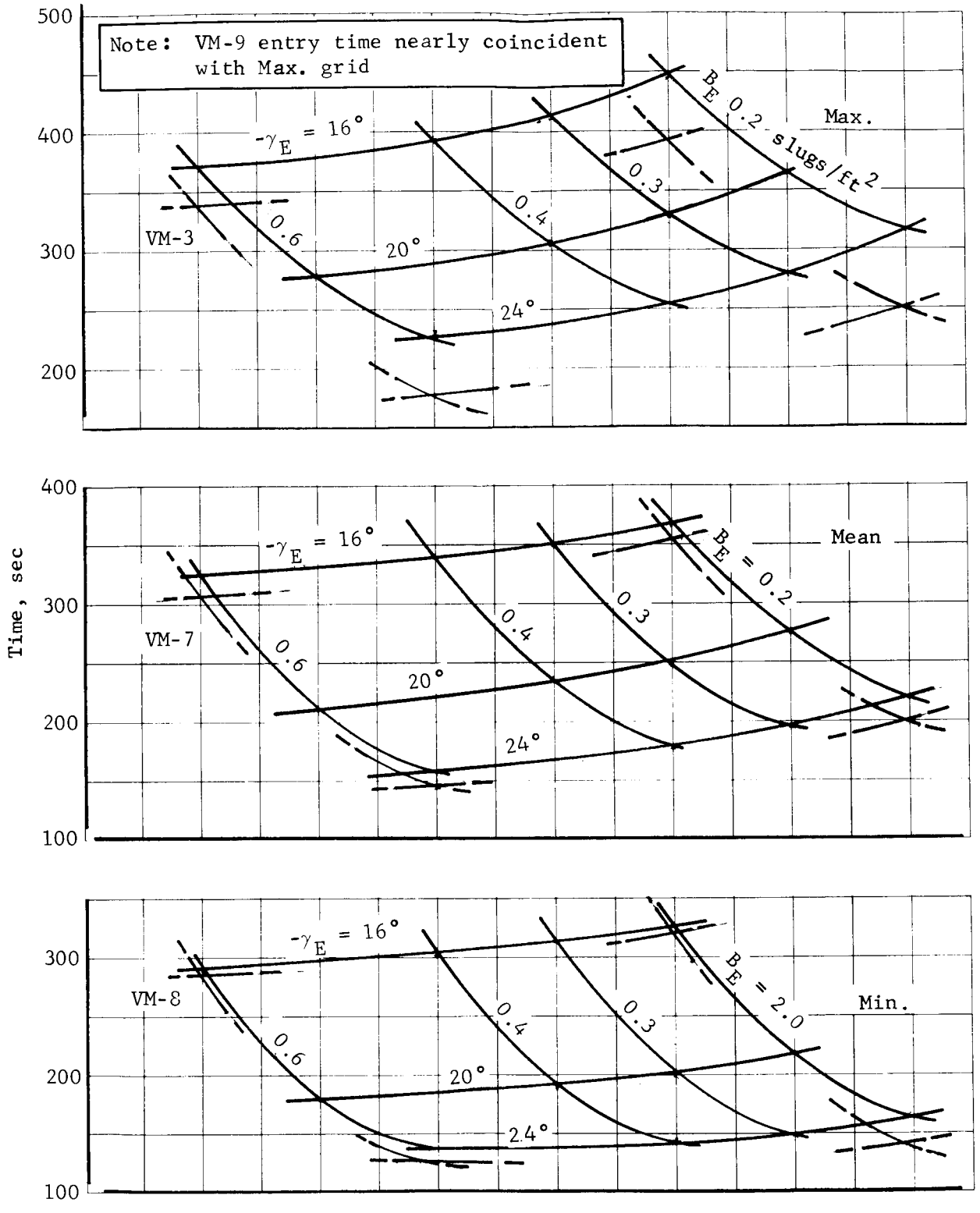

Figure 14a.- Time from Entry to 20 000-ft Altitude, MEM 5/68 Atmospheres, Orbital Entry, V_E = 16 000 fps

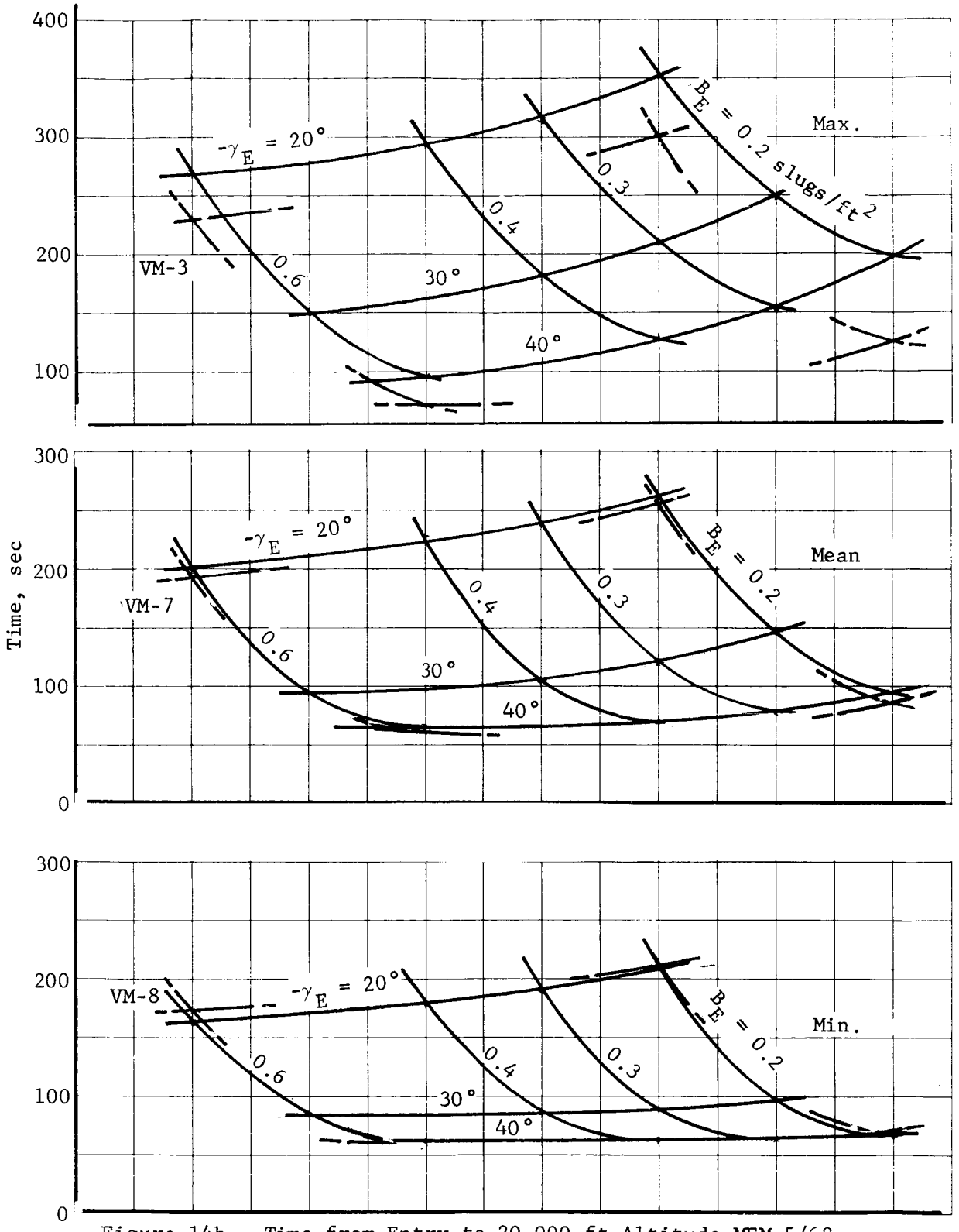

Figure 14b.- Time from Entry to 20 000-ft Altitude MEM 5/68 Atmospheres, Direct Entry, V_E = 21 000 fps

Note: Downrange angle in VM-3, -7, and -8 is <0.5° different from respective MEM 5/68 atmospheres.

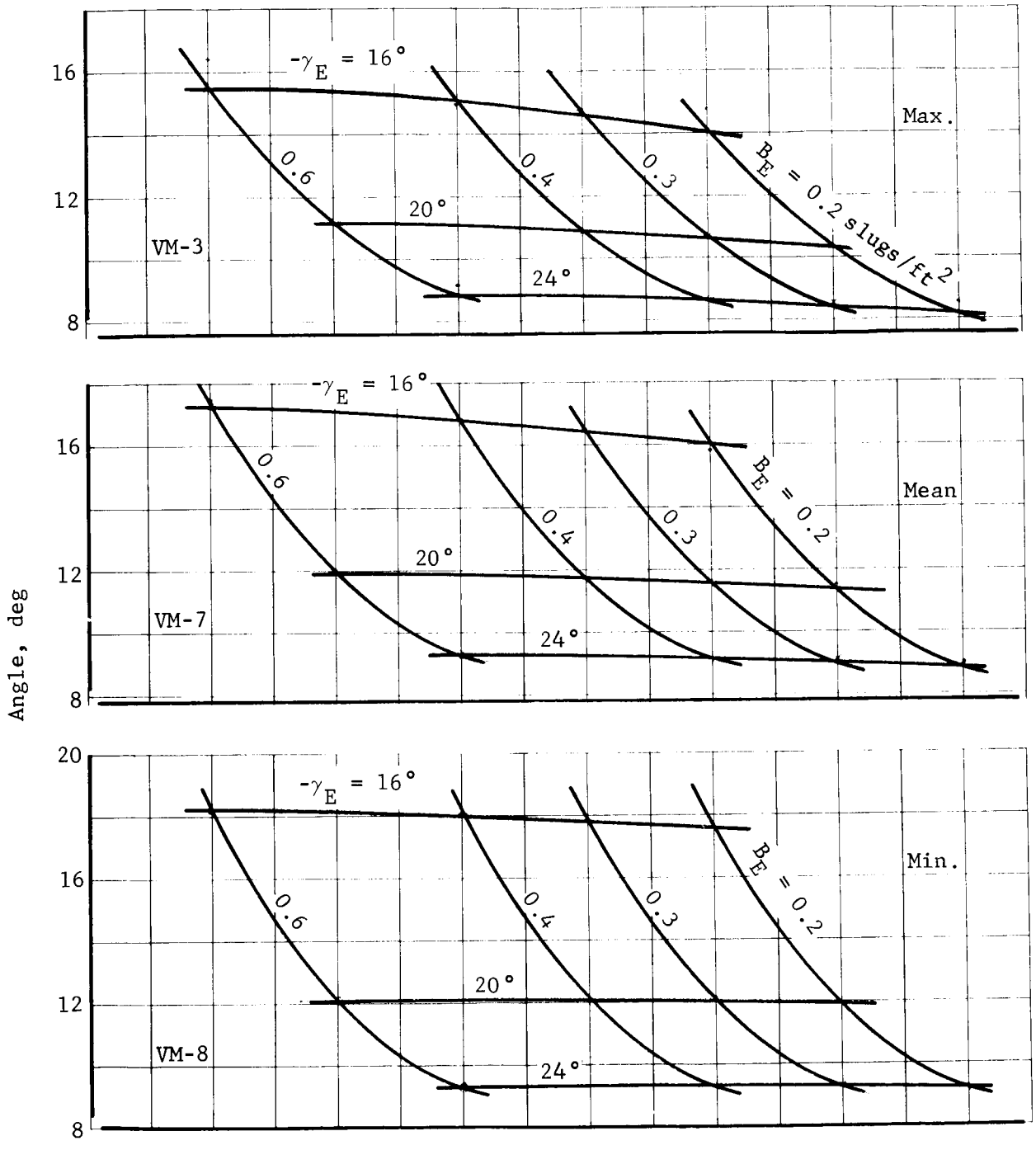

Figure 14c.- Downrange Angle Entry to 20 000 ft, MEM 5/68 Atmospheres, Orbital Entry, V_E = 16 000 fps

Note: Downrange angle in VM-3, -7, and -8 is <0.5° different from MEM 5/68 atmospheres.

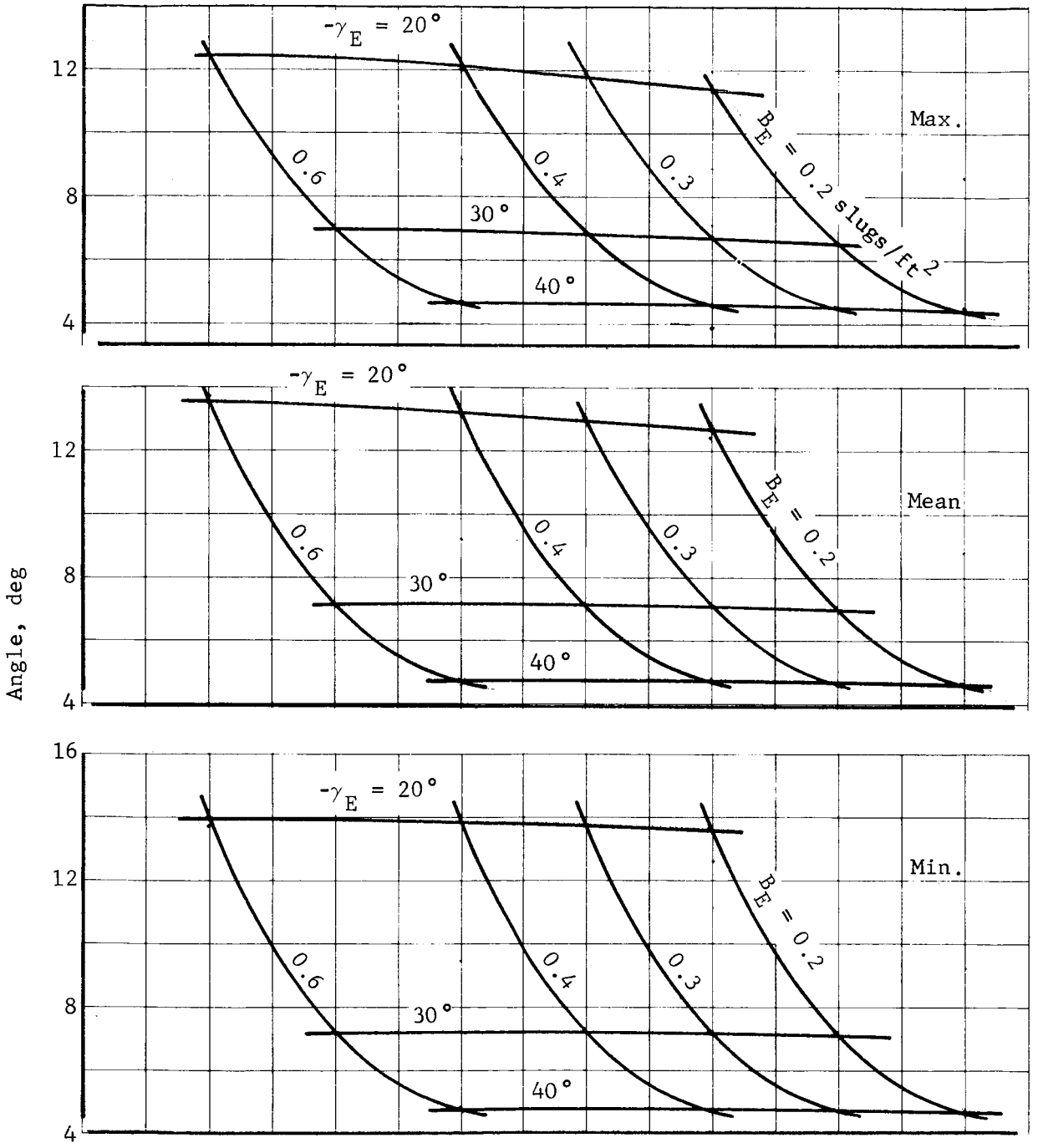

Figure 14d.- Downrange Angle Entry to 20 000-ft Altitude, MEM 5/68 Atmospheres, Direct Entry, V_E = 21 000 fps

Terminal Phase Analysis

Terminal phase initiation conditions are determined by entry trajectory characteristics, presented in the preceding section, and may be expressed in terms of entry conditions (velocity, flight-path angle, ballistic coefficient). Entry corridors (flightpath angle vs velocity at entry) result from the targeting and error analysis. Correlation with these values defines the required values over the parametric range of entry parameters used in the terminal phase analysis. Terminal phase performance is measured in terms of entry weight, aeroshell diameter, and useful landed weight. Entry weight converted to capsule system weight allows correlation with launch vehicle capability, as shown in reference 2 (Volumes I, II, and III). The end point of the terminal phase analysis defines useful landed weight as a function of aeroshell diameter and entry conditions and dispersions. Sensitivity to design parameters such as landed terrain height and decelerator size is also factored into the analysis along with the constraints under which the system is assumed to perform. This report presents the results of the MEM 5/68 atmosphere analysis compared with the VM atmosphere results taken from reference 2 (Volume IV). In addition, VM results are rerun for the direct mode (V_E = 21 000 fps) to provide a direct comparison.

The terminal descent system investigated consists of a disc-gap-band or ringsail-type parachute deployed at M = 2.0 or less. The aeroshell is separated from the lander at about M = 0.80. Final deceleration is supplied by a vernier propulsion system after parachute release. The MEM 5/68-min atmosphere is most critical for the parachute trajectory because of its low density during this phase. Initial velocities and Mach number are highest at parachute deployment in this atmosphere model. Therefore, this atmosphere determines the altitude of parachute deployment. The effect of the MEM 5/68-mean atmosphere on terrain height capability is also investigated for several point designs.

Conditions investigated for the trajectory analysis are:

1) Entry velocities of 16 000 fps (orbital mode) and 21 000 fps (direct mode);

2) Entry flightpath angles of -16 to -24° (orbital mode) and -20 to -40° (direct mode);

3) Terrain heights of 0, 3000, and 6000 ft above the mean planet surface;

4) Lateral velocity due to winds of 220 fps at aerodecelerator separation (retro system ignition).

Additional assumptions, ground rules, and constraints related to the aerodecelerator phase are as follows:

1) The aerodecelerator has completed its job at 4000 ft above terrain;

2) The flightpath angle, γ, at aerodecelerator separation must be -60° or steeper;

3) Time on aerodecelerator must be 16 sec or longer;

4) The parachute system must be sized to accomplish 1) and 2) above or separate the aeroshell, whichever is larger.

Ground rules and constraints related to the vernier system sizing are as follows:

1) Ignition at 4000 ft above the surface;

2) Velocity at ignition is 1.25 times parachute terminal velocity;

3) Flightpath angle at ignition is -60°;

4) Aerodecelerator separation at vernier ignition.

A monopropellant three-engine vernier propulsion system with a specific impulse of 225 sec is assumed for the terminal phase analysis.

The analysis is performed for a range of aeroshell diameter as follows:

1) Orbital mode - 6.5, 8.5, 12, and 15 ft;

2) Direct model - 6.5, 8.5, 12, 15, 20, 25, and 30 ft.

The launch vehicle shroud size limitation assumed for this analysis (16-ft diameter) has been interpreted in this parametric analysis to limit the aeroshell diameter to approximately 15 ft. Aeroshell diameters greater than 15 ft are obtained by deploying flaps.

These assumptions, ground rules, and constraints are identical to those used in VM atmosphere model analysis. A more detailed discussion may be found in reference 2 (Volume IV).

A discussion of the data and comparison of atmospheres follows. Reason for differences due to atmospheres is found in the summary at the end of this section.

Parachute trajectories are calculated for various B_E based on deployment at $M = 2$ in the MEM 5/68-min atmosphere. The parachute is assumed to have accomplished its purpose when a relative flightpath angle of -60° is reached at least 4000 ft above the terrain. The B_{DEC} (parachute size required to reach these final conditions) for various γ_E and B_E are shown in figures 15 thru 20 for the MEM 5/68-min atmosphere. Similar data for VM-7 and VM-8 (direct mode) are shown in figures 21 and 22. B_{DEC} for VM-7 and VM-8 for the orbit mode are partially shown for reference in figures 15 and 17. It is seen that the parachute sizes required for the MEM 5/68-min atmosphere are smaller than for VM-7 and VM-8. The parachute size used in calculations is always sufficient to separate the system from the aeroshell at $M = 0.8$. Therefore, in those cases where the parachute size required for separation is larger than shown in figures 15 thru 22, the size required for separation is used. A minimum time on the parachute of 16 sec is assumed. Time on the parachute is shown parametrically in figures 23 and 24 for the 6000-ft terrain height and parachute sizes of 0.015, 0.030, and 0.10 slug/ft^2.

The approach used in this analysis is to compare the useful payload on the ground on the basis of entry weight and aeroshell diameter. The parameter used for comparison is landed equipment weight, W_{LE}. This parameter is defined as entry weight, W_E, minus aeroshell weight, aerodecelerator system, vernier system, entry thermal control, ACS, landed structure including legs, pyro subsystem, and diameter sensitive cabling. Thus, W_{LE} is the effective usable weight on the ground comprised of entry G&C, all communications and data handling subsystems, power subsystems, surface thermal control, and surface science subsystems. The parametric weight equations used for the delivery system weight are shown in reference 2, (Volume VI).

A sample of the basic data calculated is shown in figure 25 for the MEM 5/68-min and VM-7, VM-8 atmospheres. The results for the MEM 5/68-min atmosphere, compared to the VM-7, VM-8 results, show higher landed equipment weights for a given entry weight or a given diameter. Illustrated in figure 25 are the maximum W_{LE} contour and the maximum W_{LE}/W_E envelope. The maximum W_{LE}/W_E envelope optimizes landed equipment weight per pound entry weight at the expense of higher aeroshell diameters.

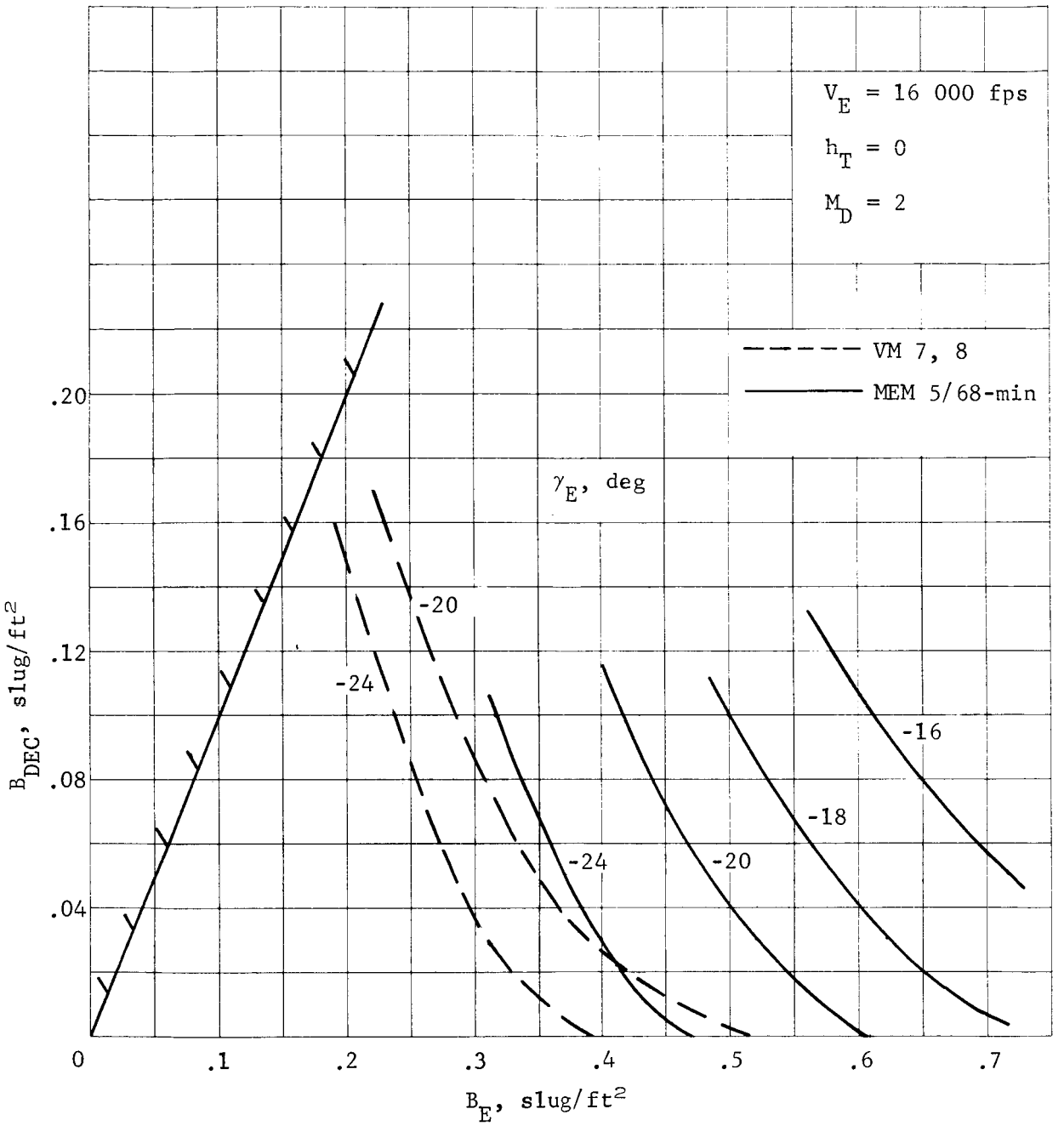

Figure 15.- B_{DEC} vs B_E, Orbit Mode

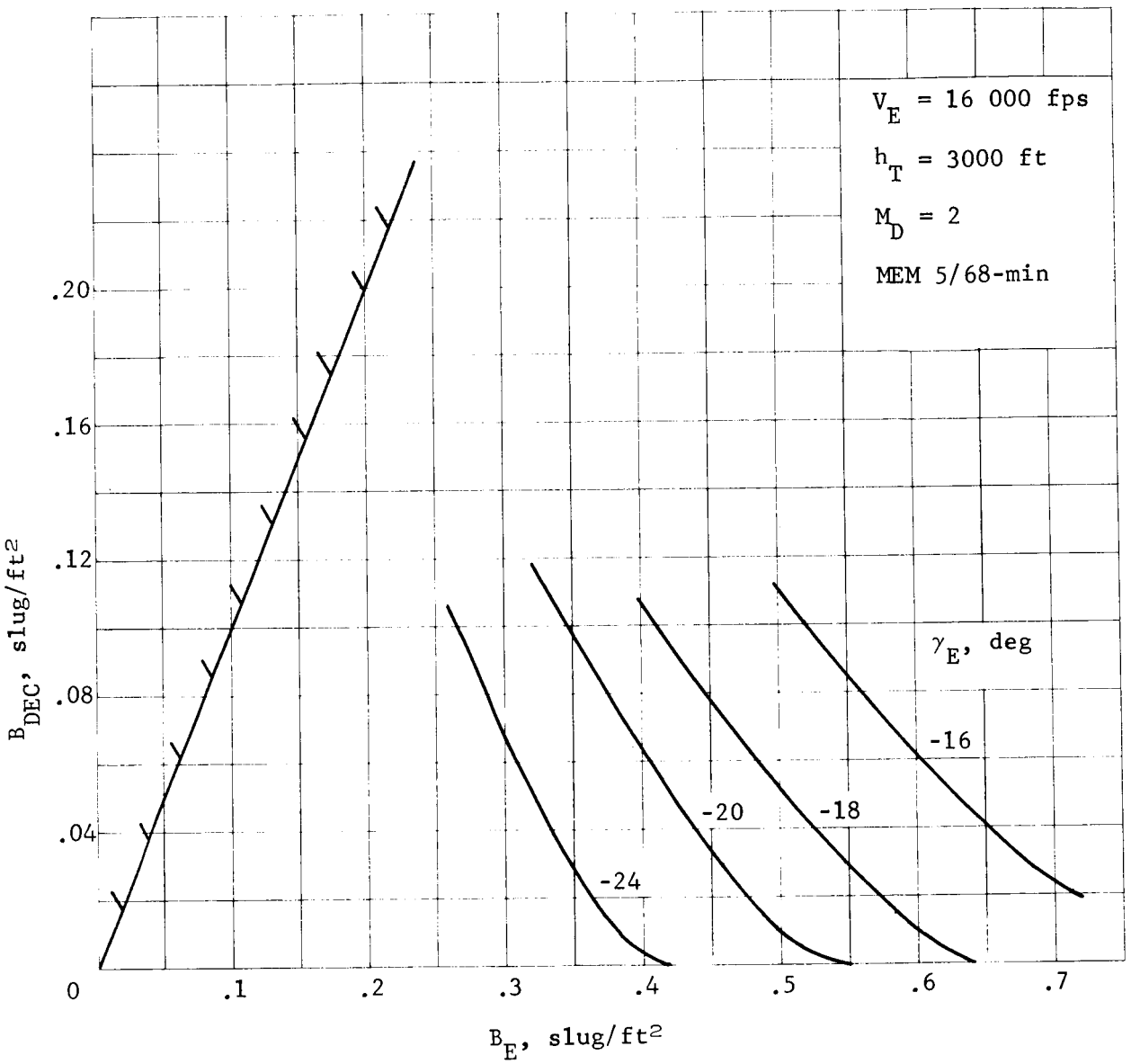

Figure 16.- B_{DEC} vs B_E, Orbit Mode

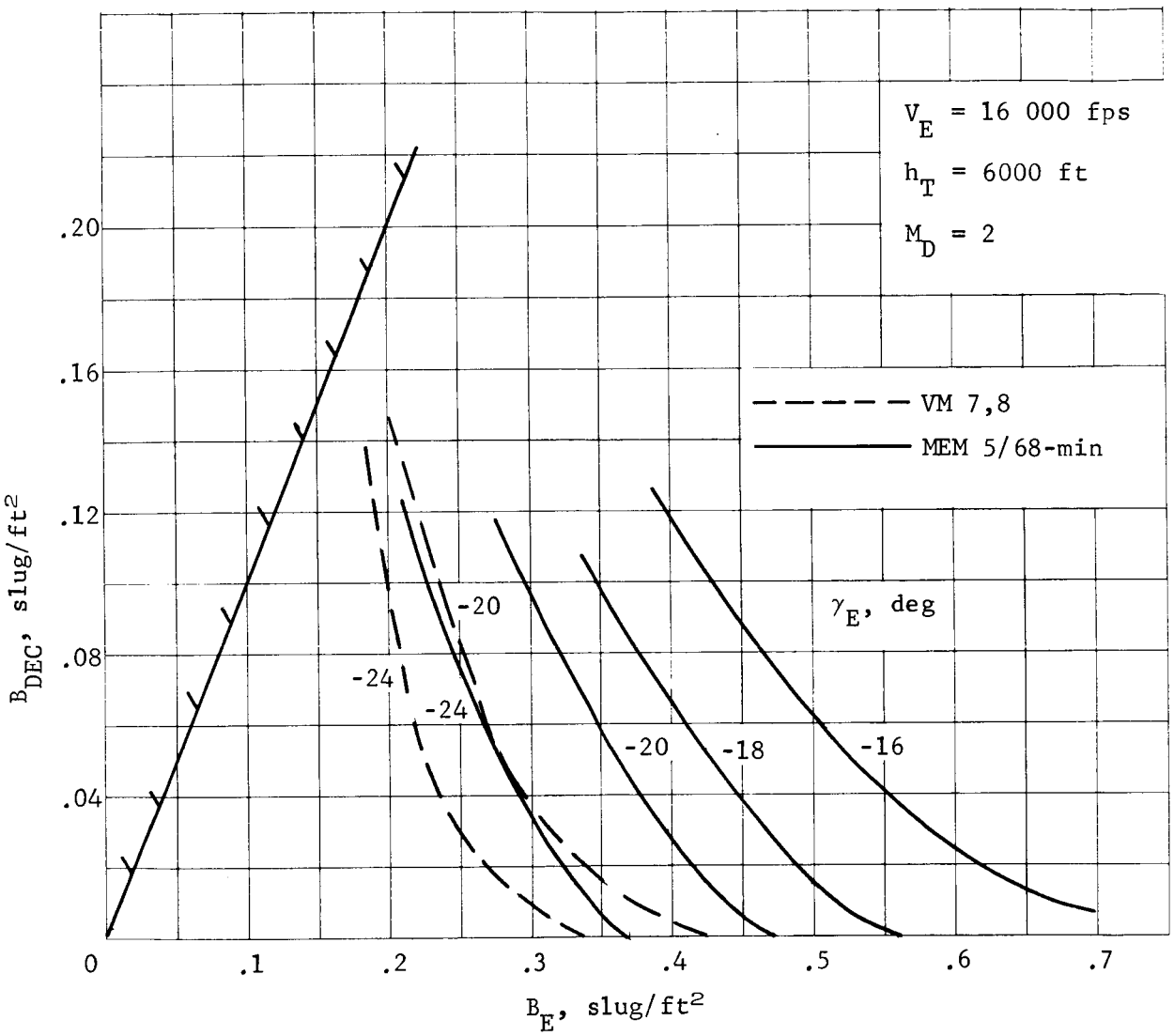

Figure 17.- B_{DEC} vs B_E, Orbit Mode

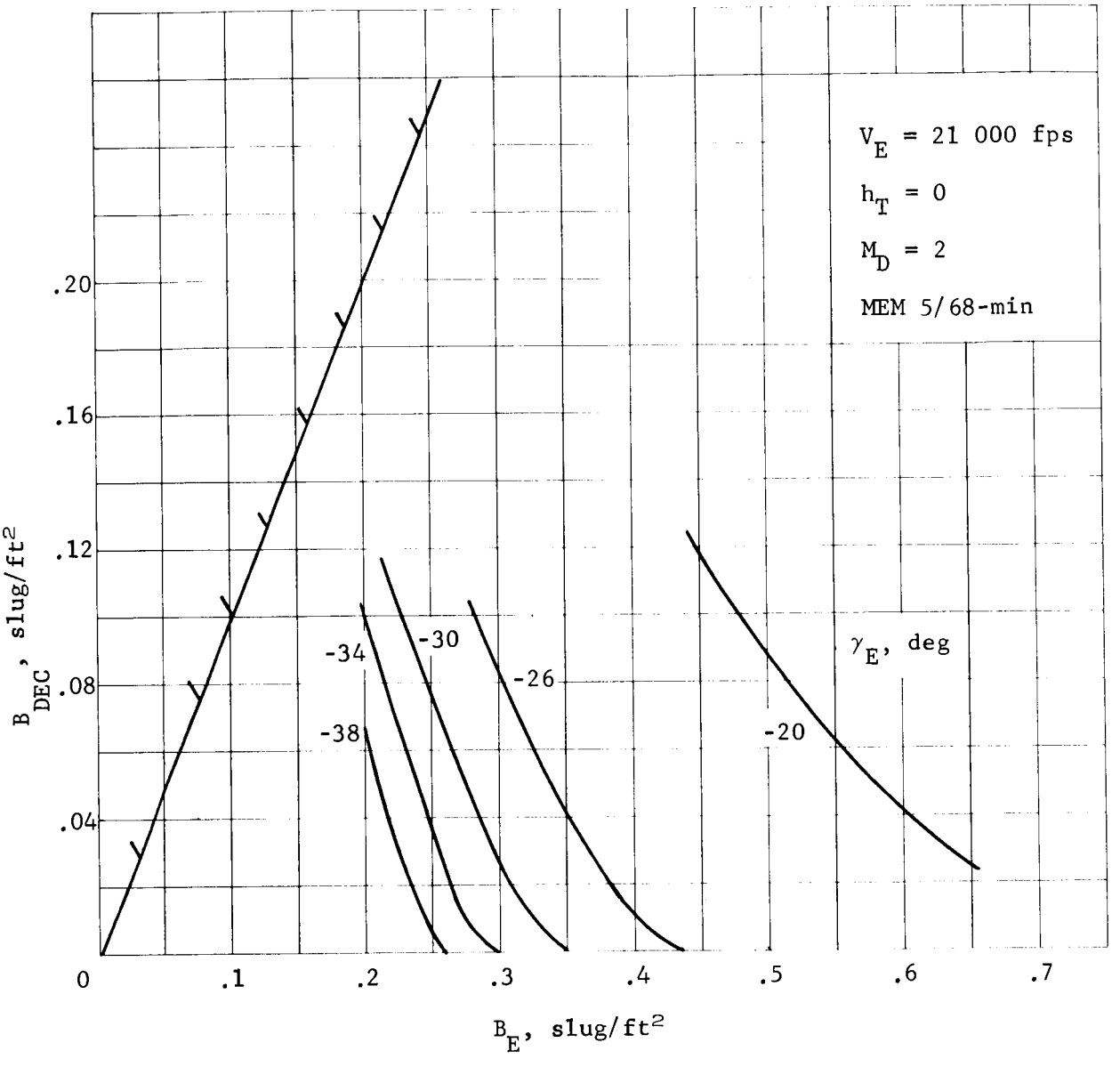

Figure 18.- B_{DEC} vs B_E, Direct Mode

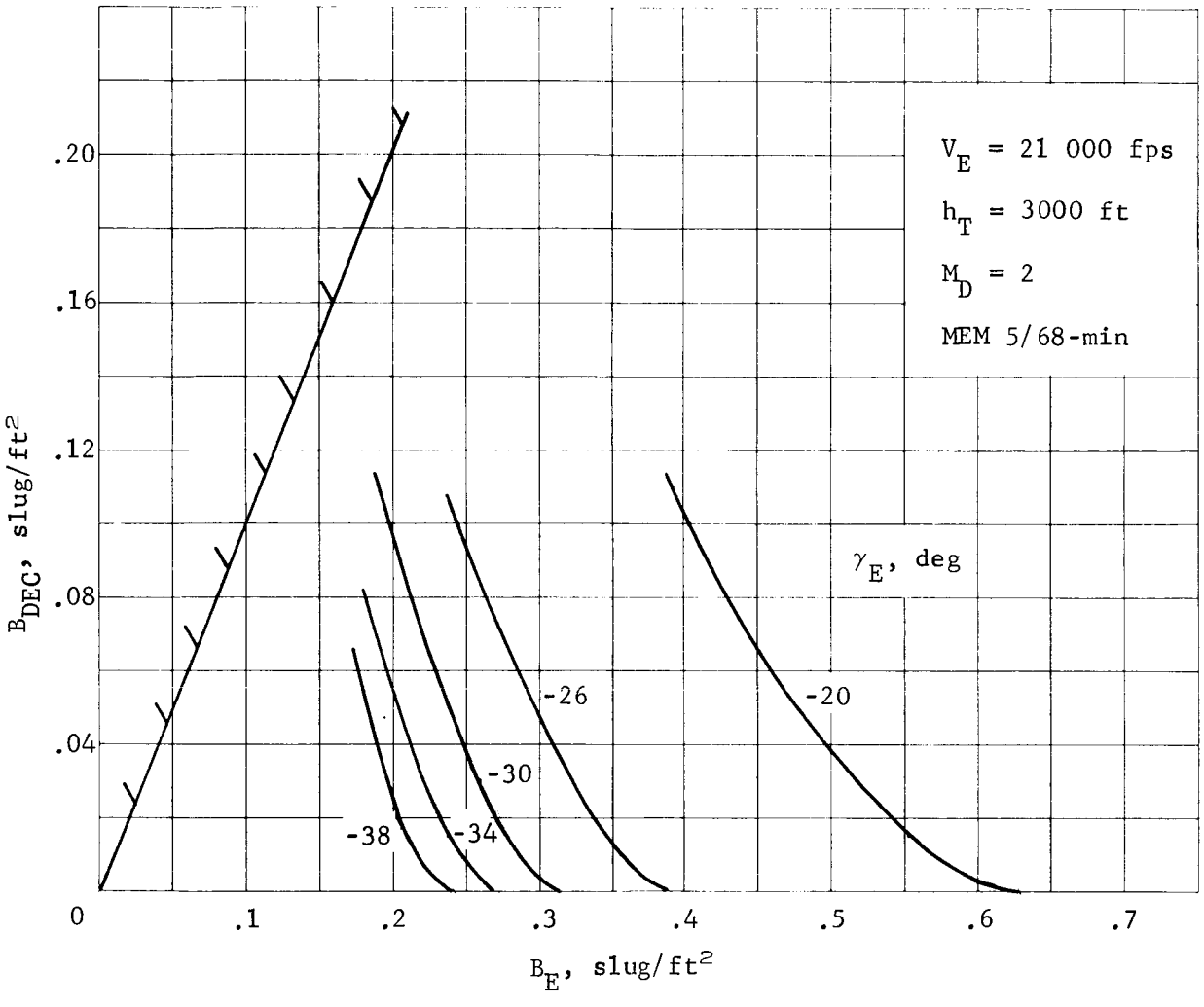

Figure 19.- B_{DEC} vs B_E, Direct Mode

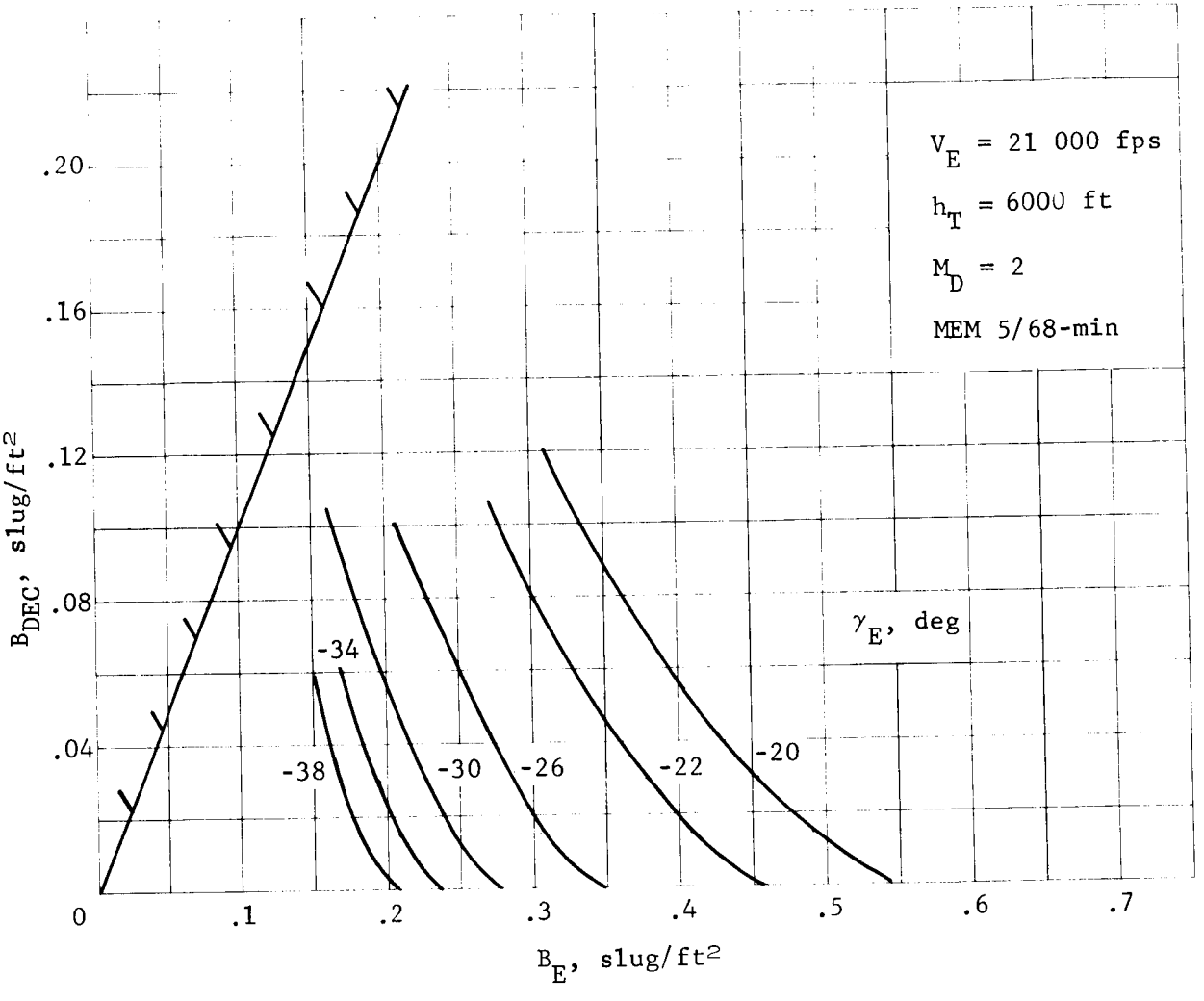

Figure 20.- B_{DEC} vs B_E, Direct Mode

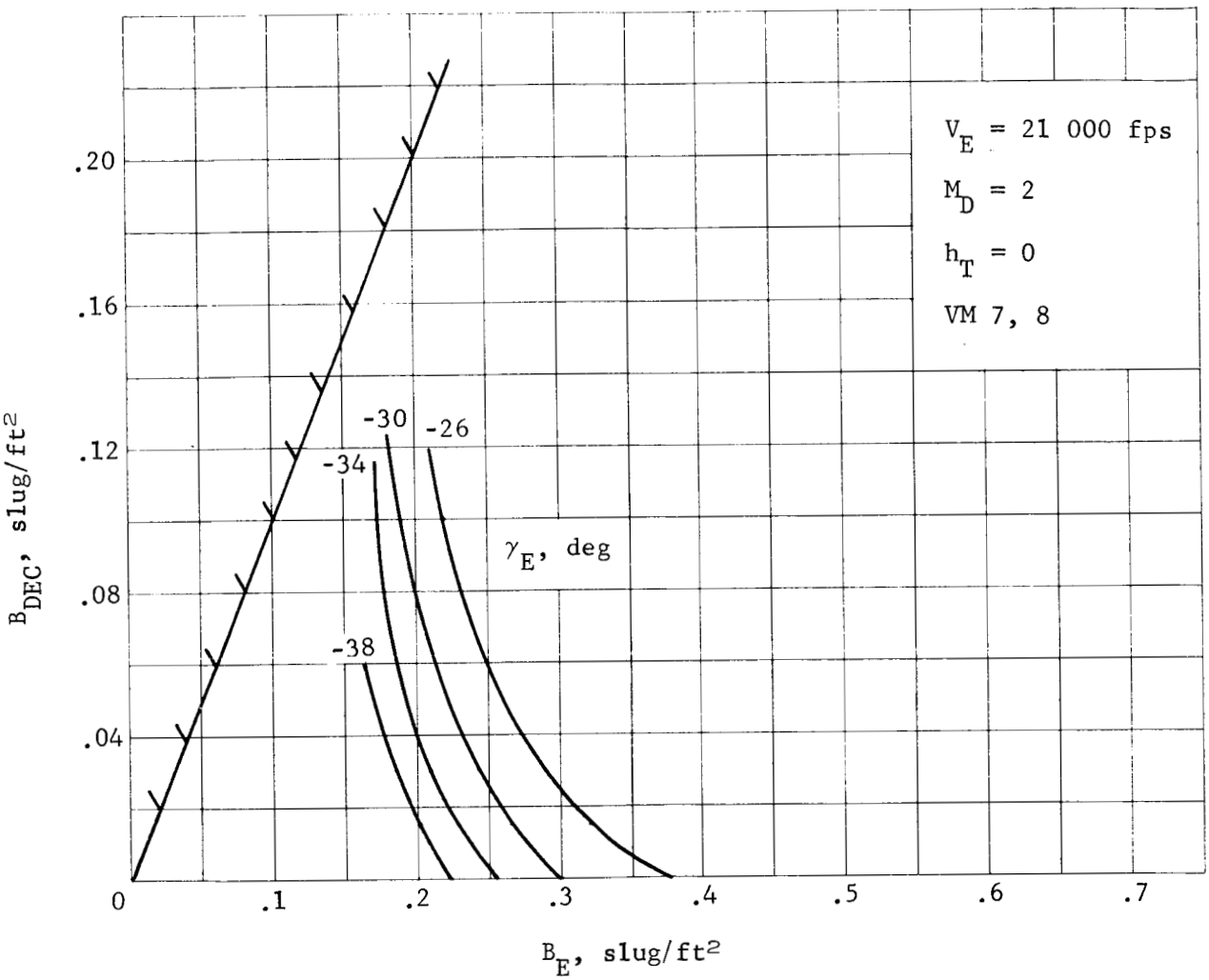

Figure 21.- B_{DEC} vs B_E, Direct Mode

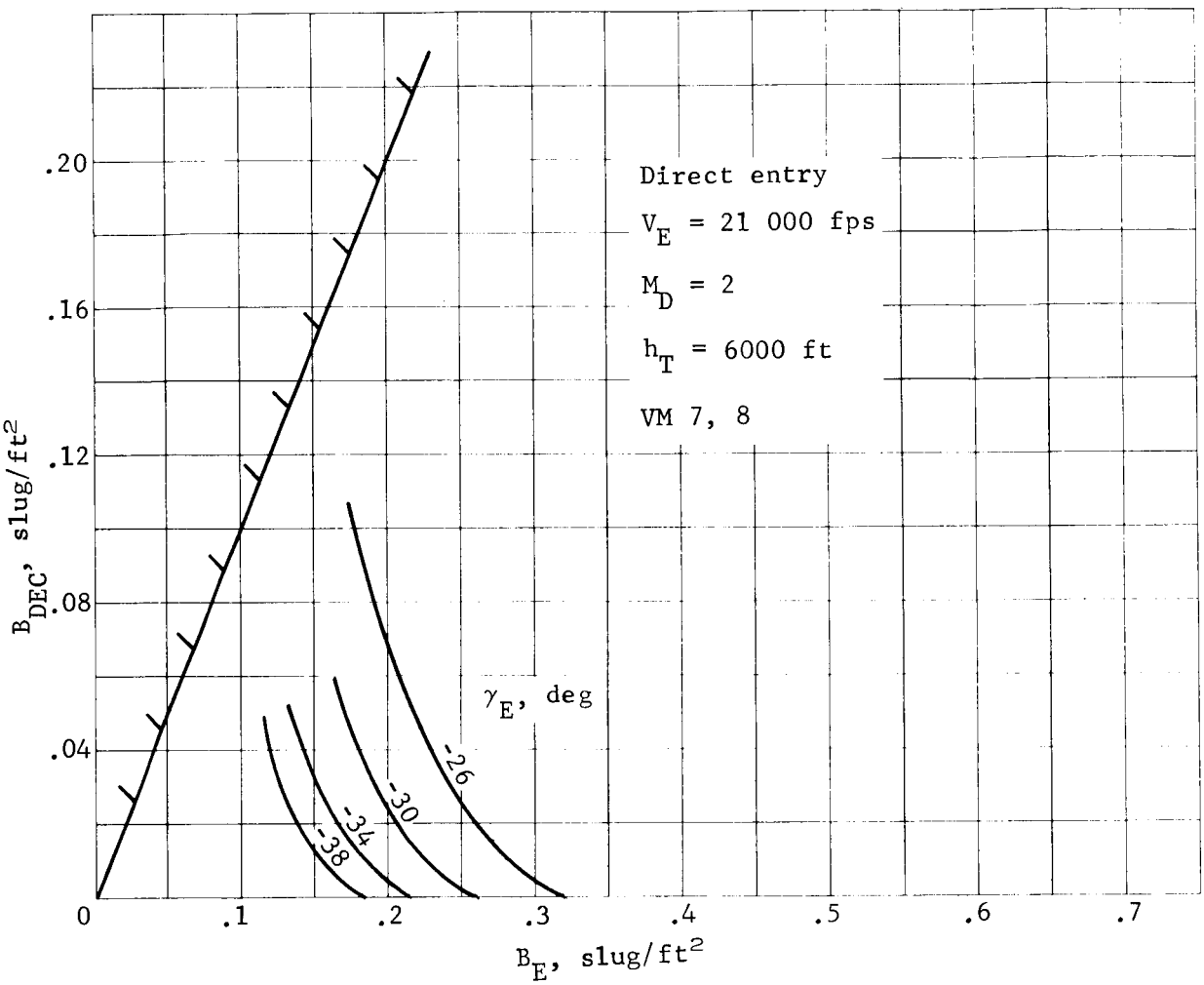

Figure 22.- B_{DEC} vs B_E, Direct Mode

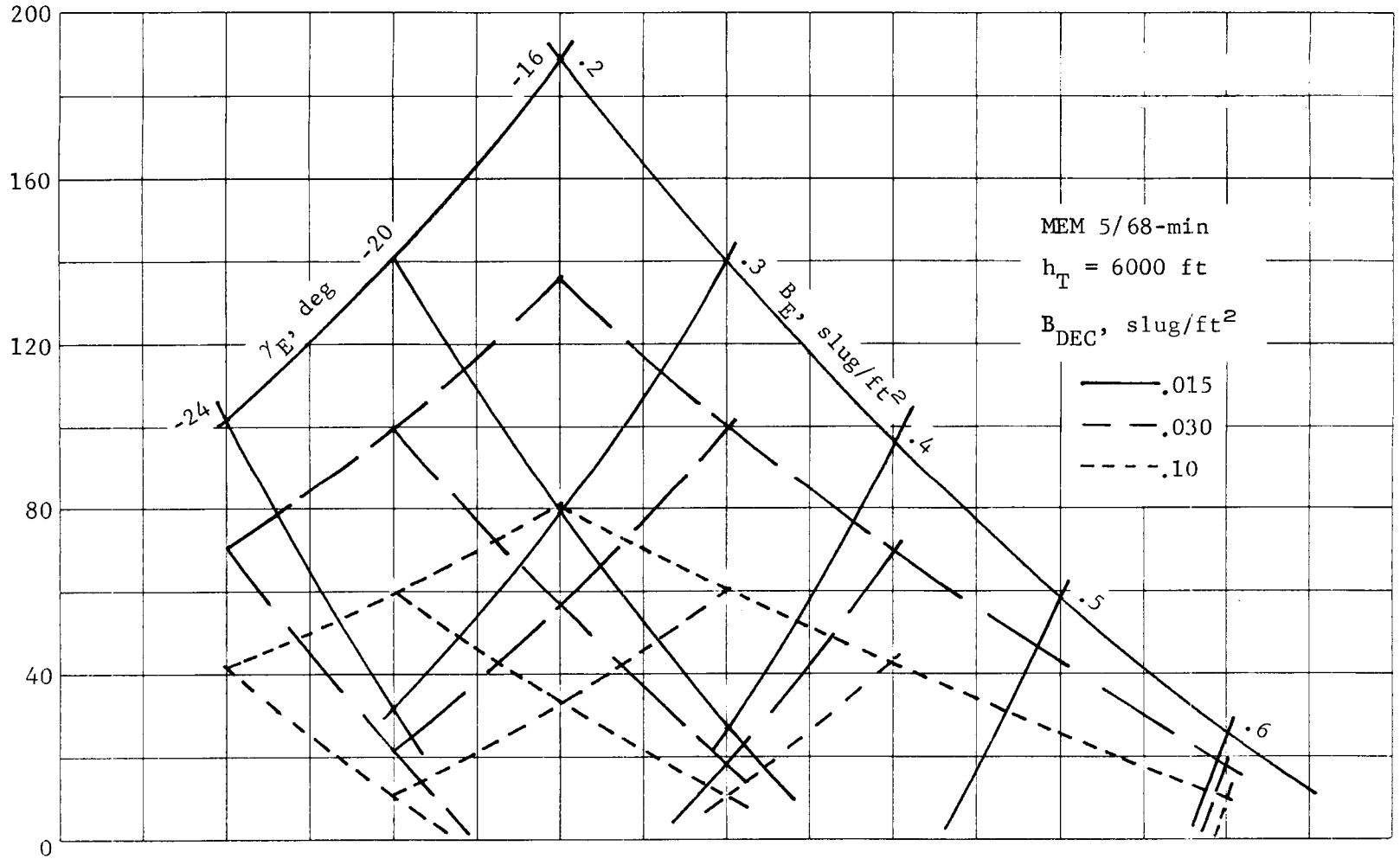

Figure 23.- Time on Parachute, Orbit Mode

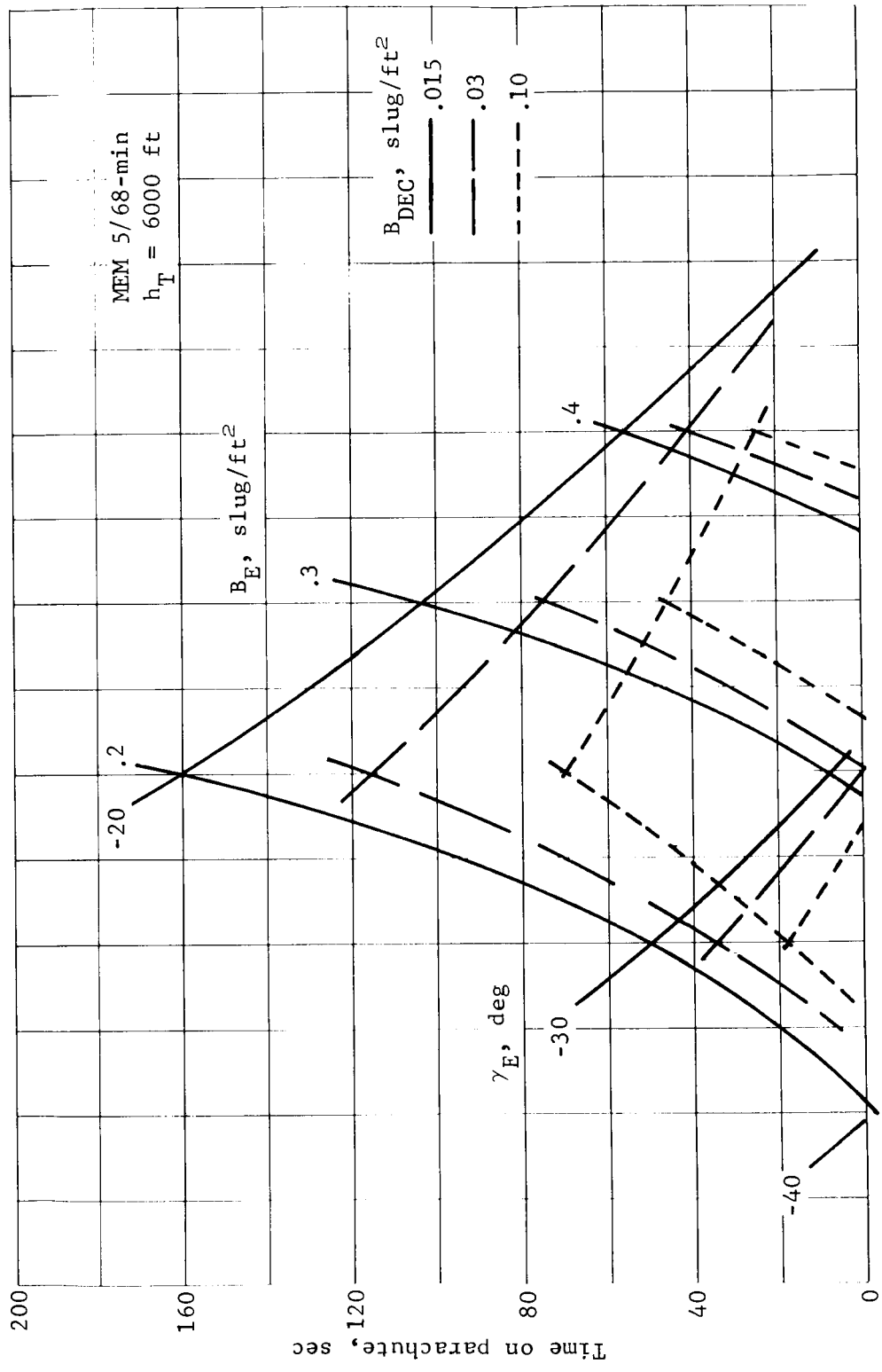

Figure 24.- Time on Parachute, Direct Mode

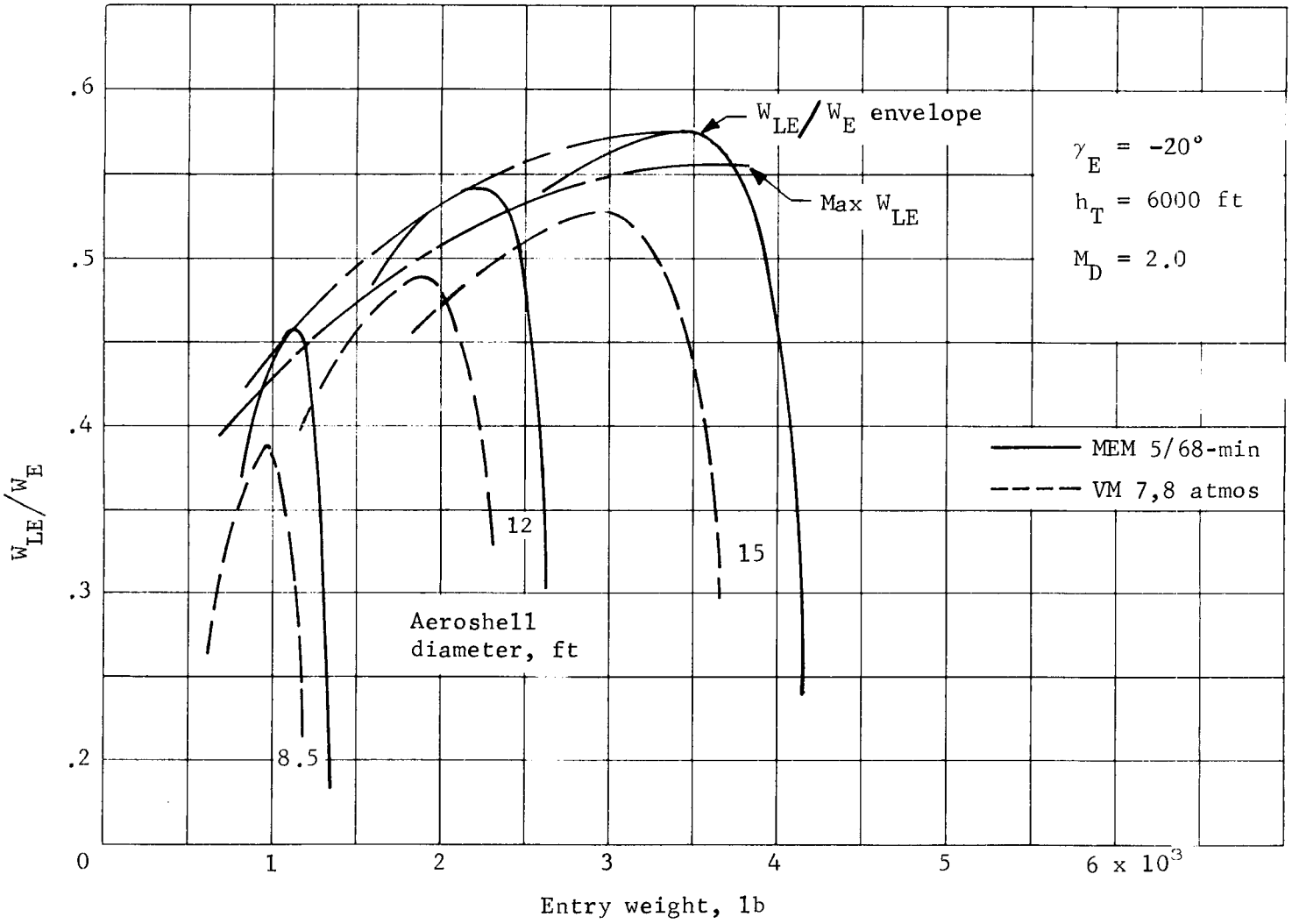

Figure 25.- Landed Weight Ratio vs Entry Weight, Orbit Mode

Those points maximizing W_{LE} for a given diameter aeroshell do so at the expense of higher entry weight. The data following are for the maximum W_{LE} or the maximum W_{LE}/W_E envelope. Maximum landed equipment weight always occurs at a higher entry weight than maximum landed weight ratio.

Heat shield ablator weights for direct entry depend on whether the flow is laminar or turbulent. In previous work (ref. 2) flow transition was assumed to occur at $B_E = 0.3$ for all conditions. However the transition B_E is actually a function of aeroshell diameter and entry flightpath angle. This is illustrated in figure 26 which shows the transition B_E that are used in this report. Values for VM-7, VM-8 are also calculated for comparison purposes. Weight curves were not faired as in reference 2; **rather**, an abrupt change in ablator weight is used at the transition B_E. This is illustrated in figure 27.

The maximum landed equipment and entry weights for the MEM 5/68-min atmosphere are shown in figure 28 thru 33 for orbital entry and terrain heights of 0, 3000, and 6000 ft. Some values using VM-7 and VM-8 atmospheres are superimposed for comparison. The new atmospheres in all cases yields greater landed equipment weights than the VM atmospheres for a given diameter. For example, in figure 32 at $\gamma_E = -16°$ for a 10-ft aeroshell, the landed equipment weight for the minimum atmosphere is 1350 lb $(W_E = 2475$ lb) compared with 940 lb $(W_E = 1910$ lb) for VM-7, VM-8. The MEM 5/68-min atmosphere also allows smaller aeroshells to be used for a given W_{LE}. From figure 32 for $W_{LE} = 1000$ lb and $\gamma_E = 16°$, the MEM 5/68-min atmosphere requires an aeroshell diameter of 8.8 ft; the VM-7, VM-8 atmospheres require a 10.2-ft-diameter aeroshell. Corresponding entry weights are 1900 and 1970 lb, a small variation. Note also, that the new atmosphere permits a greater dispersion in entry angle to obtain a given $W_{LE} - D_{A/S}$ combination. It should be pointed out that the VM-7, VM-8 data shown for comparison are based on a $V_E = 4.5$ km/sec (14 760 fps). Thus, the improvement shown by the MEM 5/68-min atmosphere results $(V_E = 16\ 000$ fps) is slightly conservative; a slightly larger improvement might be expected using equal entry velocities. The effect of terrain height shown in figure 34 for orbital entry, is

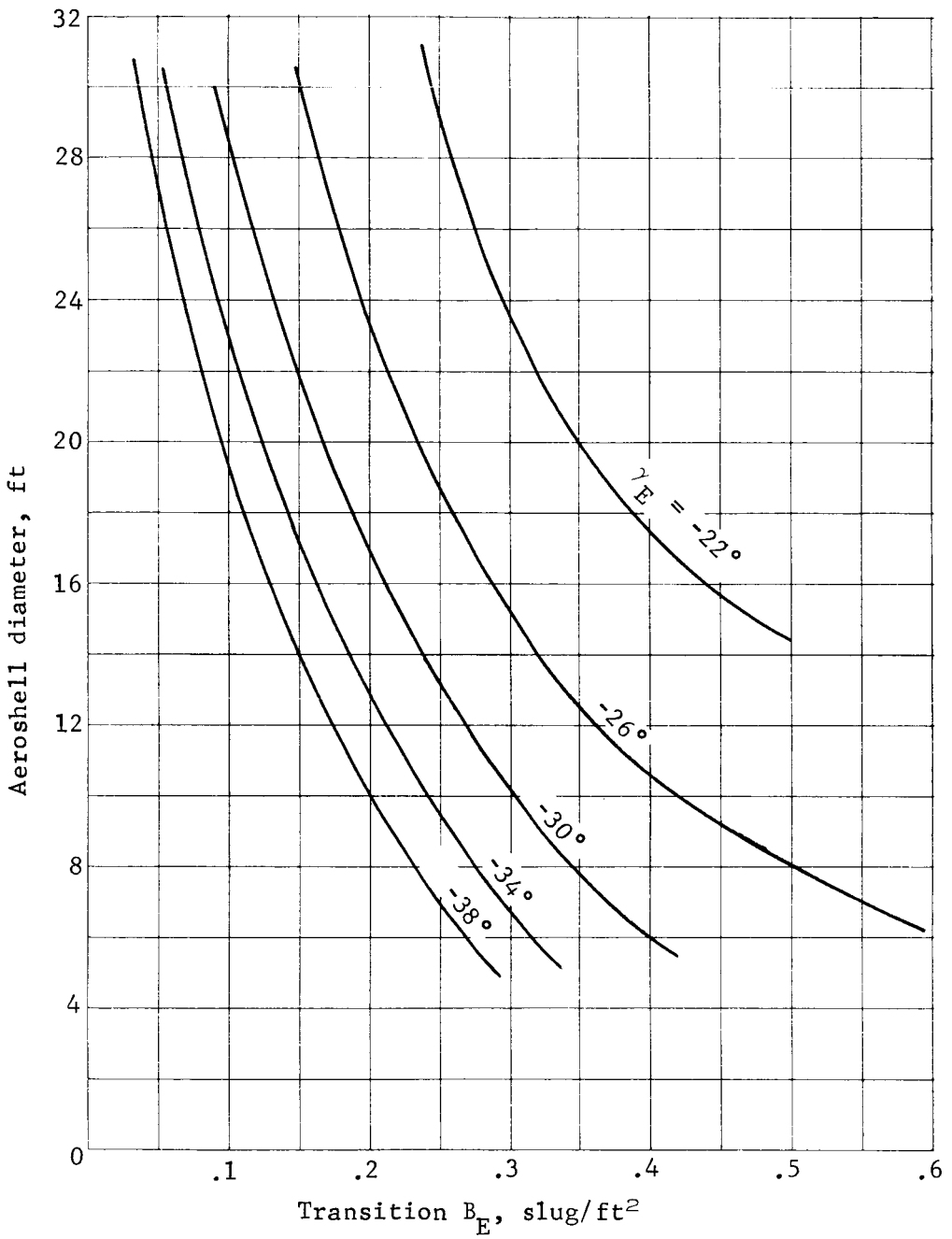

Figure 26.- Transition Ballistic Coefficient, Direct Entry

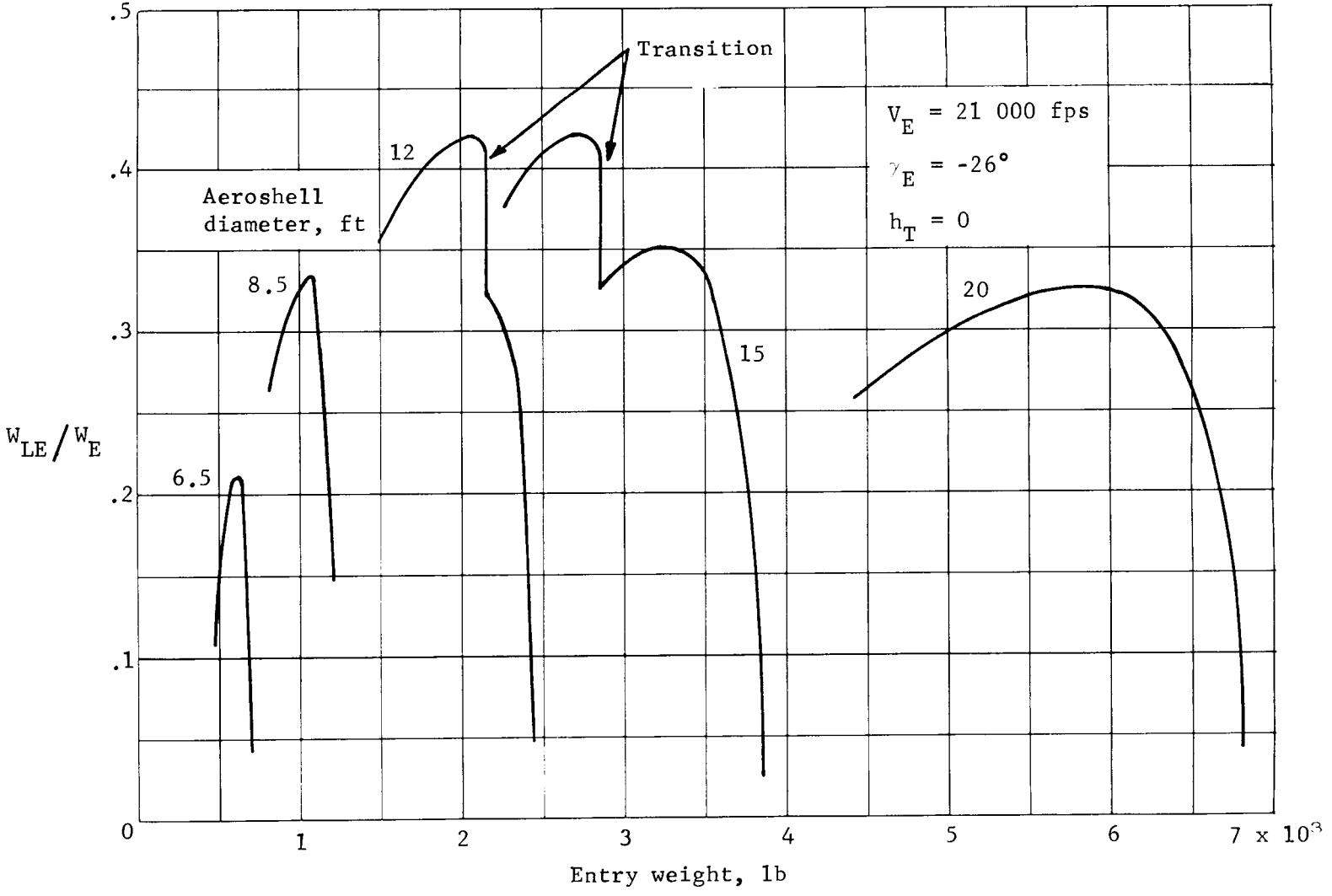

Figure 27.- Effect of Transition Ablator Weights, Direct Mode

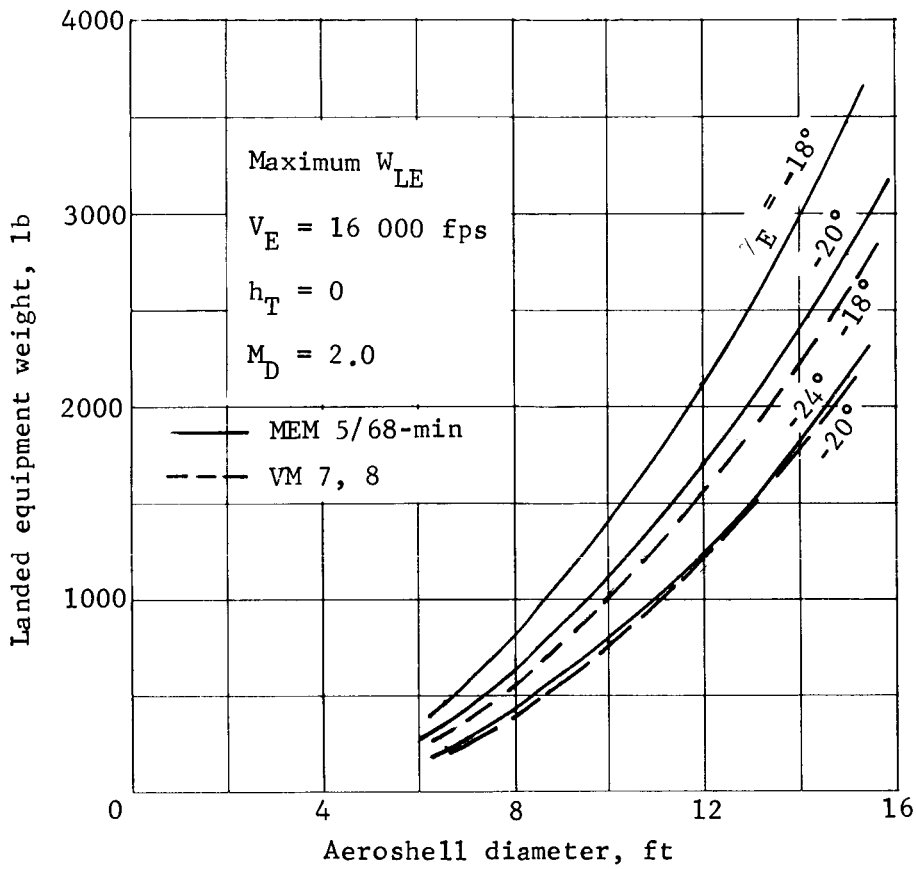

Figure 28.- W_{LE} vs Aeroshell Diameter, Orbit Mode

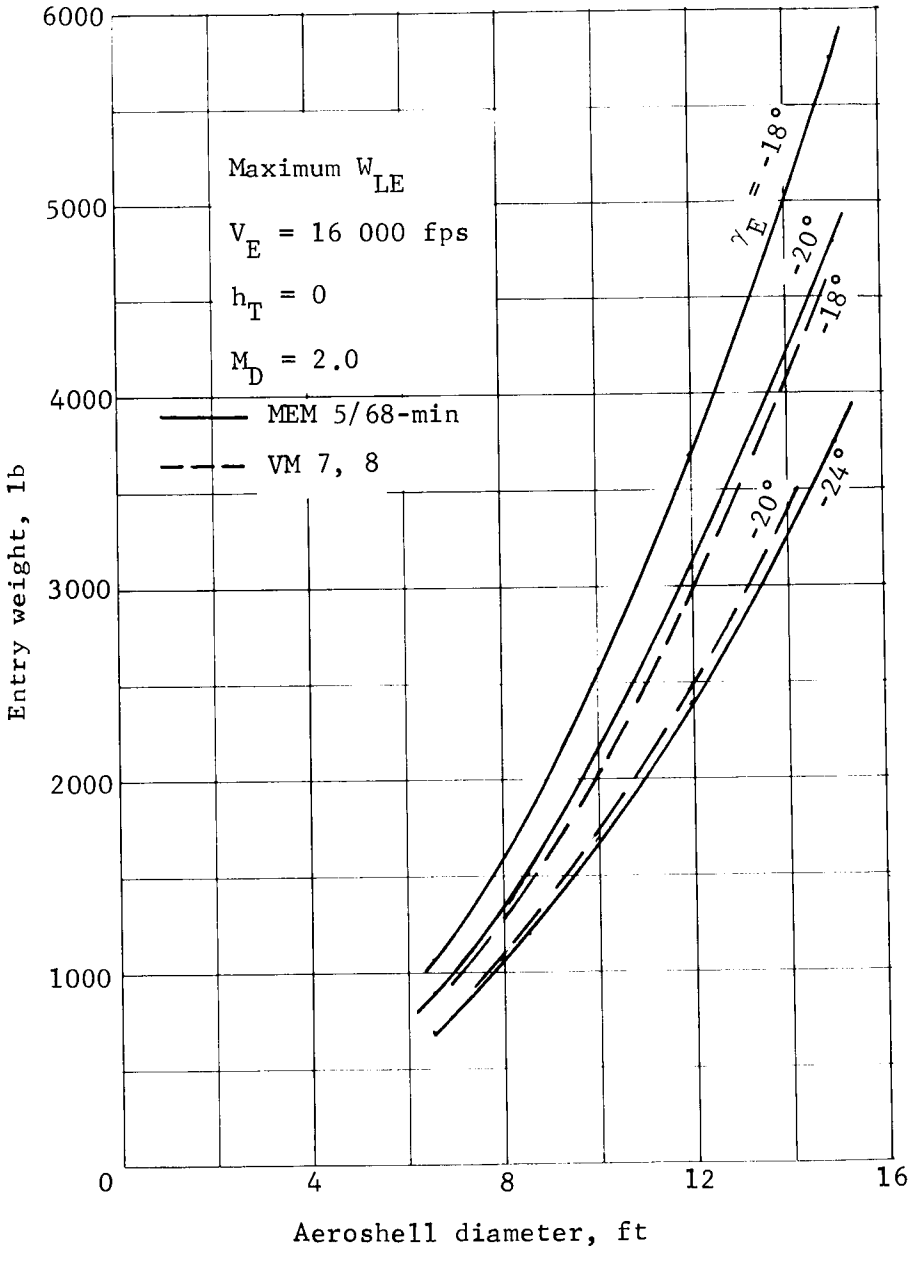

Figure 29.- W_E vs Aeroshell Diameter, Orbit Mode

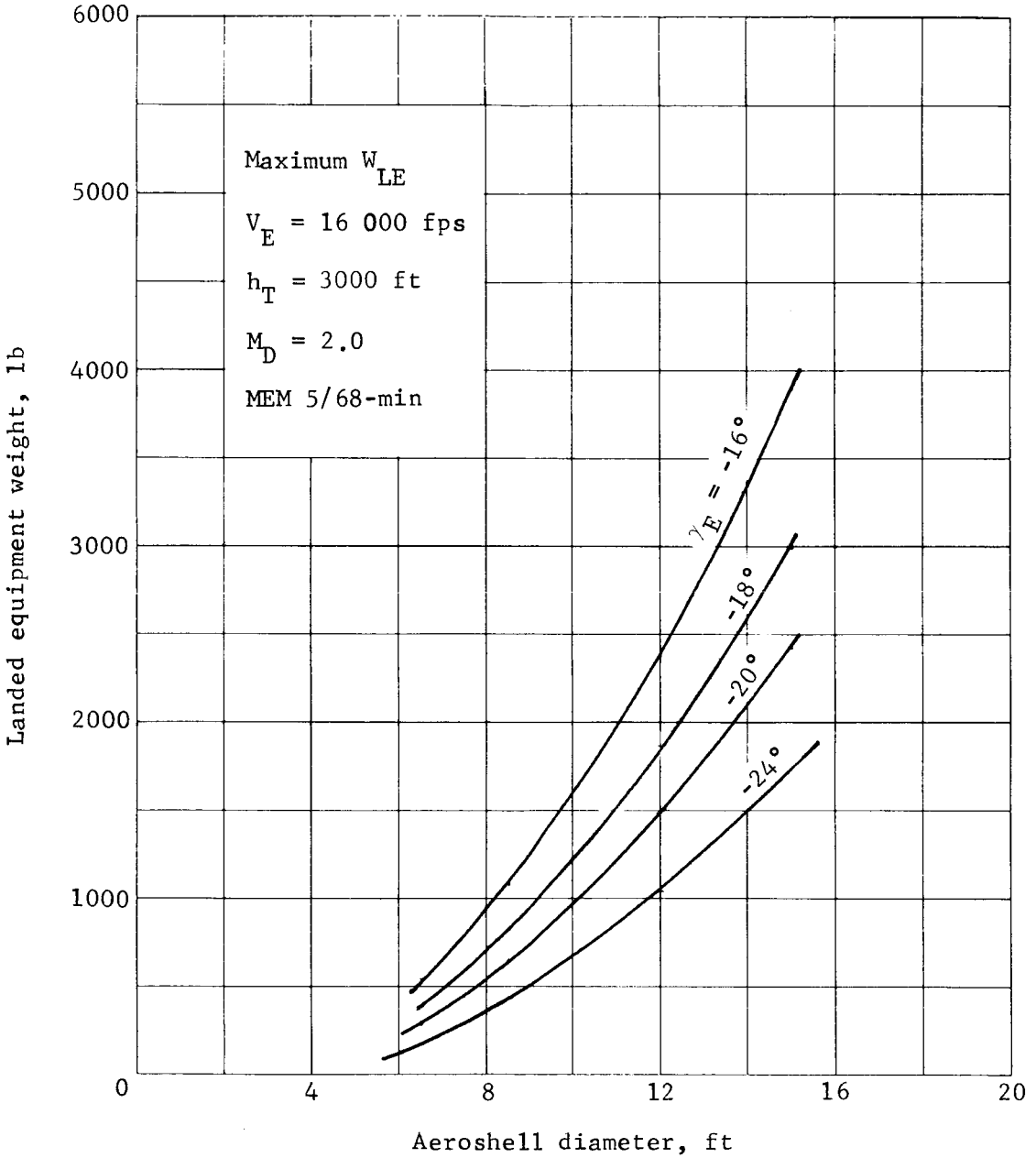

Figure 30.- W_{LE} vs Aeroshell Diameter, Orbit Mode

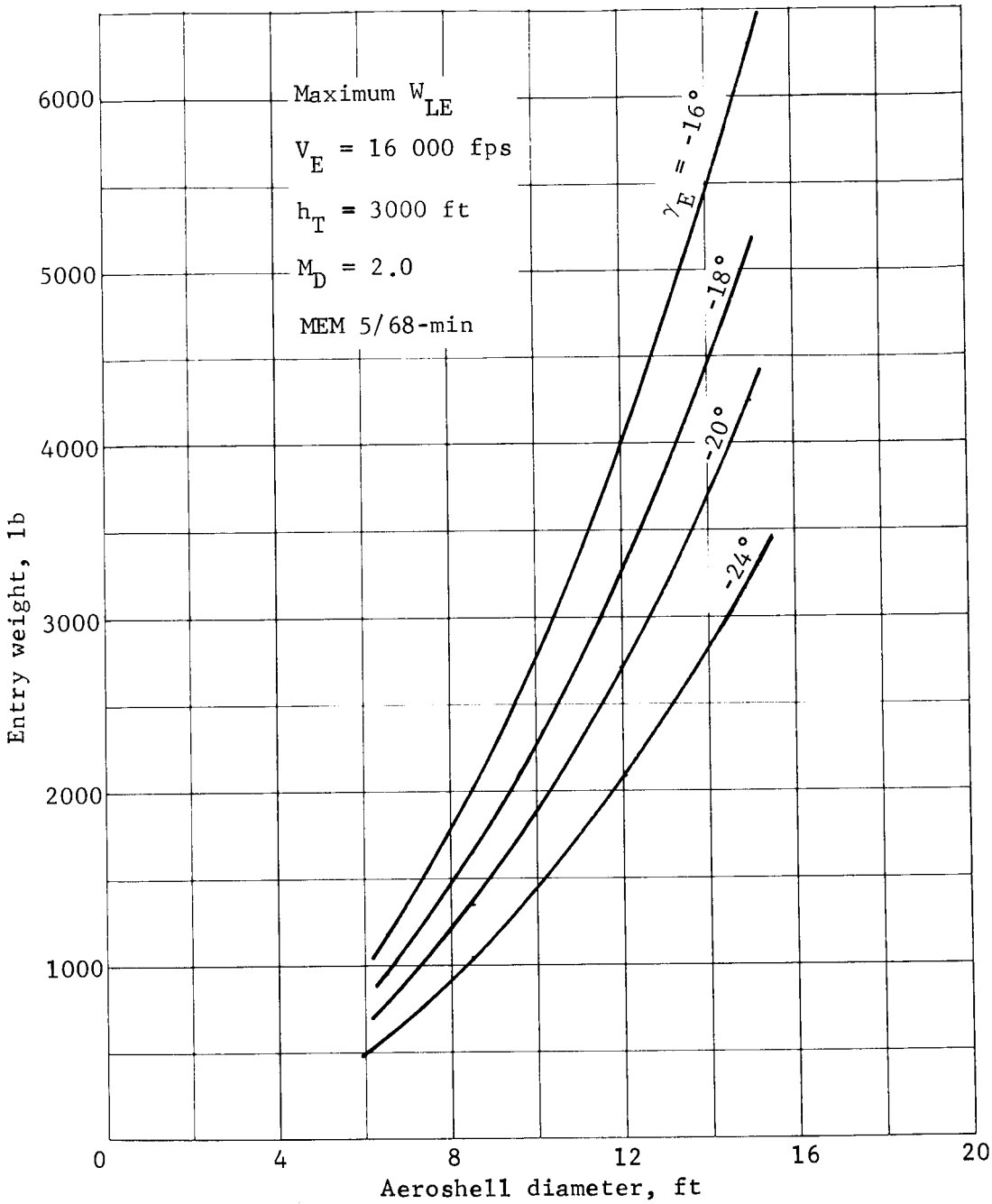

Figure 31.- W_E vs Aeroshell Diameter, Orbit Mode

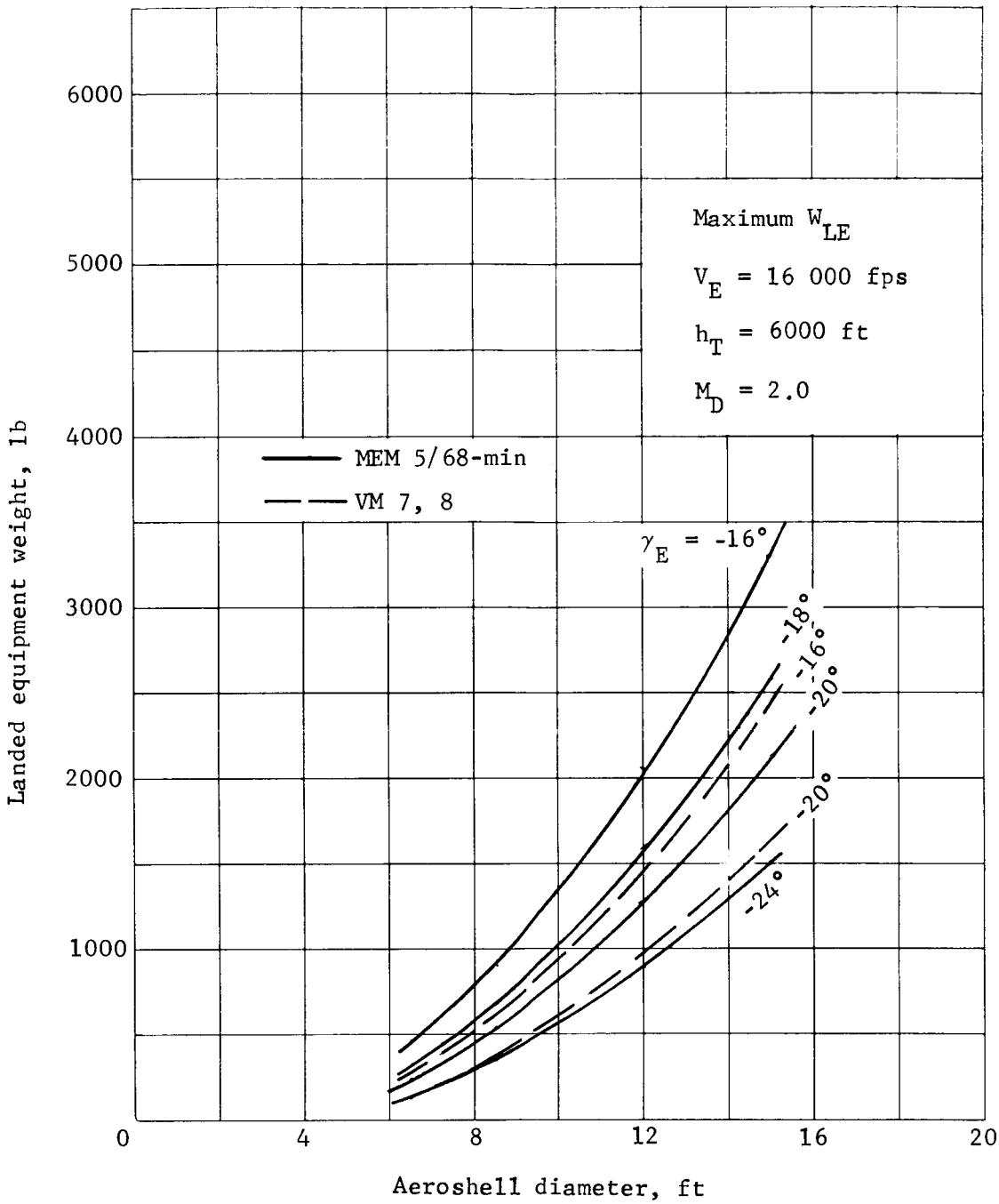

Figure 32.- W_{LE} vs Aeroshell Diameter, Orbit Mode

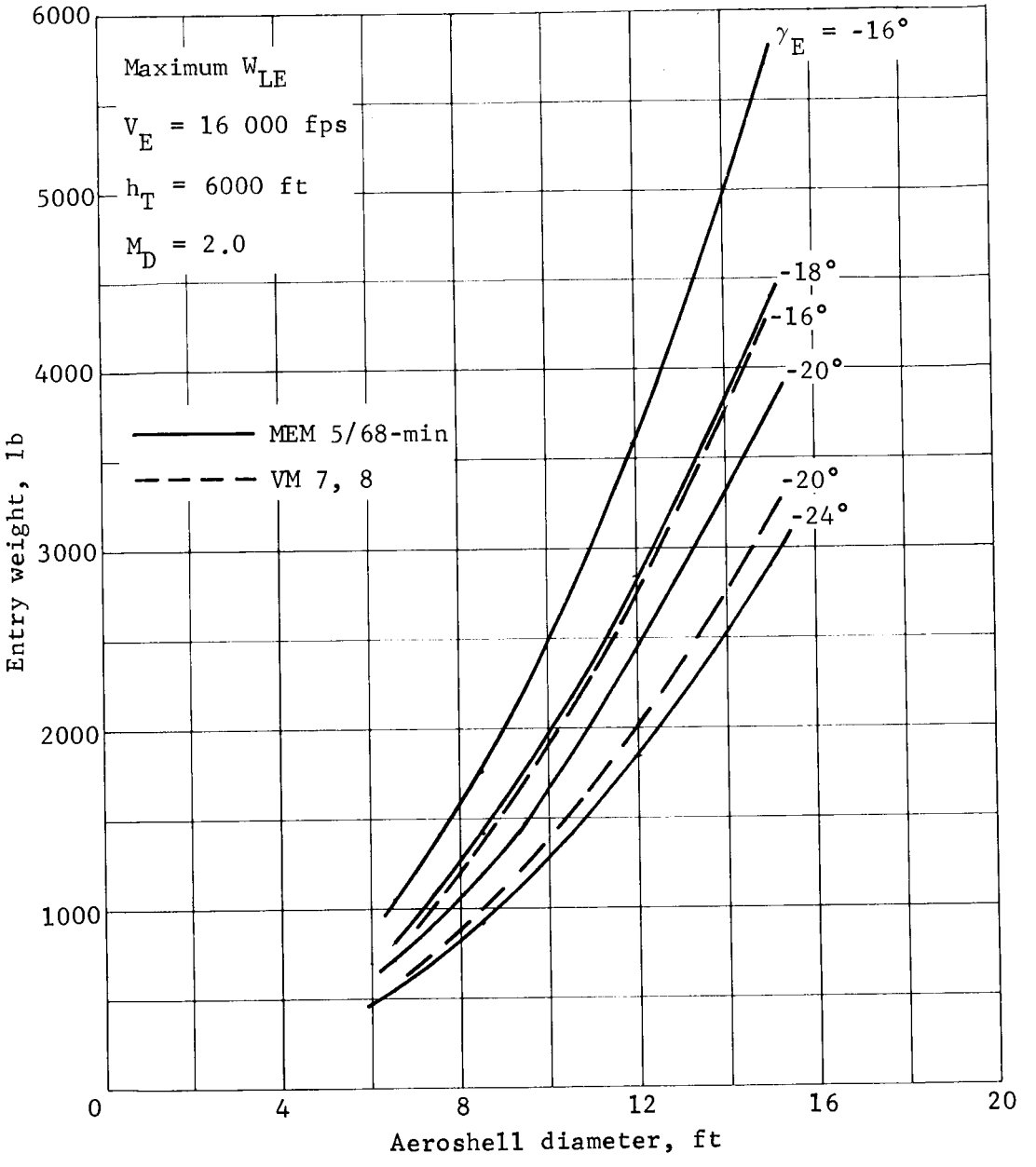

Figure 33.- W_E vs Aeroshell Diameter, Orbit Mode

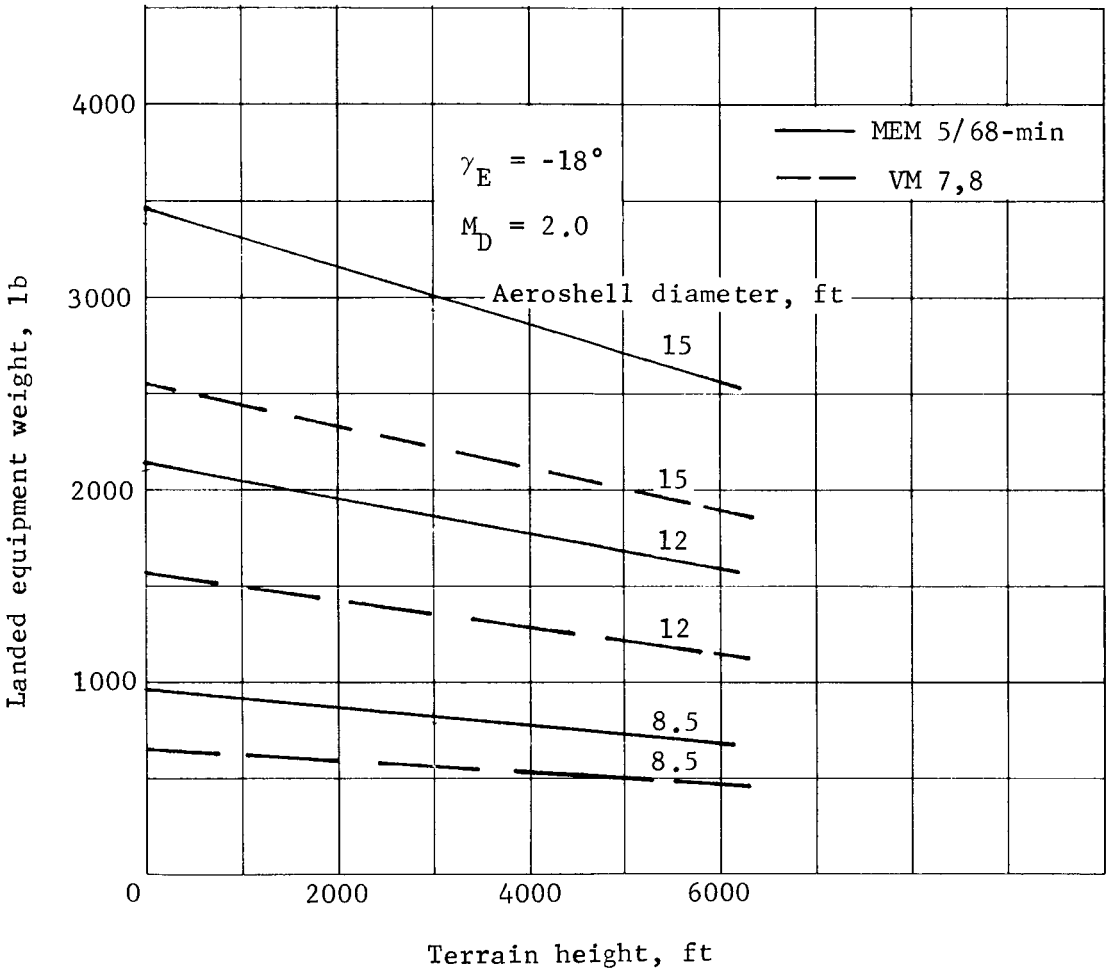

Figure 34.- Effect of Terrain Height, Orbit Mode

essentially linear. Plots of maximum landed equipment weight and entry weight for the VM-7 and VM-8 atmospheres for direct entry are shown in figures 35 thru 38. Minimum atmosphere plots for direct entry are shown in figures 39 thru 44. The irregularity in the curves is caused by a change in ablator weights at flow transition illustrated previously in figure 26. The results show the same trends as for the orbit mode.

W_{LE} and W_E are summarized in figures 45 thru 52 for both modes. The figures are in such form that interpolations may be made readily. Some VM-7, VM-8 points are also shown in these figures for reference.

Landed equipment weight and entry weight for the landed weight ratio envelope are shown in figures 53 thru 60. These data may be used for design when entry weight rather than aeroshell diameter is the limiting design parameter.

The figures in this section are plotted for constant entry flightpath angles. They show that increasing γ_E will decrease the landed equipment weight for a particular B_E. This holds true for nearly every point for direct and orbital modes.

Several point designs are evaluated to determine the effect of atmosphere uncertainty on terrain height capability. These points are for landed equipment weights of 600 lb, orbital mode, and nominal $\gamma_E = -16°$ and maximum $\gamma_E = -18°$. Design conditions are for both maximum W_{LE} and W_{LE}/W_E envelope. Parachute deployment is at $M \leq 2.0$ in two atmospheres, MEM 5/68-min and -mean. The design points and calculated final altitudes on the parachute are given in table 3.

TABLE 3.- DESIGN POINTS AND CALCULATED FINAL ALTITUDES ON THE PARACHUTE

						MEM 5/68-min atmosphere, ft			MEM 5/68-mean atmosphere, ft			
Design condition	γ_E, deg	$D_{A/S}$, ft	W_E, lb	B_E	B_{DEC}	$h_{D\ M=2}$	h_F	h_t	$h_{M=2}$	h_D	h_f	h_t
W_{LE}/W_E	16	7.5	1220	0.523	0.051	17 000	10 000	6000	42 490	32 800	25 800	21 800
W_{LE}/W_E	18	8.4	1240	0.423	0.053	17 000	10 000	6000	43 300	31 700	24 700	20 700
W_{LE}	16	7.2	1280	0.595	0.025	14 000	10 000	6000	37 730	30 000	26 000	22 000
W_{LE}	18	8.1	1300	0.478	0.024	14 000	10 000	6000	38 760	30 000	26 000	22 000

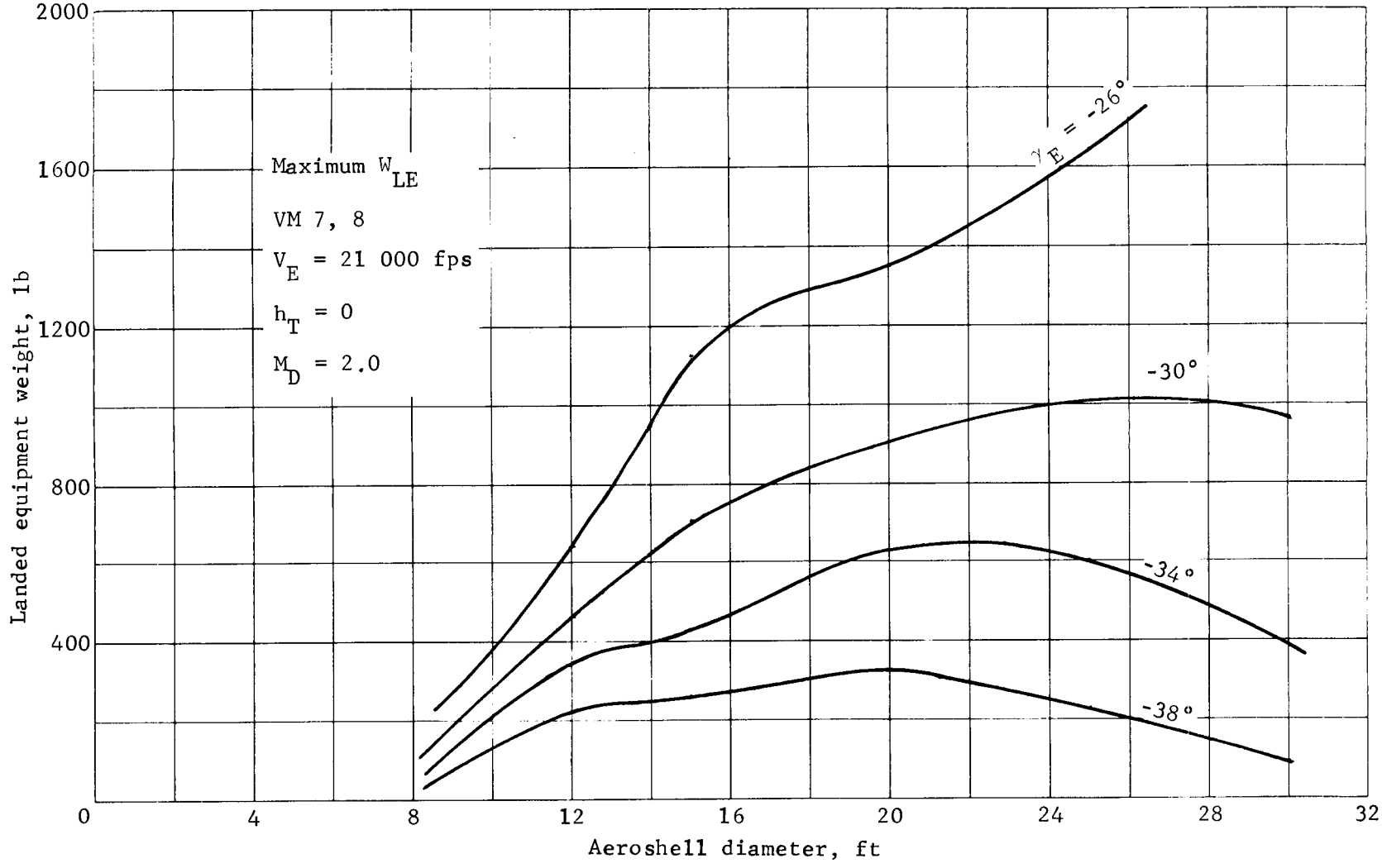

Figure 35.- W_{LE} vs Aeroshell Diameter, Direct Mode

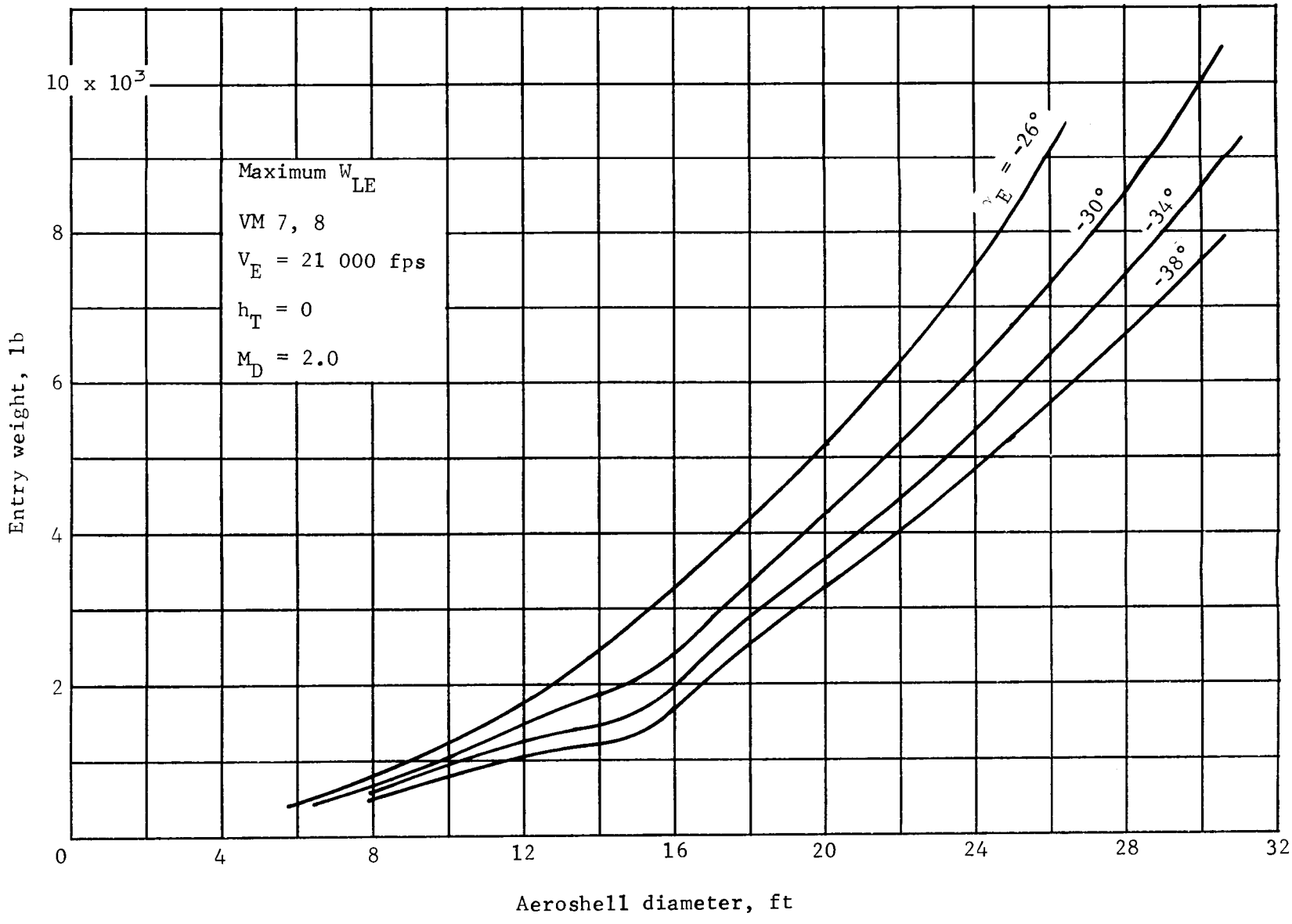

Figure 36.- W_E vs Aeroshell Diameter, Direct Mode

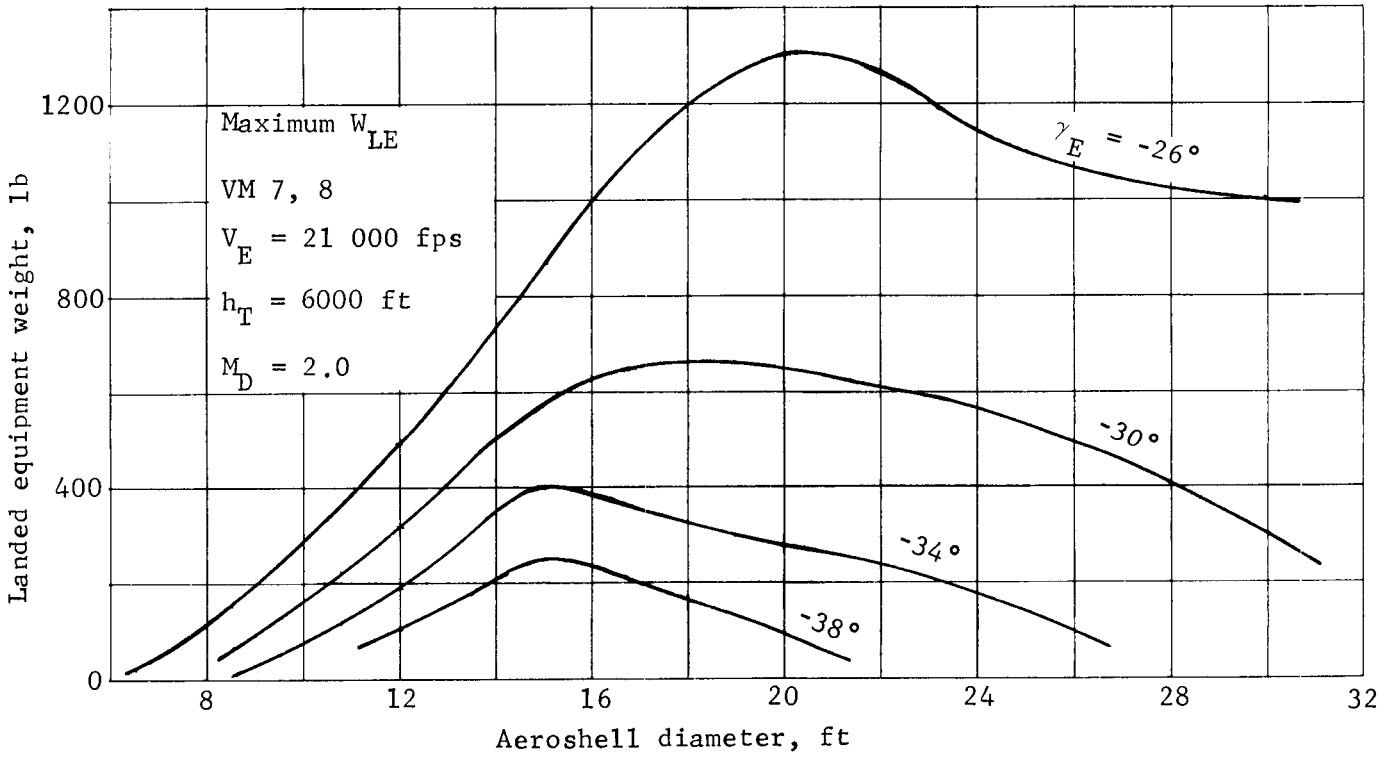

Figure 37.- W_{LE} vs Aeroshell Diameter, Direct Mode

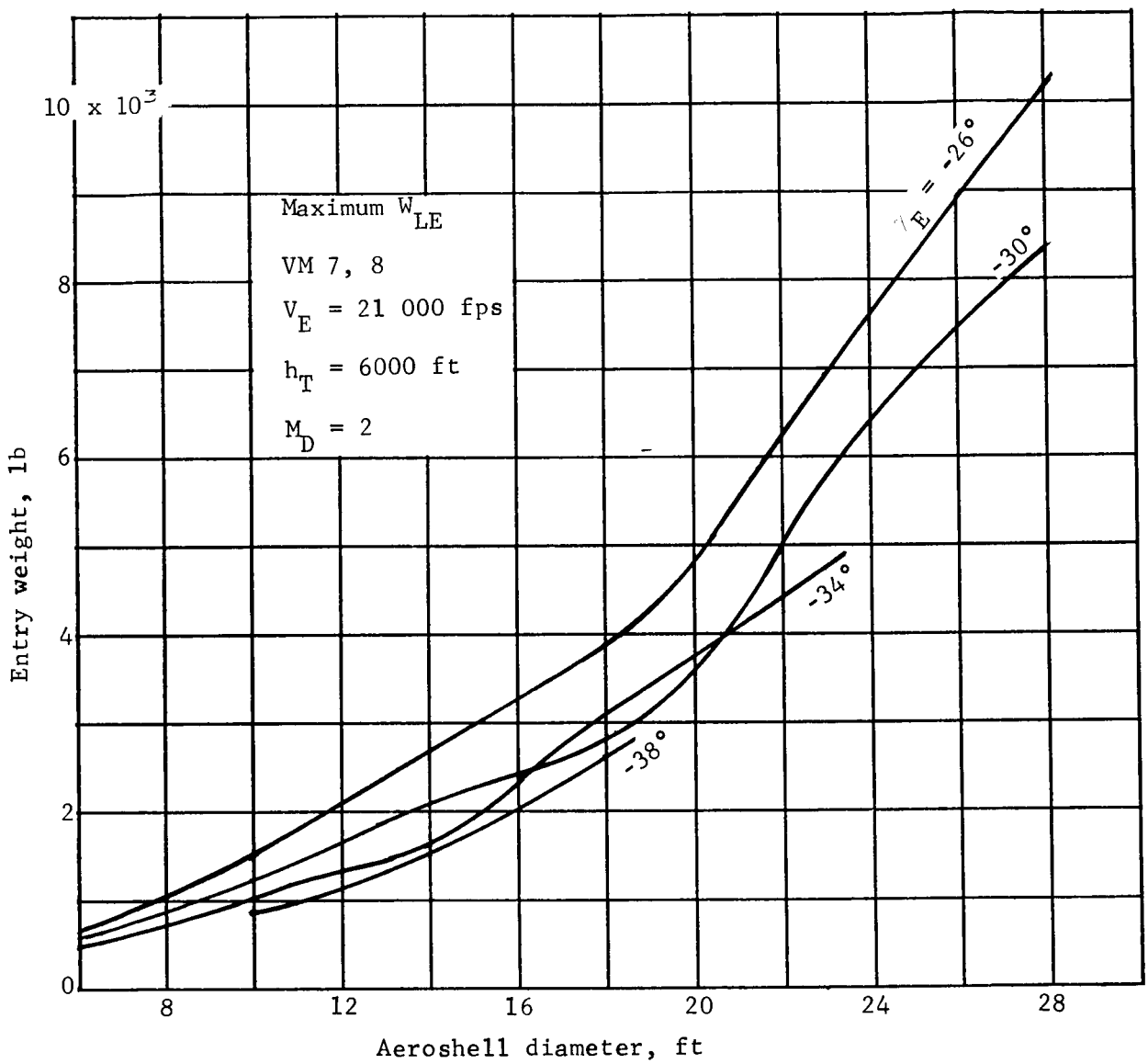

Figure 38.- W_E vs Aeroshell Diameter, Direct Mode

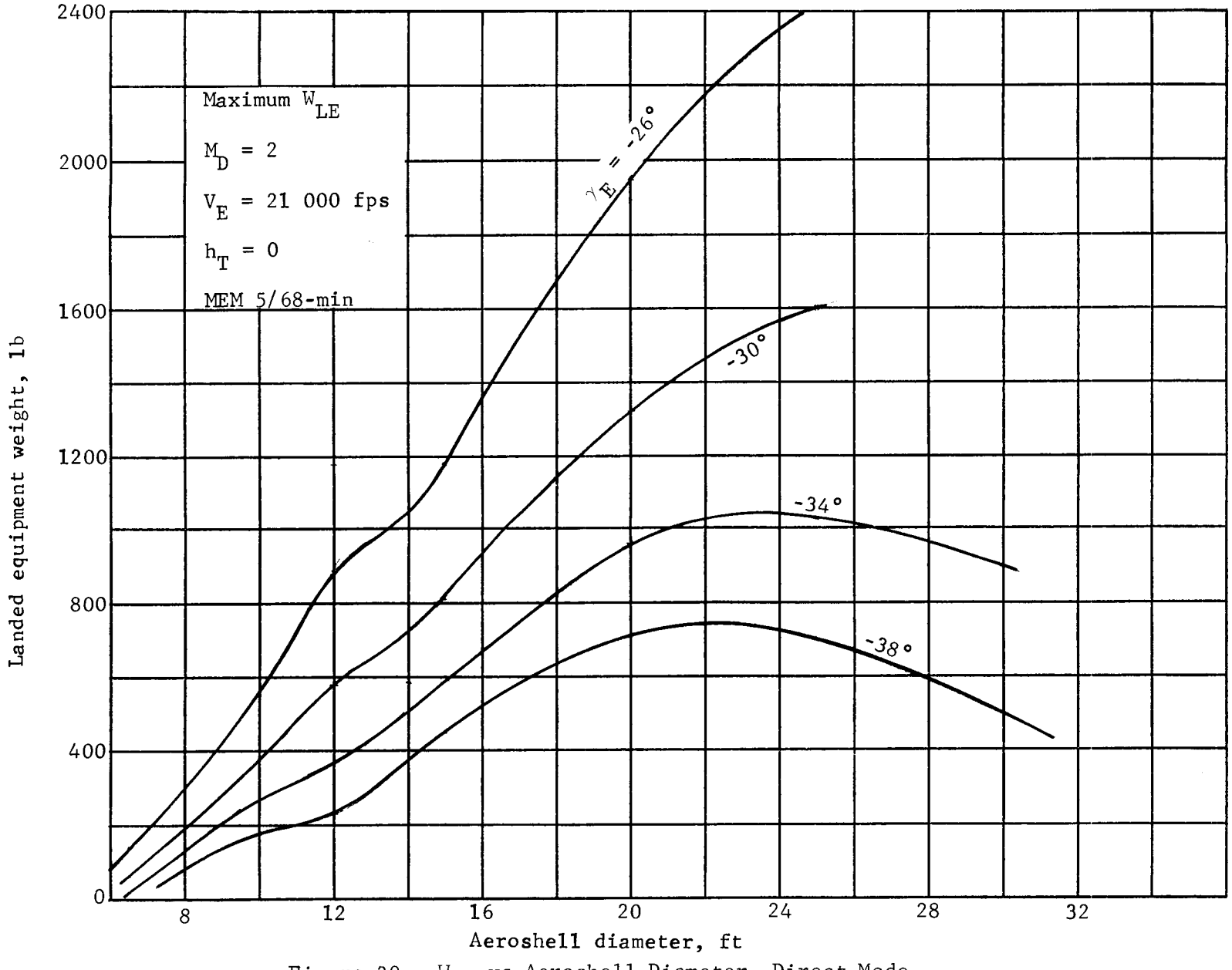

Figure 39.- W_{LE} vs Aeroshell Diameter, Direct Mode

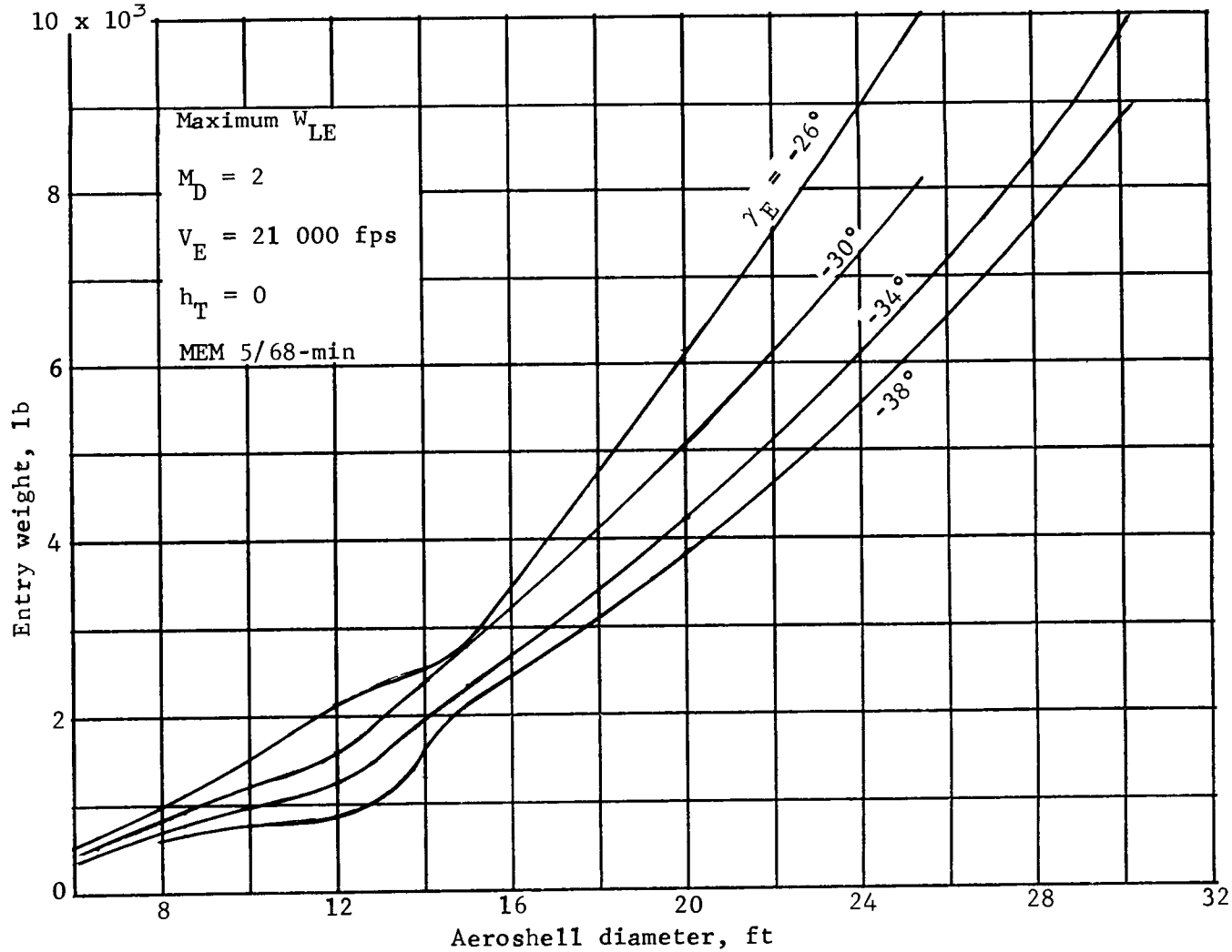

Figure 40.- W_E vs Aeroshell Diameter, Direct Mode

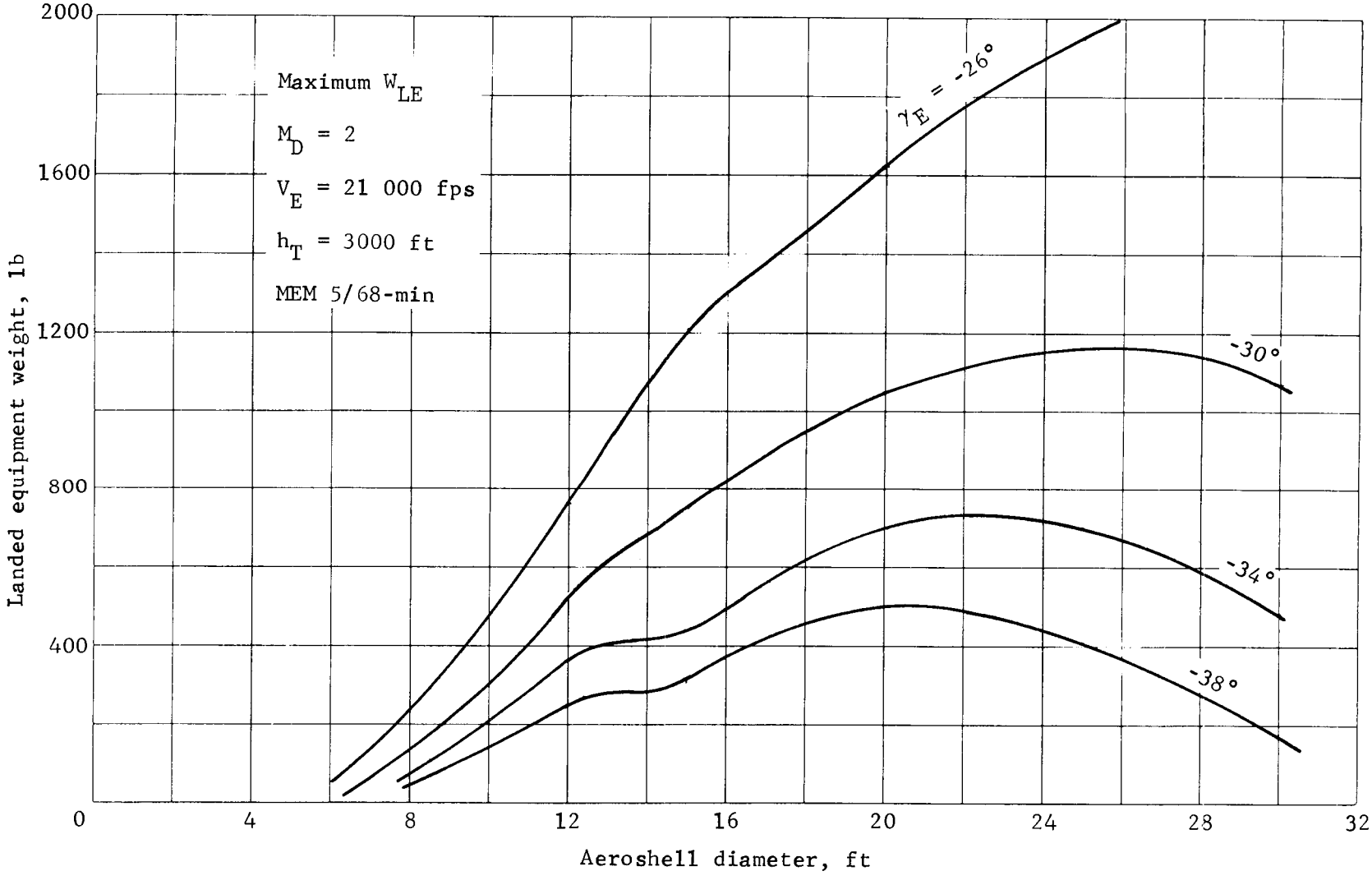

Figure 41.- W_{LE} vs Aeroshell Diameter, Direct Mode

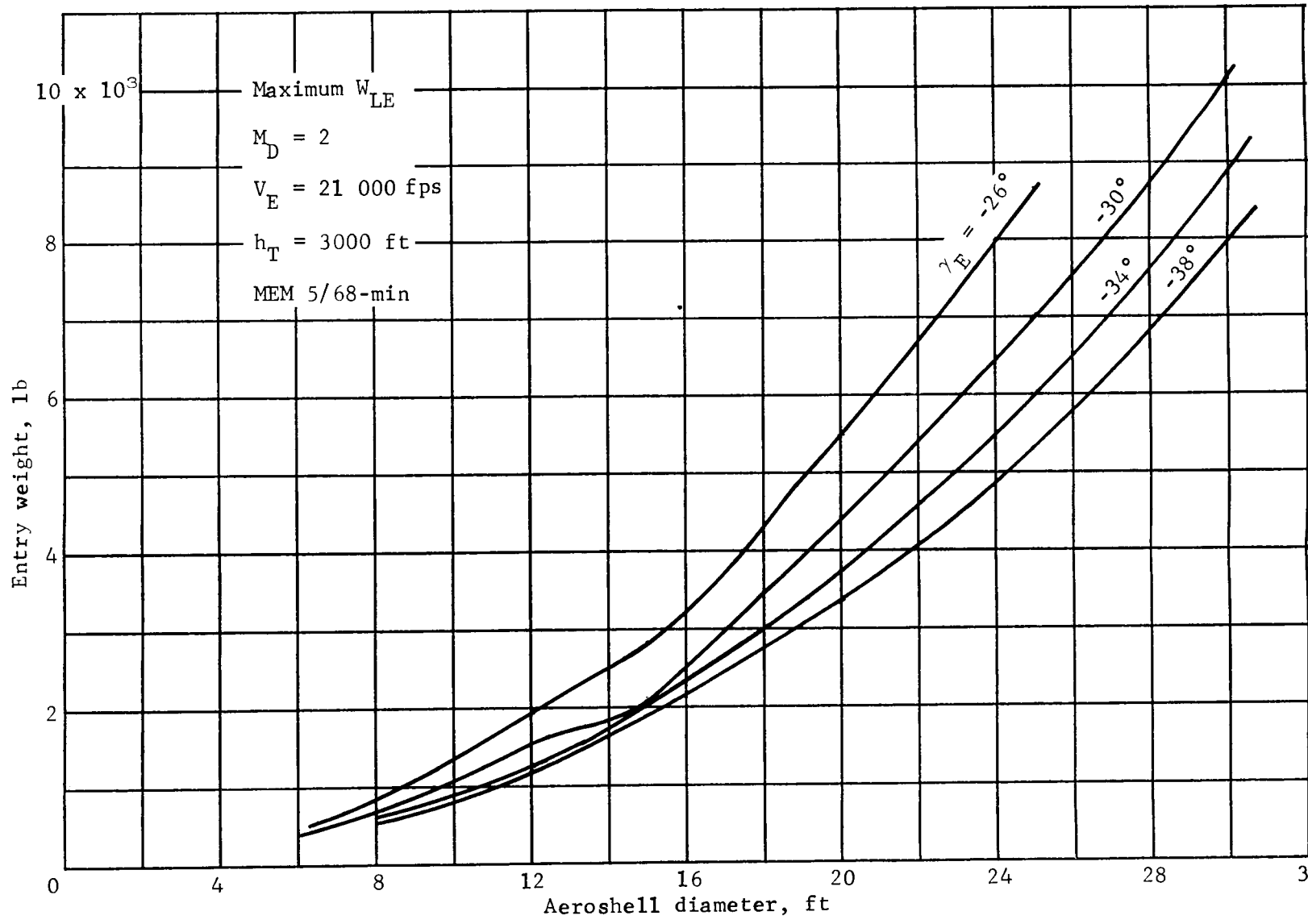

Figure 42.- W_E vs Aeroshell Diameter, Direct Mode

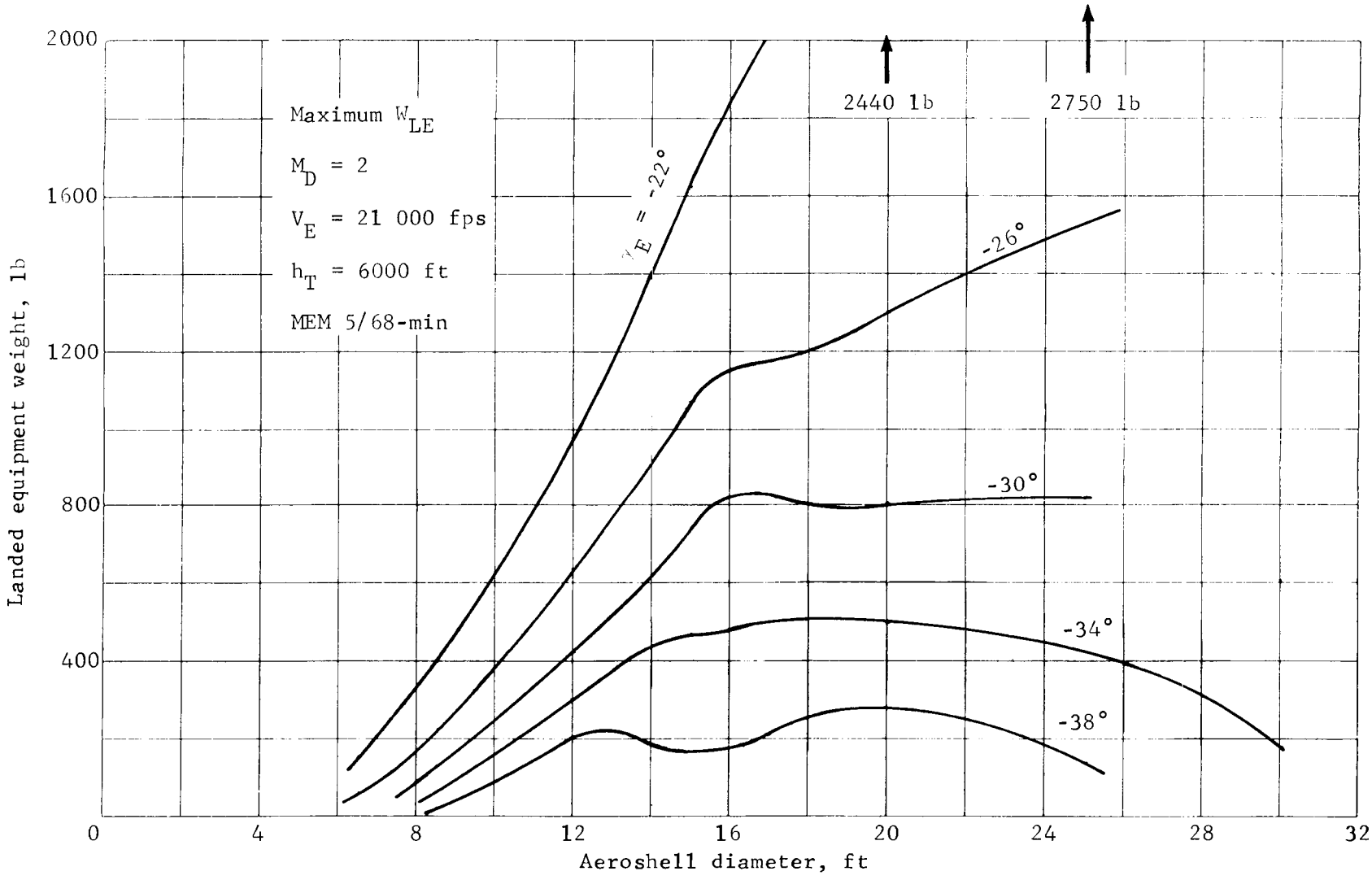

Figure 43.- W_{LE} vs Aeroshell Diameter, Direct Mode

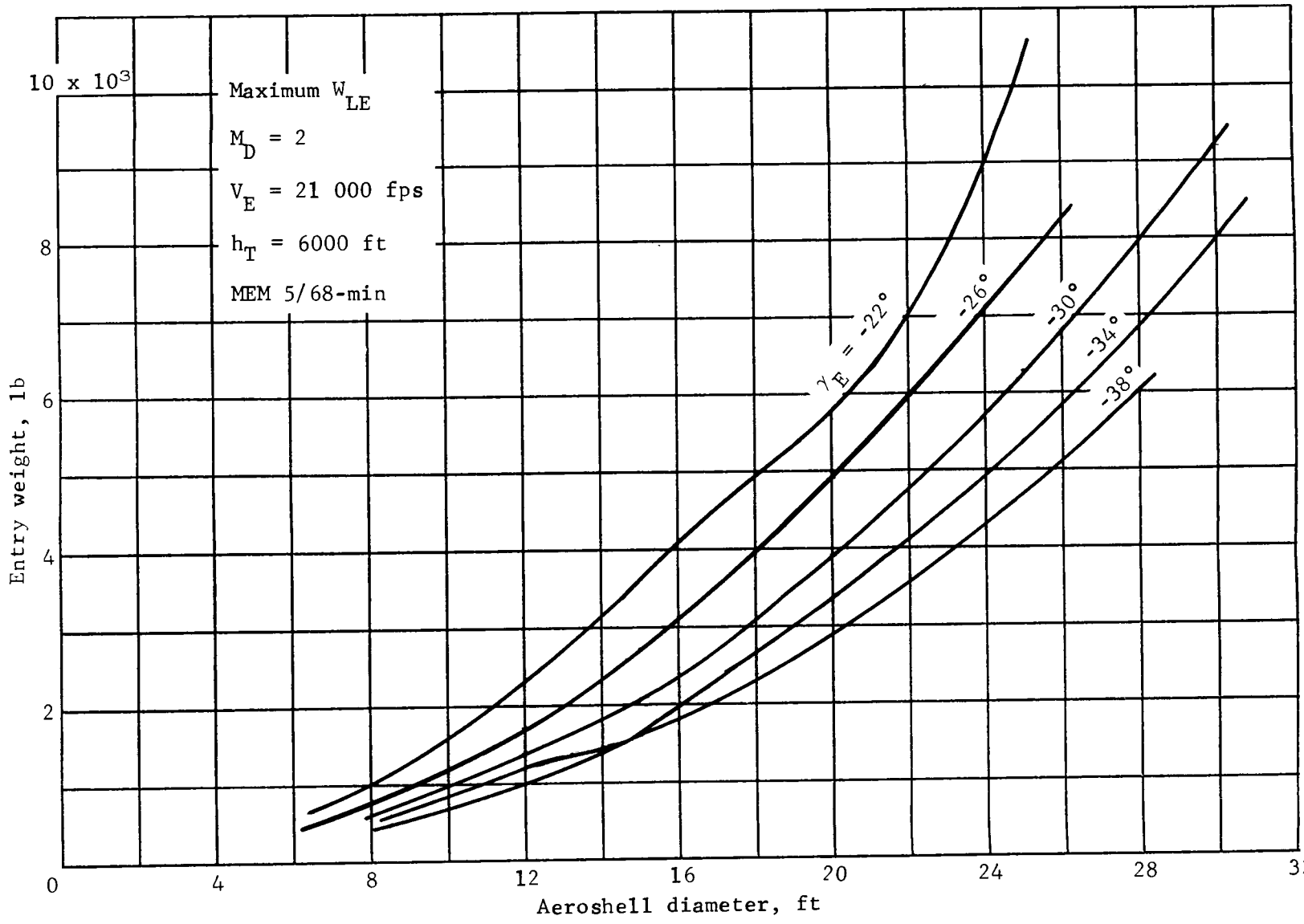

Figure 44.- W_E vs Aeroshell Diameter, Direct Mode

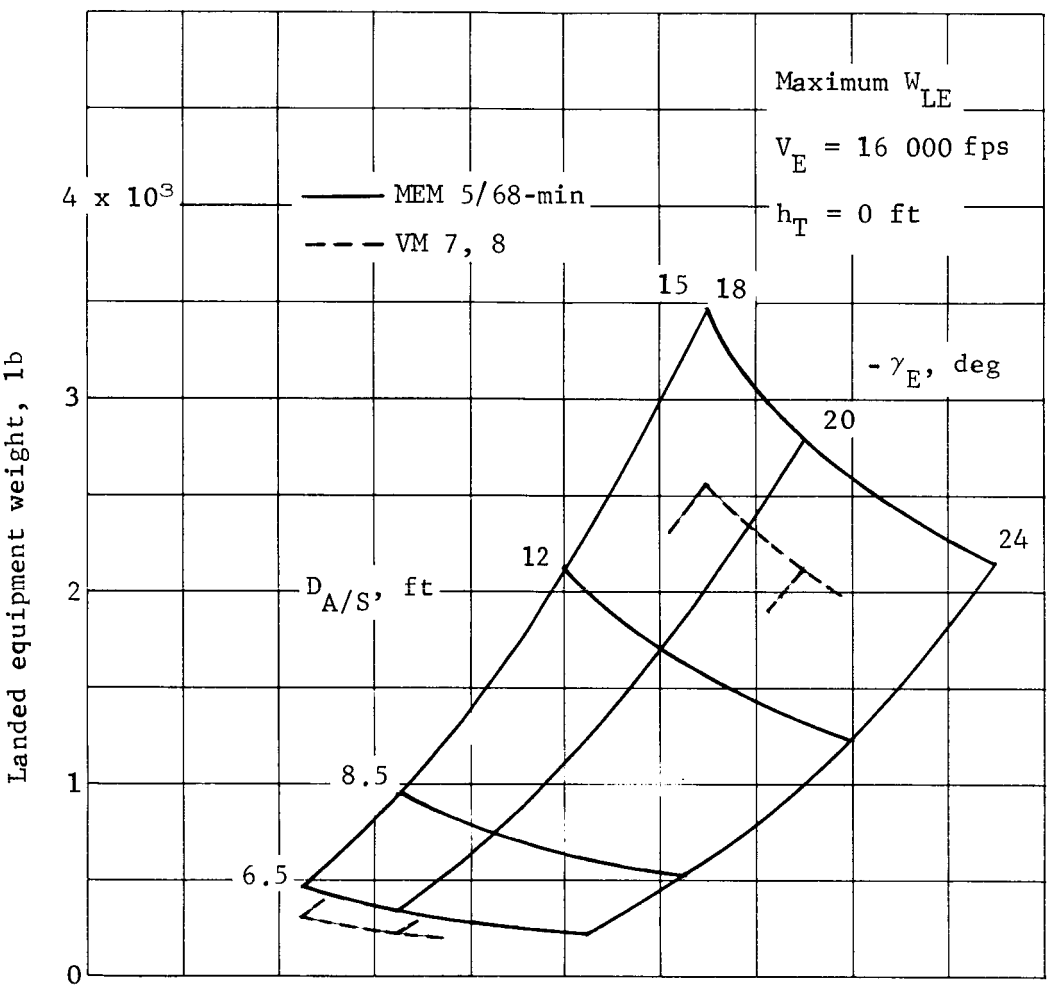

Figure 45.- Landed Equipment Weight, Orbit Mode

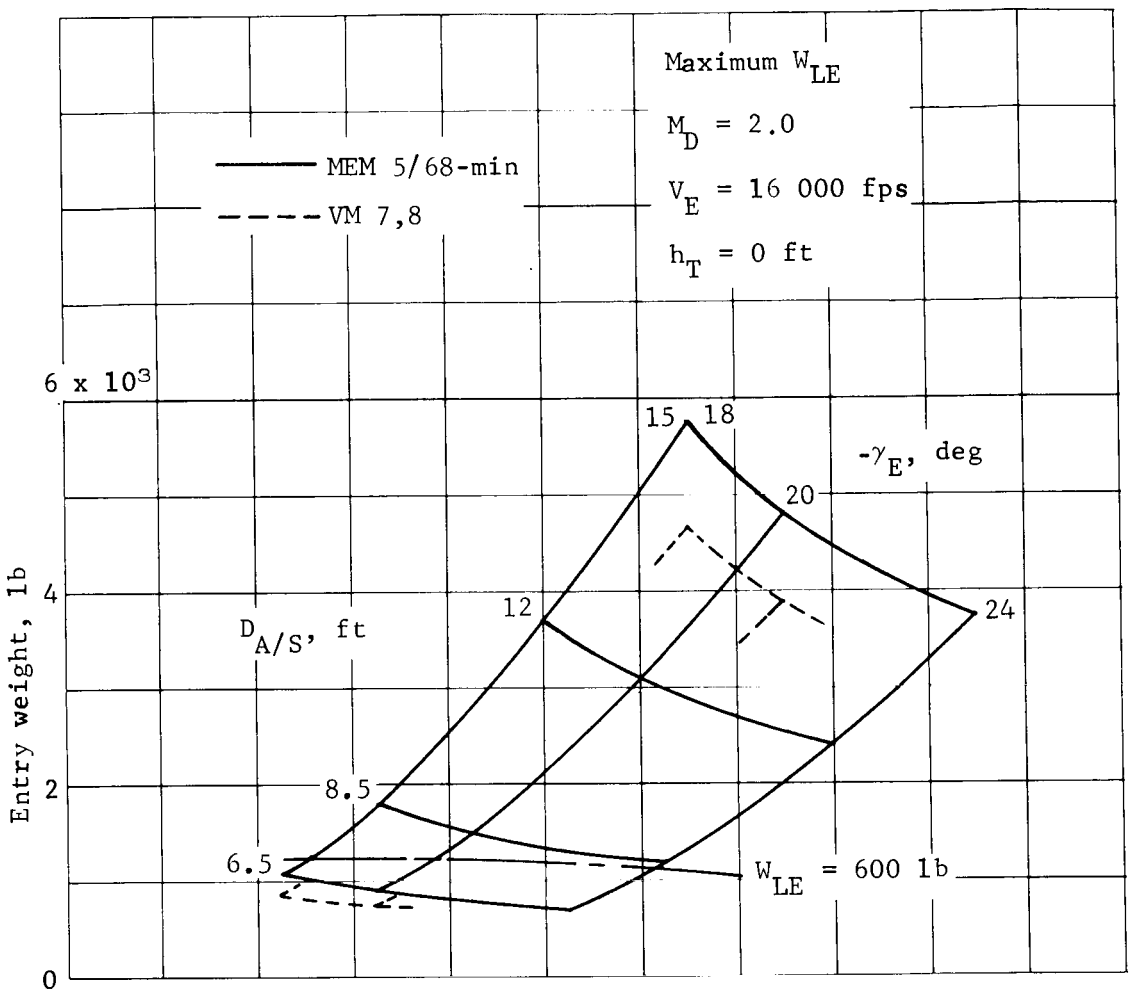

Figure 46.- Entry Weight, Orbit Mode

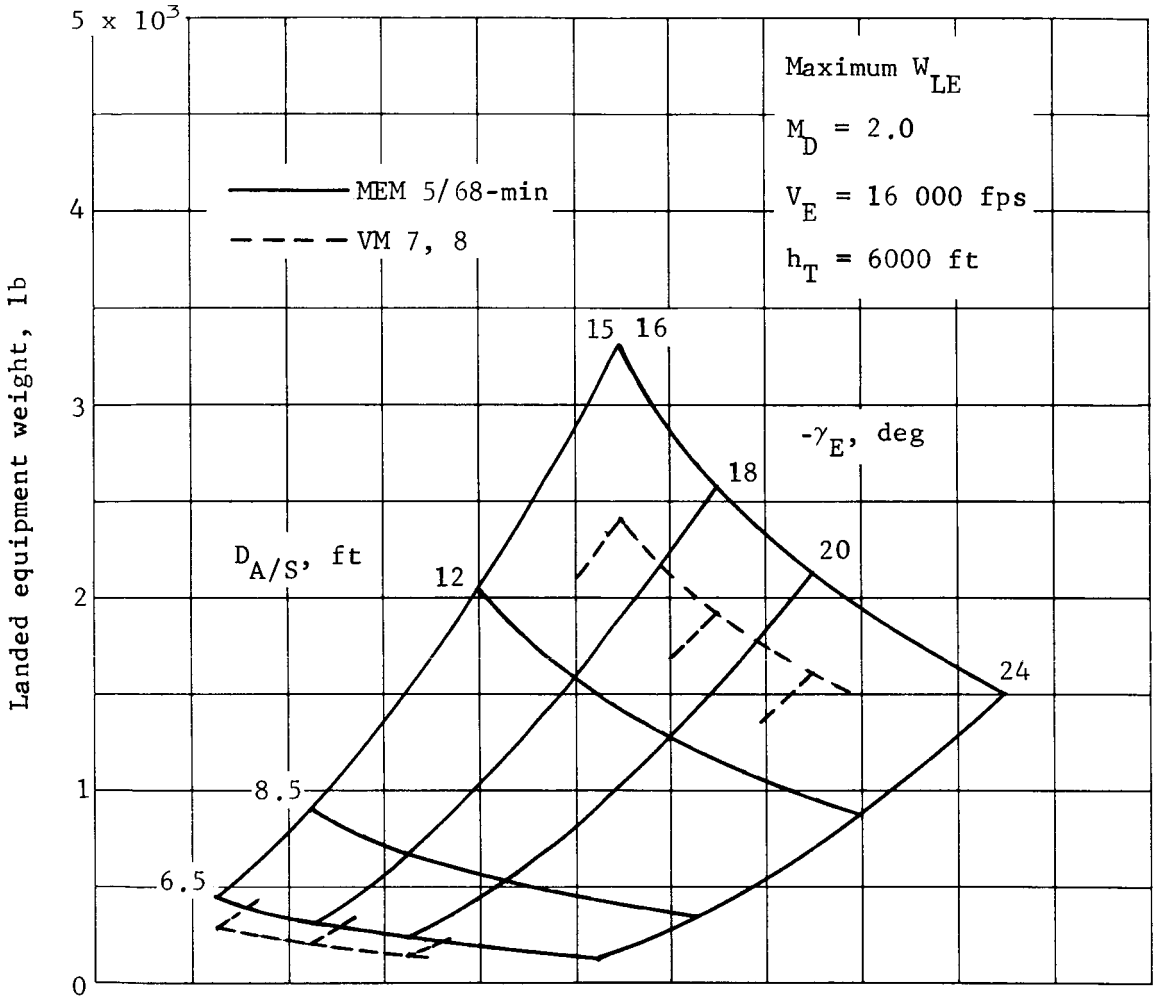

Figure 47.- Landed Equipment Weight, Orbit Mode

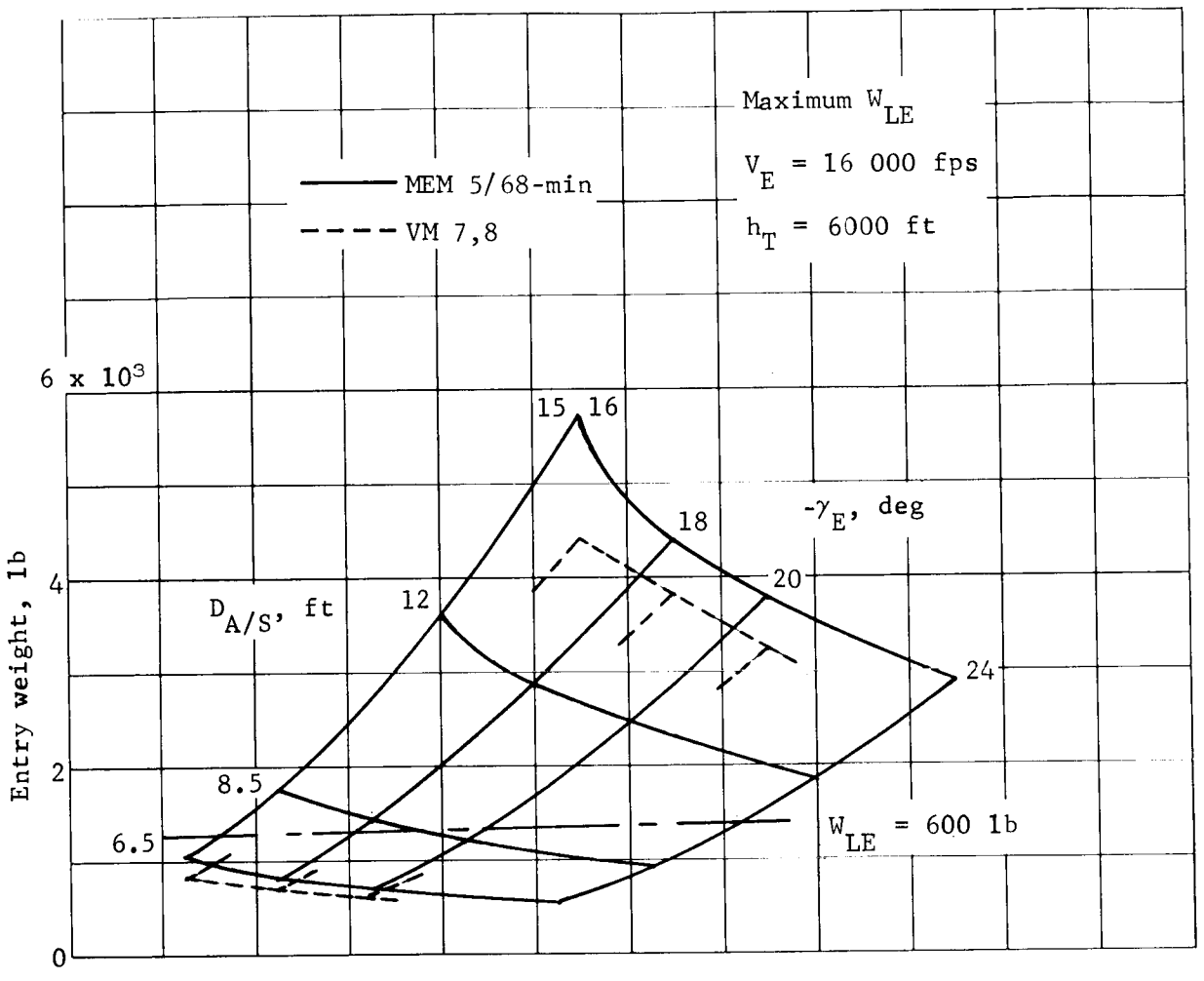

Figure 48.- Entry Weight, Orbit Mode

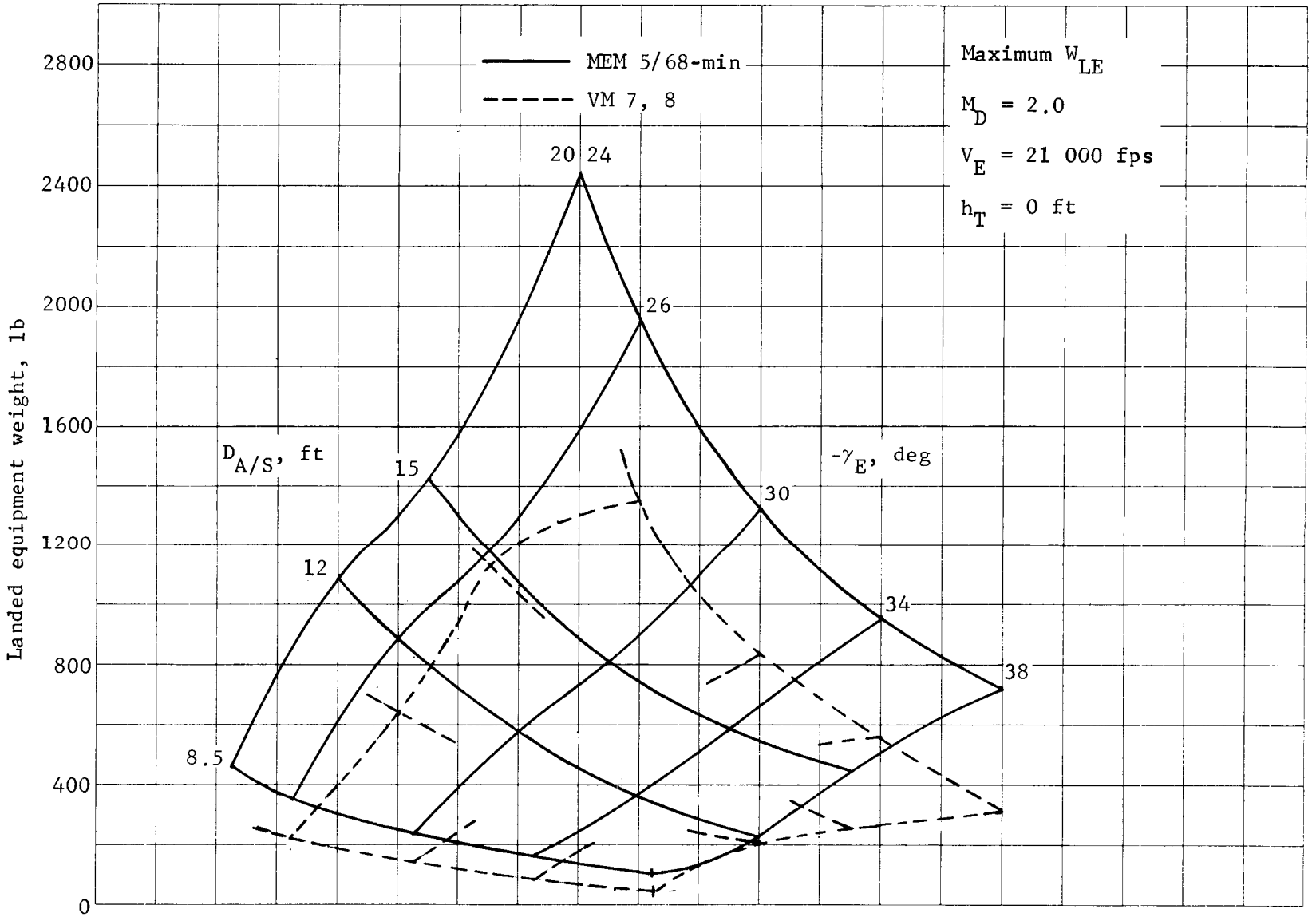

Figure 49.- Landed Equipment Weight, Direct Mode

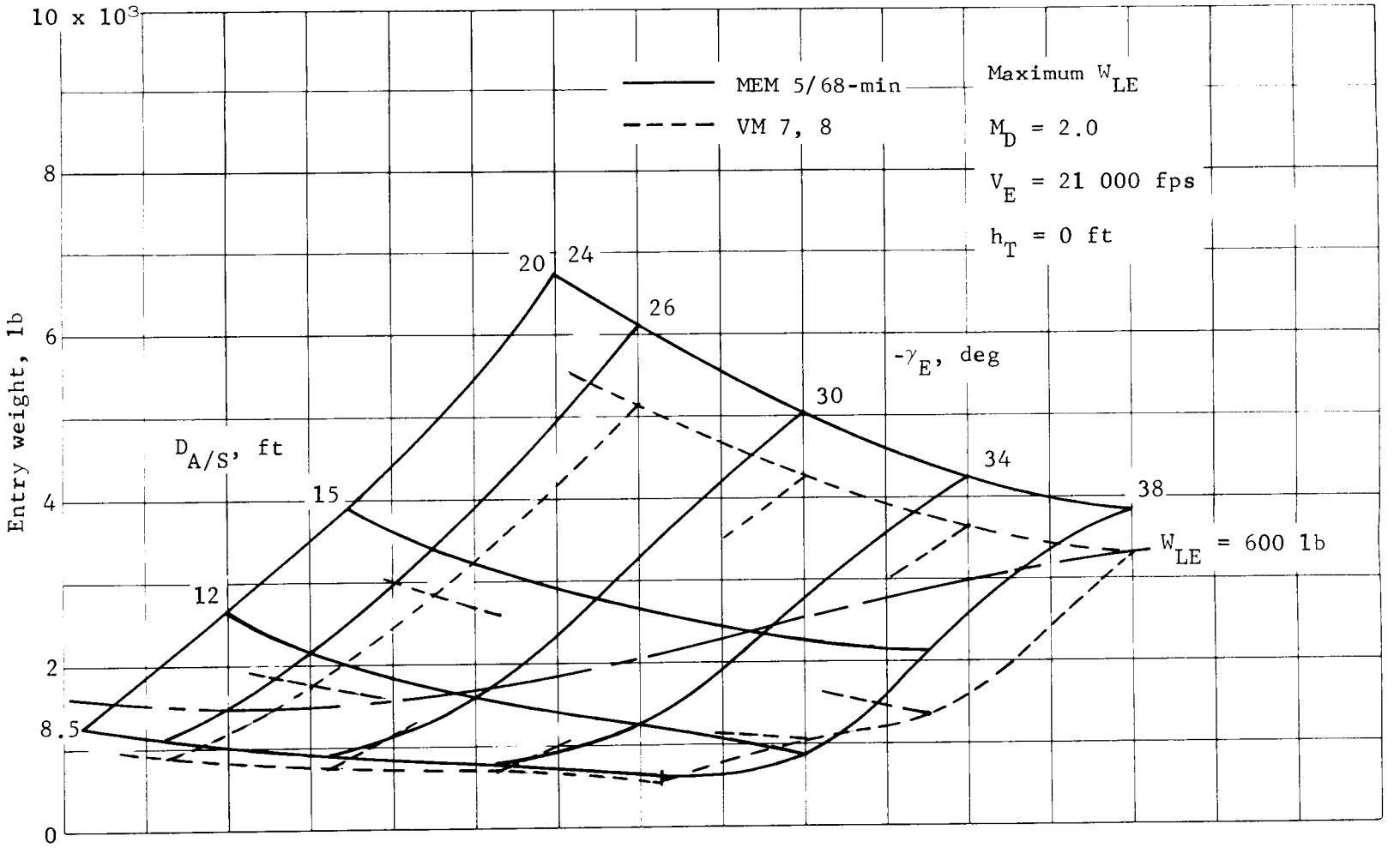

Figure 50.- Entry Weight, Direct Mode

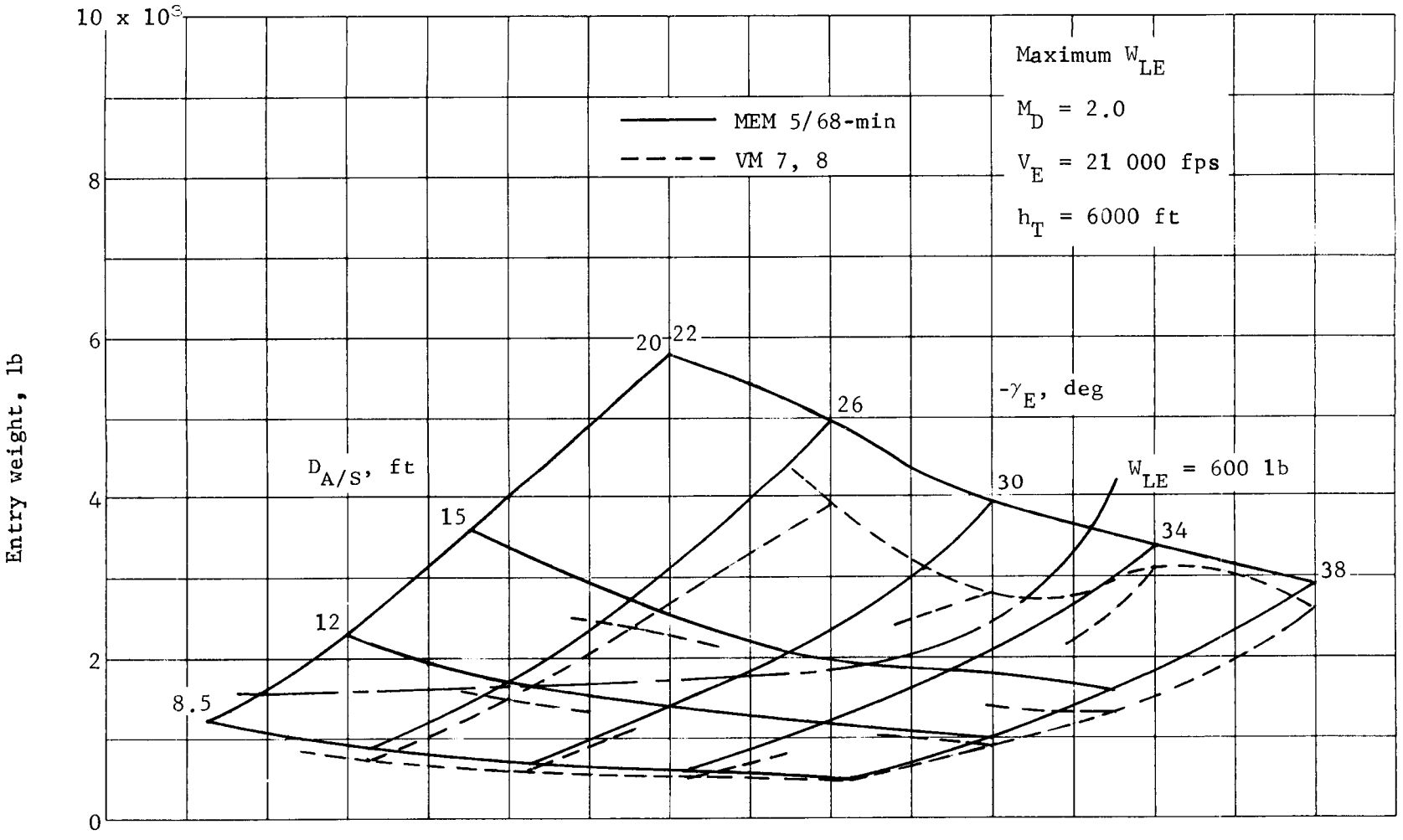

Figure 51.- Entry Weight, Direct Mode

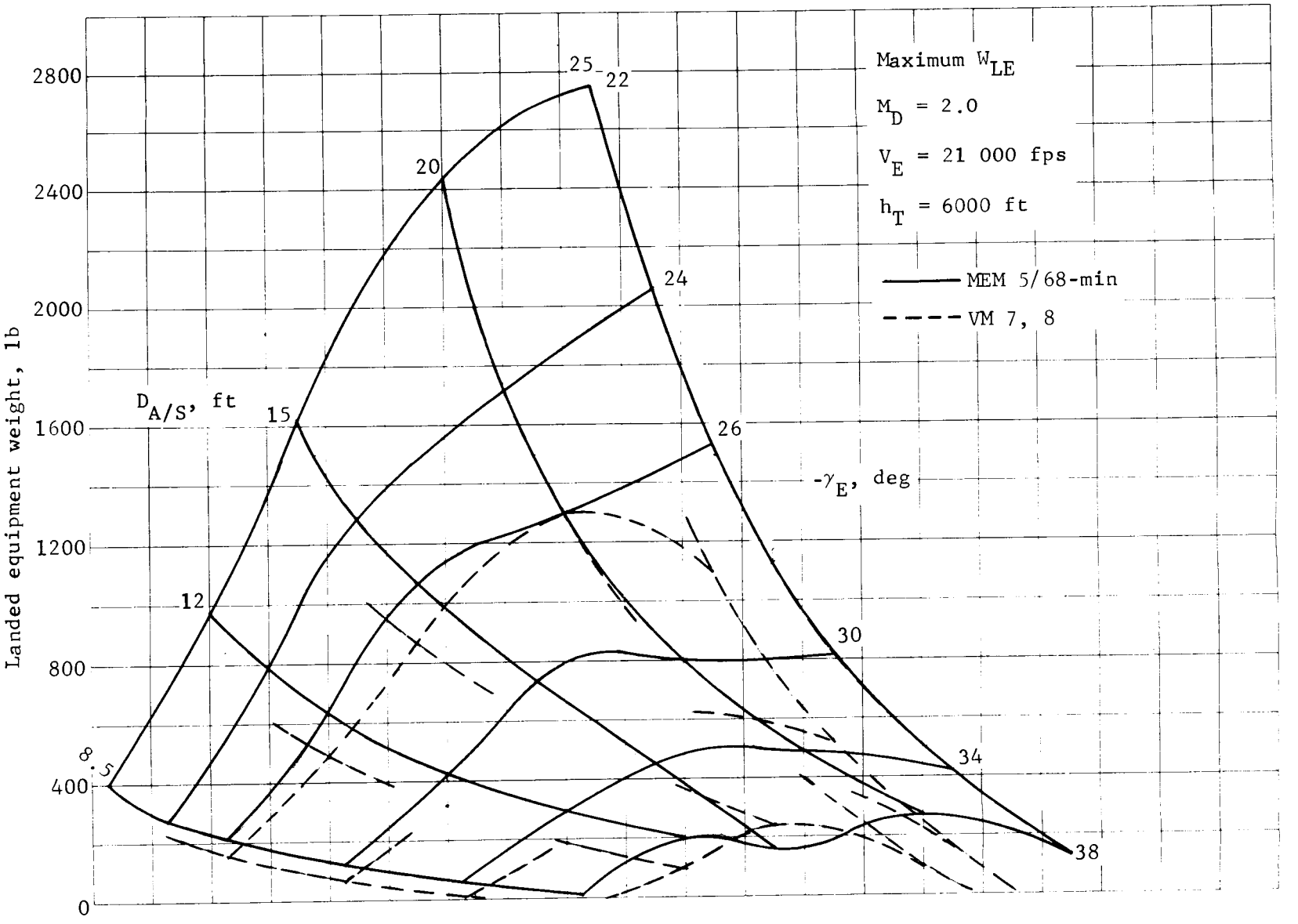

Figure 52.- Landed Equipment Weight, Direct Mode

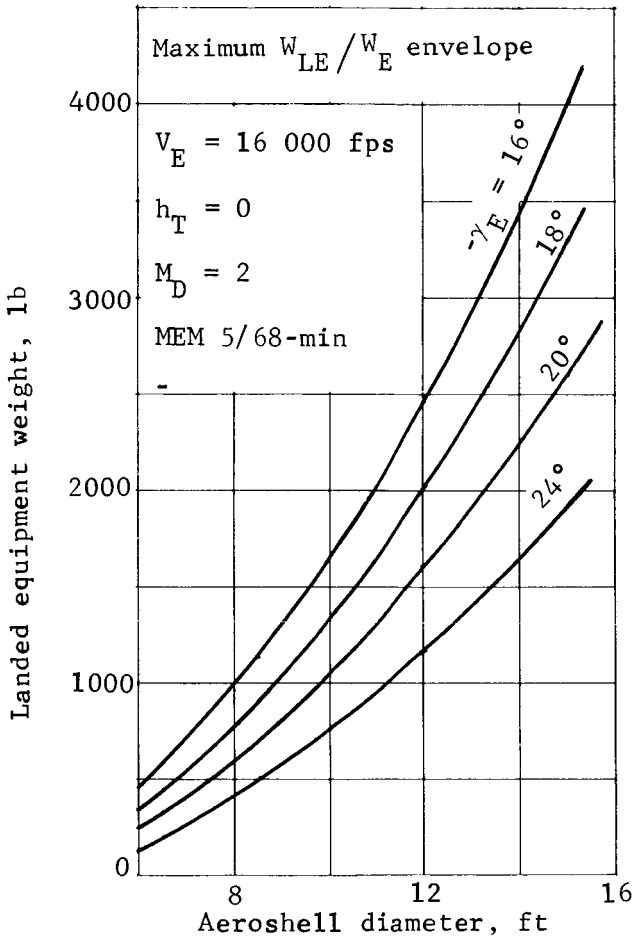

Figure 53.- W_{LE} vs Aeroshell Diameter, Orbit Mode

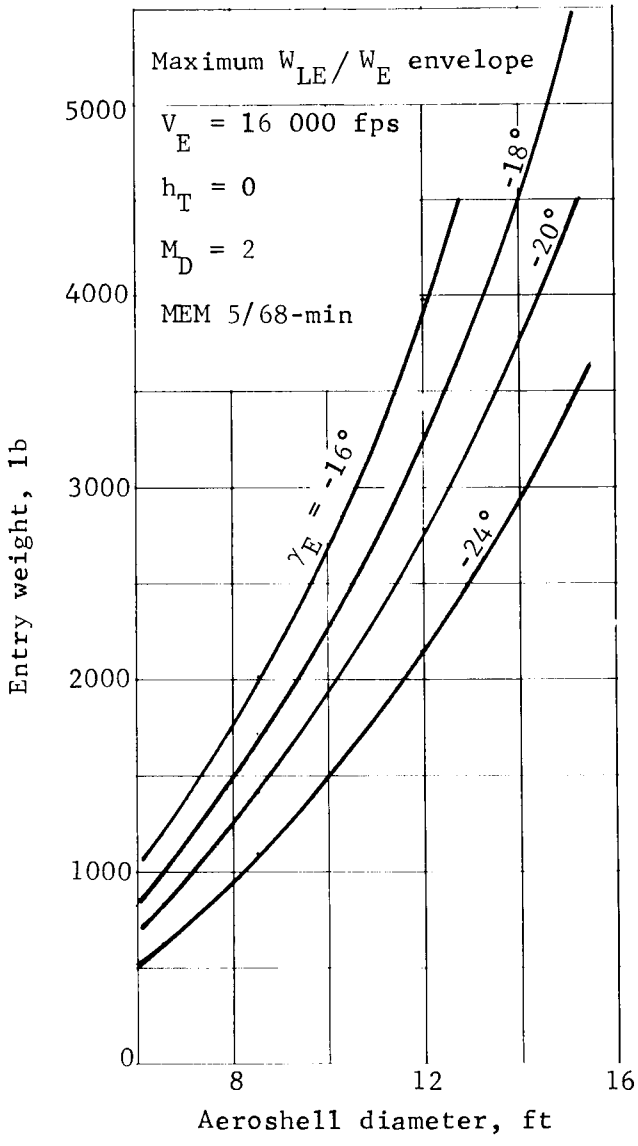

Figure 54.- W_E vs Aeroshell Diameter, Orbit Mode

Maximum W_{LE}/W_E envelope

V_E = 16 000 fps

h_T = 6000 ft

M_D = 2

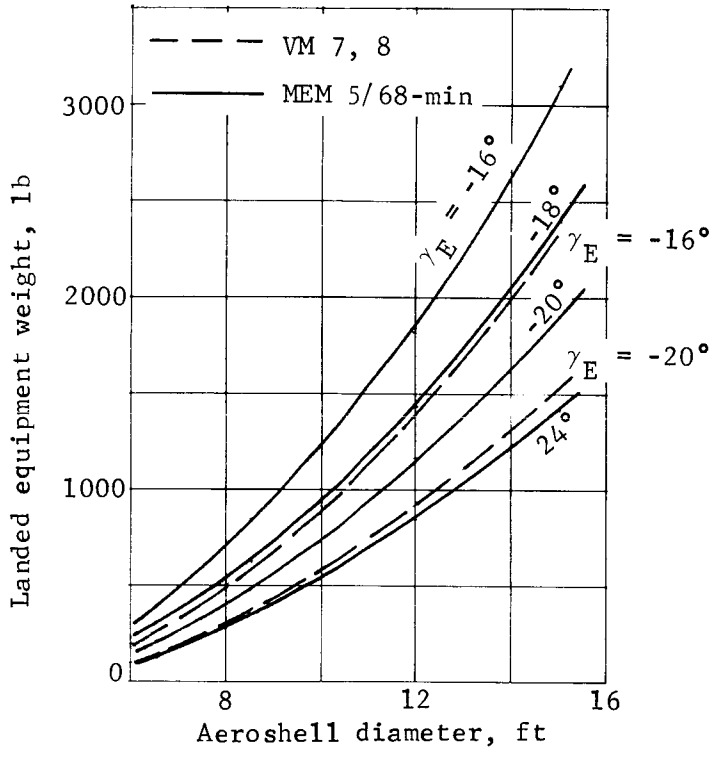

Figure 55.- W_{LE} vs Aeroshell Diameter, Orbit Mode

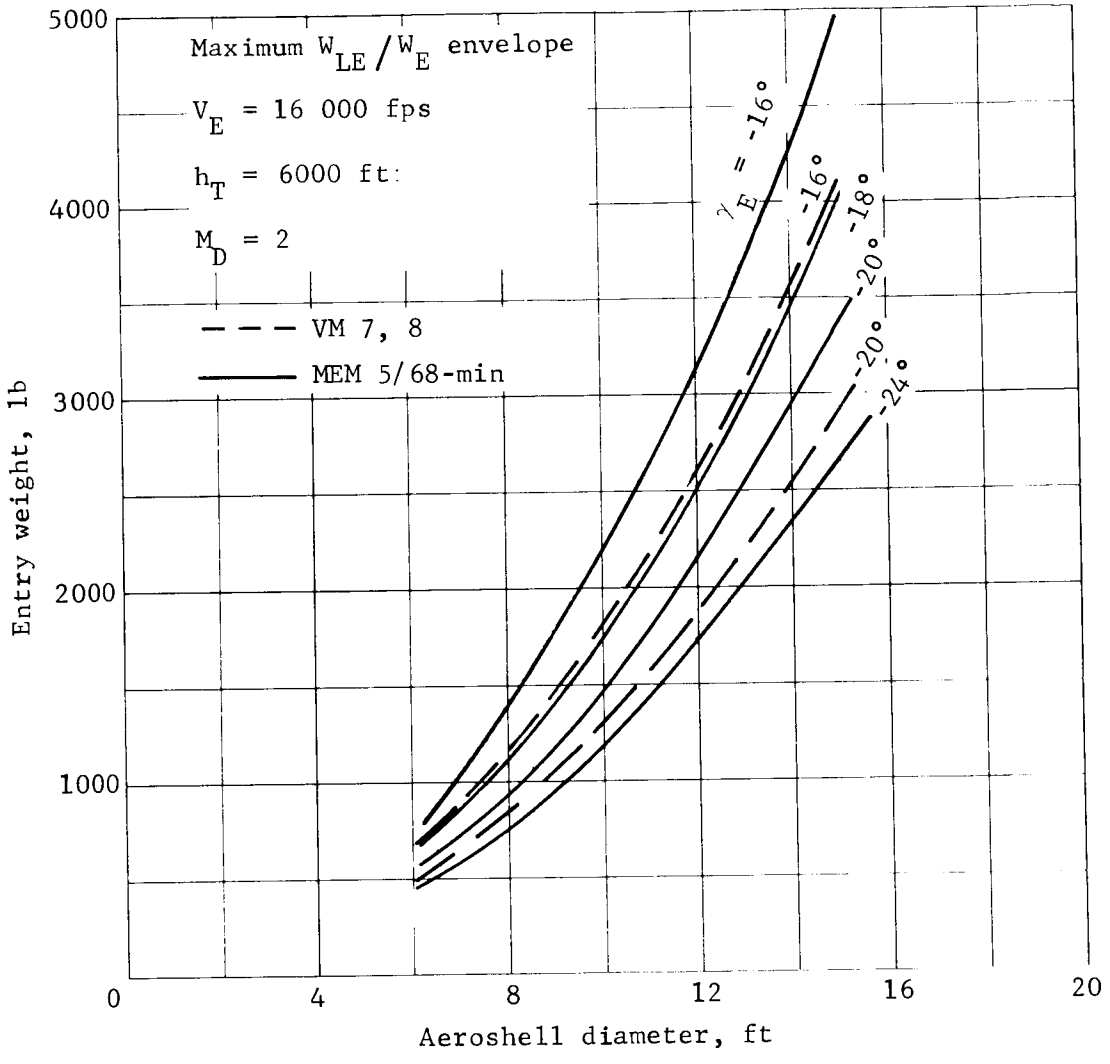

Figure 56.- W_E vs Aeroshell Diameter, Orbit Mode

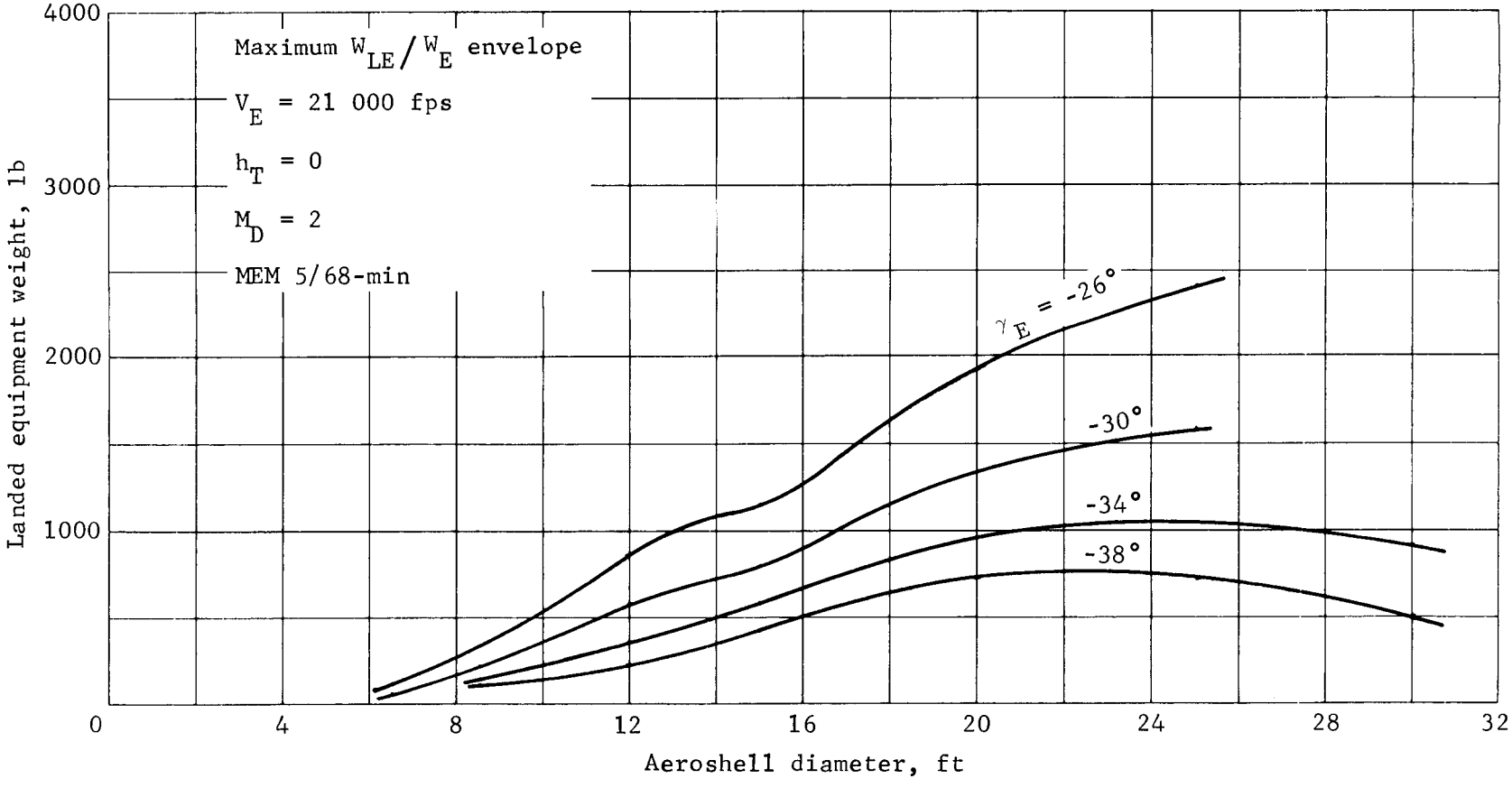

Figure 57.- W_{LE} vs Aeroshell Diameter, Direct Mode

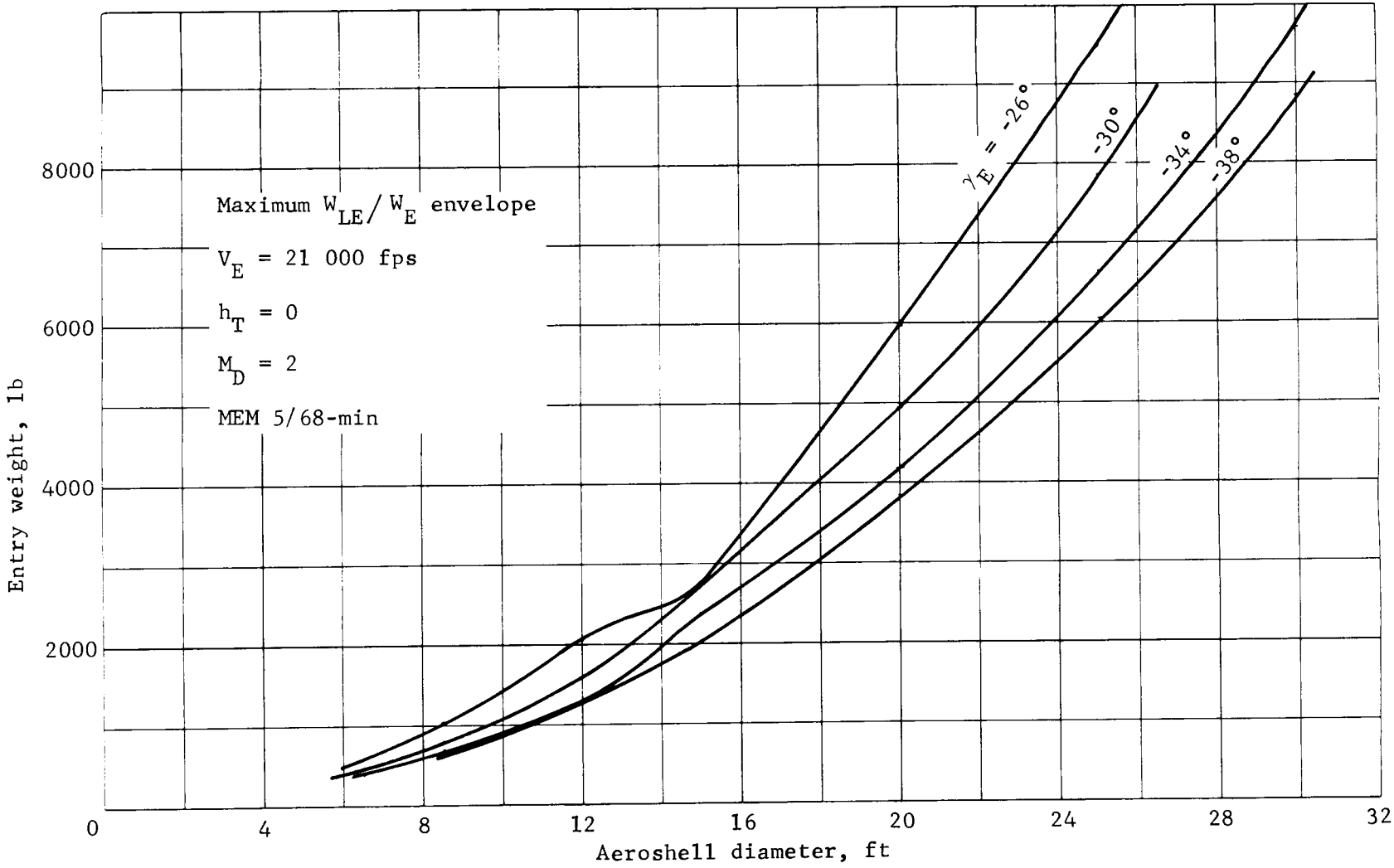

Figure 58.- W_E vs Aeroshell Diameter, Direct Mode

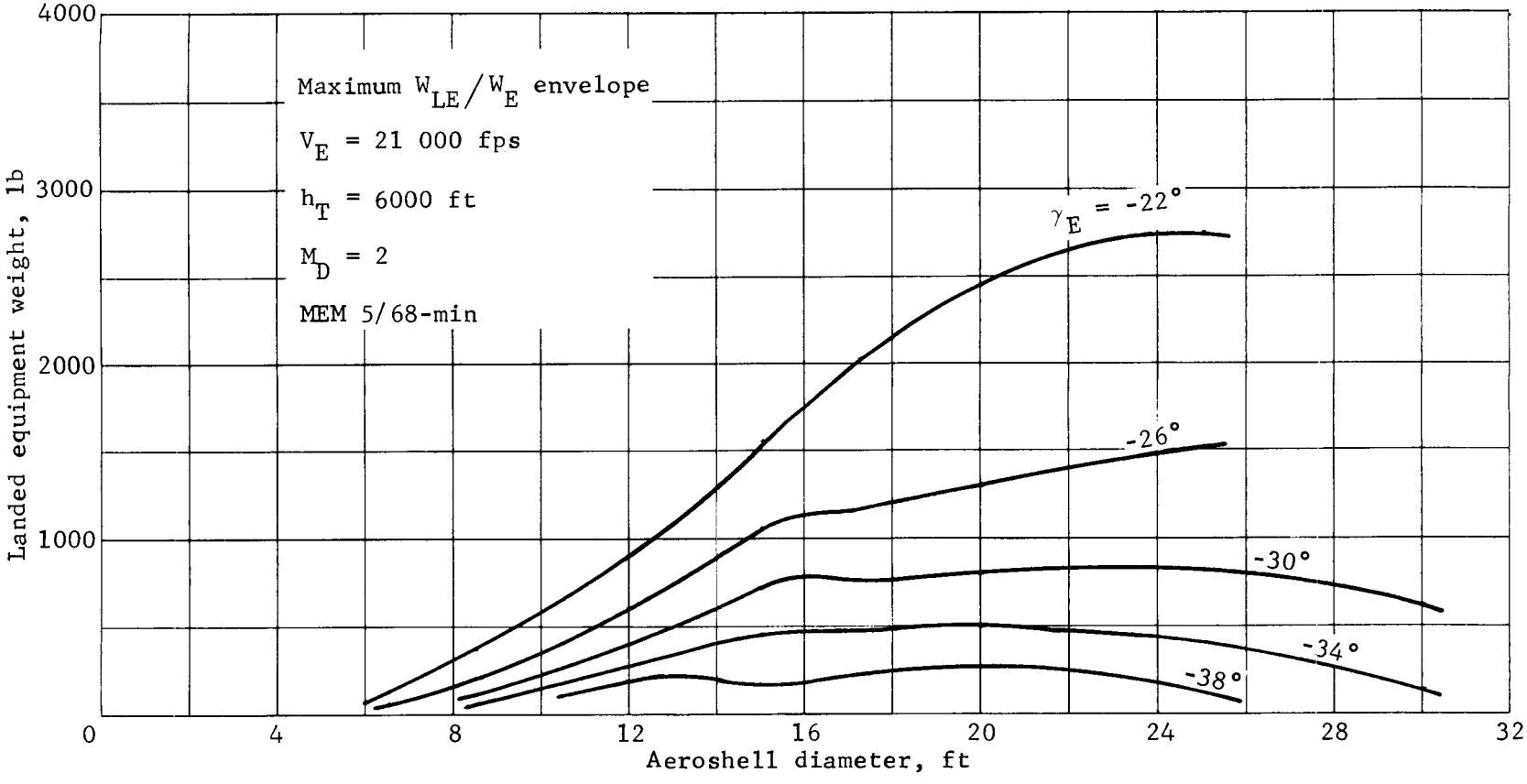

Figure 59.- W_{LE} vs Aeroshell Diameter, Direct Mode

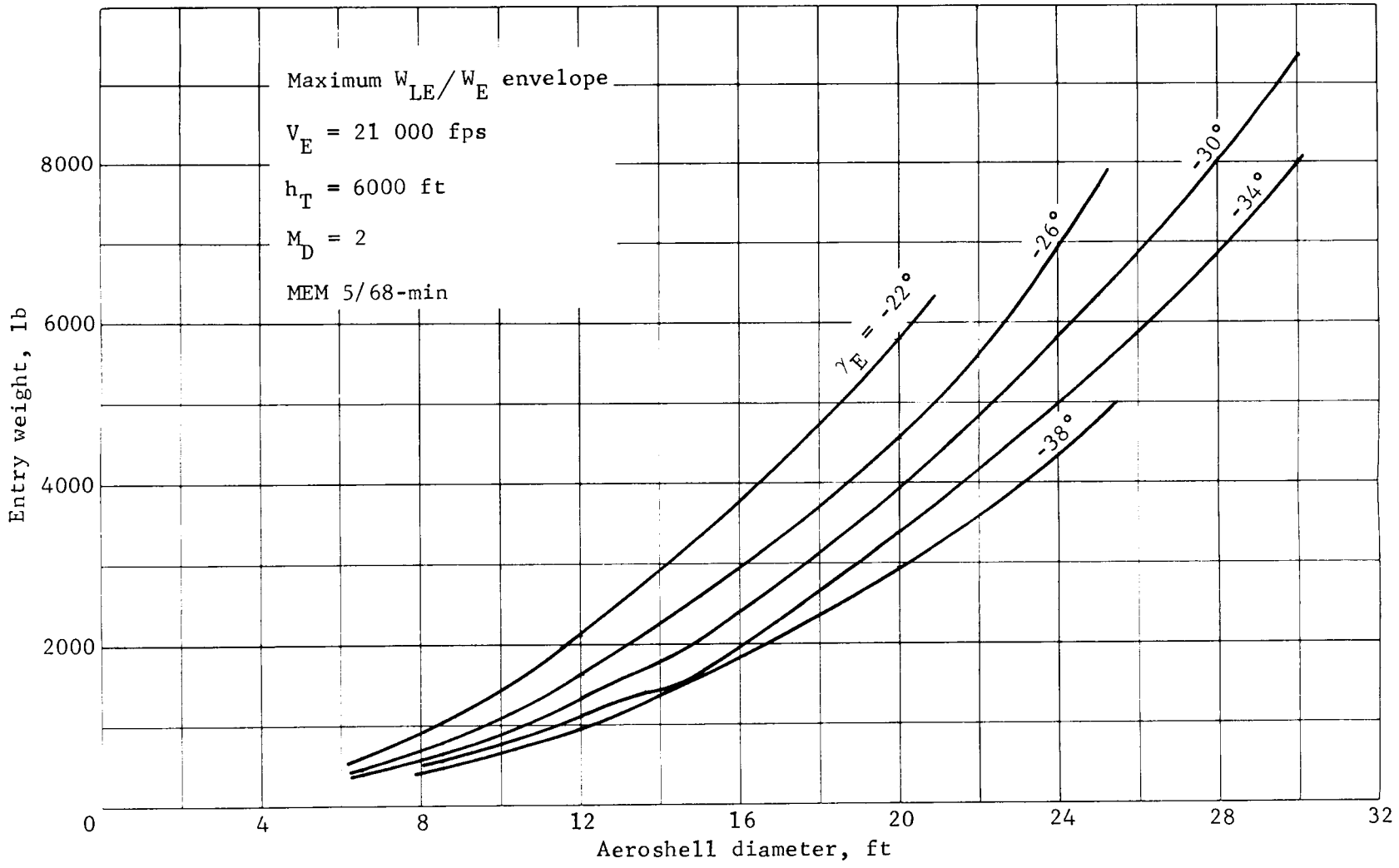

Figure 60.- W_E vs Aeroshell Diameter, Direct Mode

The deployment altitude is below the Mach 2 altitude in the MEM 5/68-mean atmosphere. This is necessary to obtain the same Δh to vernier ignition velocity as in the MEM 5/68-min atmosphere, assuming system design based on $M = 2$ deployment in the MEM 5/68-min atmosphere. The terrain height capability in the MEM 5/68-mean atmosphere is 20 700 to 22 000 ft compared to 6000 ft for the MEM 5/68-min atmosphere.

Capsule system weight required to land various landed equipment weights for orbital and direct modes for $h_T = 6000$ ft is shown in figure 61. A comparison of modes may be made from this plot. For example a 500-lb landed equipment weight with a $\gamma_E = -18°$ for the orbital mode requires a 1400-lb capsule system weight and a $D_{A/S} \approx 7.5$ ft. The direct mode, for a $\gamma_E = -24°$ requires 1600-lb capsule system weight and a $D_{A/S} \approx 10.5$ ft. This trend holds true for all points comparing mission modes. The orbit mode is superior in amount of landed equipment weight. This is primarily due to higher entry flightpath angles required for direct entry. The effect of entry angle may be readily seen from this figure. Increasing γ_E increases required capsule system weight for the same W_{LE} particularly at the higher γ_E.

Summary of Atmosphere Change on Performance

Two small changes in trajectory characteristics in the new atmospheres have led to greater performance capability (i.e., greater W_{LE} per $D_{A/S}$). The first is the altitude at Mach 2 as a function of B_E and γ_E (figs. 4 and 5), which is basically the same at low B_E, γ_E, but shows an advantage in the new atmospheres at higher B_E, γ_E. The second characteristic is the Δ-altitude required by the parachute to complete the job. These data are summarized in figures 62 and 63 for the MEM 5/68-min and VM-7, VM-8 atmospheres, respectively. Comparison of these data at constant B_{DEC} show that less altitude is required for a given parachute size in the MEM 5/68-min atmosphere. This, coupled with the data in figures 4 and 5, tends to shift the optimum performance point for a given aeroshell diameter to higher B_E and, therefore, greater pounds on the ground. Little gain is realized at nonoptimum points.

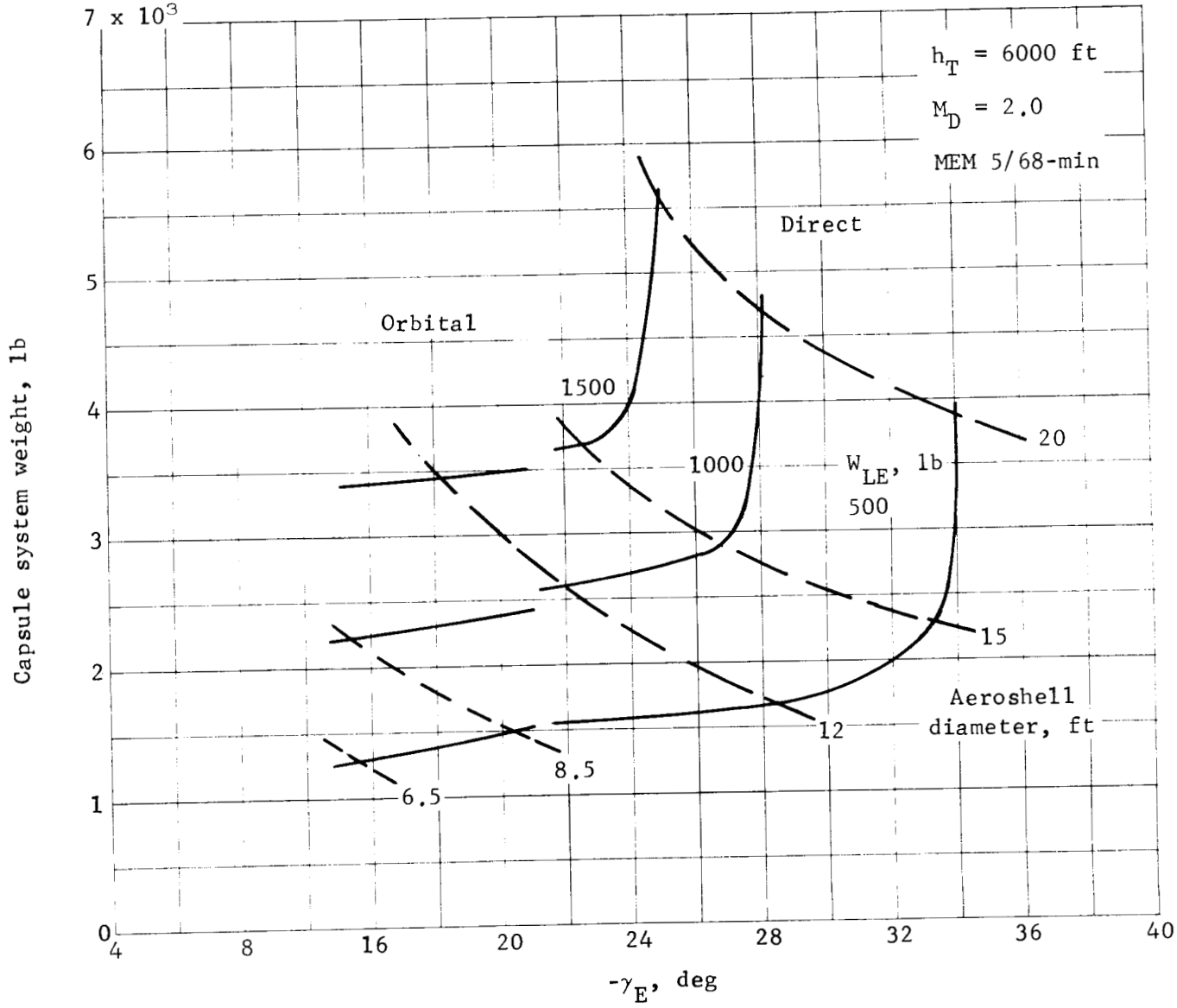

Figure 61.- Delivery Mode Performance Comparison

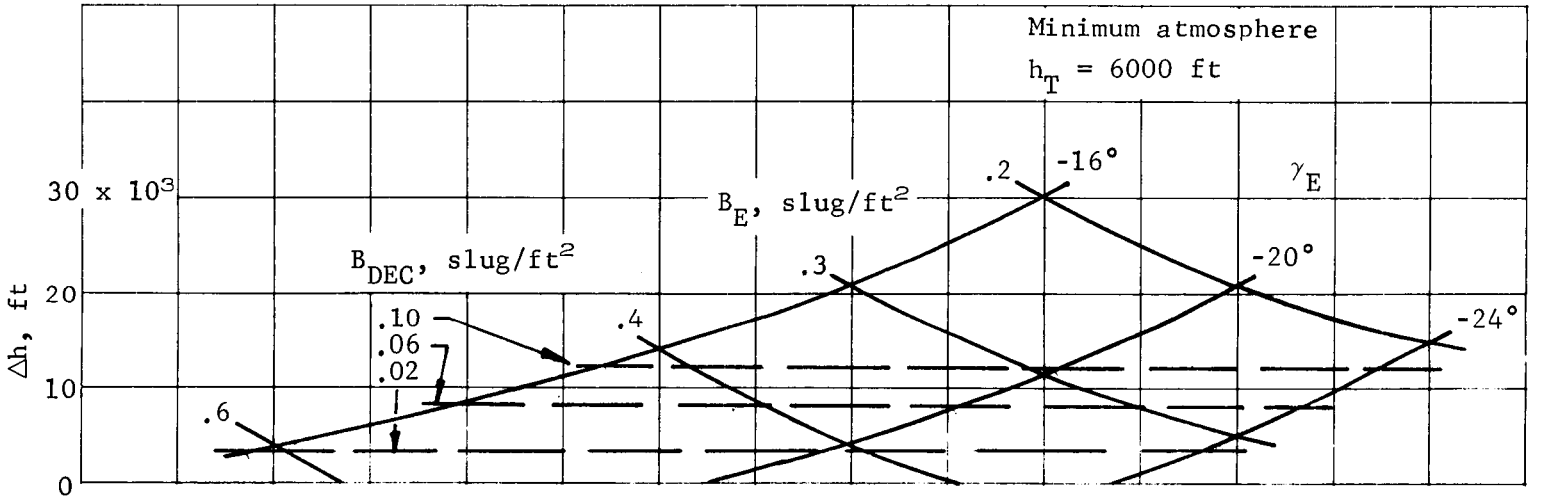

Figure 62.- Altitude Loss on Parachute, Minimum Atmosphere

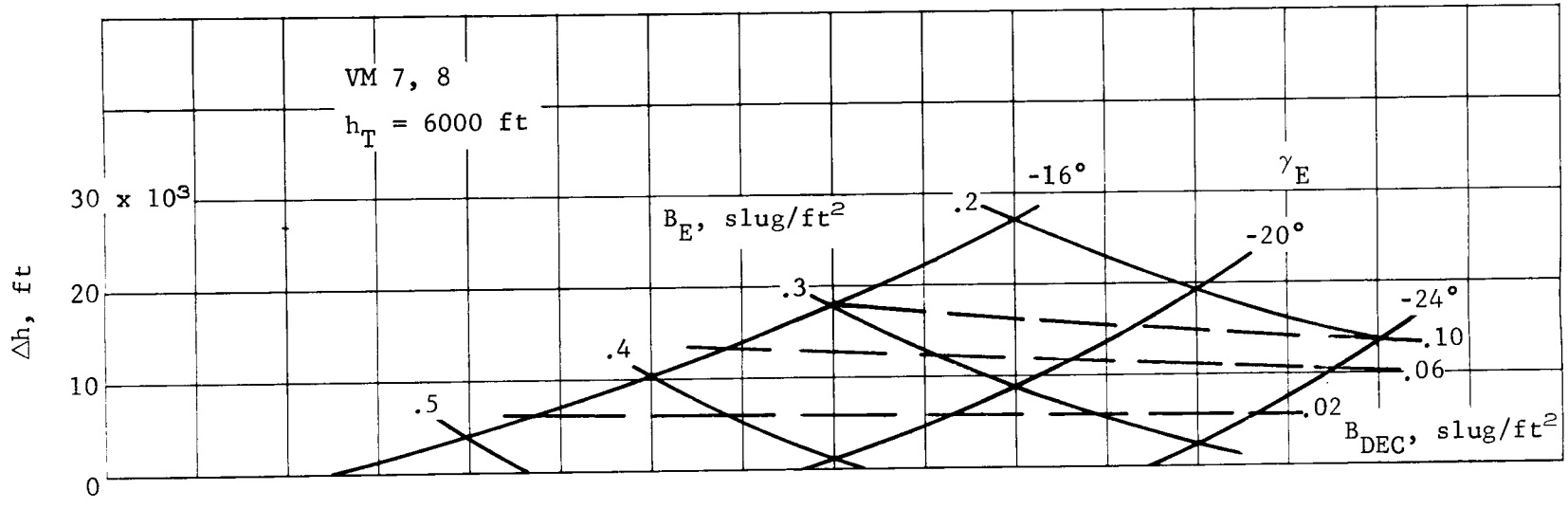

Figure 63.- Altitude Loss on Parachute, VM-7, 8 Atmosphere

A second factor that leads to greater performance in the new atmospheres is that the higher low-altitude densities allow smaller parachutes to reach a given terminal velocity. This characteristic, coupled with the vernier propulsion system characteristics, tends to shift the optimum parachute/vernier system optimization to lower terminal velocities and smaller vernier systems. Although this optimization was not made as part of this study, the characteristics are indicated in the parametric data.

A more quantitative comparison showing the effect of the new atmospheres is presented for specific point designs in tables 4 and 5 for orbital mode and tables 6 and 7 for direct mode. A typical maximum performance case derived from the parametric data in reference 2 is used as a reference point design. From table 4, this point design for the orbital mode has an entry weight of 1488 lb and W_{LE} = 711 lb for an aeroshell diameter of 8.5 ft $(B_E = 0.5)$. Four different point designs derived from the current study with the new atmospheres are shown for comparison. The first two have $D_{A/S}$ = 8.5 ft with one holding the same W_E, the second being the optimum W_{LE} point for that $D_{A/S}$. The second two point design are similar, one having the same W_E as the reference, the second the same W_{LE}. These two cases make use of the optimum aeroshell diameter for each case.

The data in tables 4 and 6 comparing these point designs show improved net performance for all of the cases with the new atmospheres. The tendency for higher B_E and, generally, smaller parachute sizes is apparent.

The weight data in tables 4 and 6 have been normalized by both W_E and W_{LE} and are presented in this form in table 5 and 7. First, the W_{LE}/W_E for the new atmosphere point designs are all greater than that for the reference. This is largely a result of the greater W_E or W_{LE}. As a generalization, the greater W_E leads to a more efficient configuration from a W_{LE}/W_E viewpoint, because the allowable weights are greater relative to the basic, relatively fixed weights such as structure, cabling, entry science, etc., which are required just to support the useful payload (i.e., fig. 25).

TABLE 4.- COMPARISON OF POINT DESIGNS, ORBIT MODE

	Typical VM-7,8 maximum performance	MEM 5/68-min atmosphere			
		Constant $D_{A/S}, W_E$	Constant $D_{A/S}$ maximum performance	Constant W_E maximum performance	Constant W_{LE} maximum performance
W_E, lb	1488	1488	1830	1488	1450
W_{LE}, lb	711	778	920	725	711
$W_{A/S}$, lb	121	121	128	110	107
W_{PAR}, lb	151	66	225	135	131
W_{VS}, lb	222	234	249	218	213
$D_{A/S}$, lb	8.5	8.5	8.5	7.8	7.7
B_E, slug/ft^2	.5	.5	.615	.59	.59
D_{PAR}, ft	70	44	78	59	58
B_{DEC}, slug/ft^2	.02	.0504	.02	.028	.028
Δh_{PAR}, ft	8000	8000	2900	4000	4000

Note: $\gamma_E = -16°$, $h_T = 6000$ ft, $V_E = 16\,000$ fps.

TABLE 5.- PERCENTAGE COMPARISON OF DELIVERY SYSTEMS, ORBIT MODE

	Typical VM-7,8 maximum performance	MEM 5/68-min atmosphere			
		Constant $D_{A/S}, W_E$	Constant $D_{A/S}$ maximum performance	Constant W_E maximum performance	Constant W_{LE} maximum performance
W_{LE}/W_E	0.478	0.523	0.503	0.487	0.490
$W_{A/S}/W_E$	0.082	0.082	0.070	0.074	0.074
W_{PAR}/W_E	0.102	0.044	0.123	0.091	0.090
W_{VS}/W_E	0.149	0.157	0.136	0.147	0.147
$\Sigma W_{DEL}/W_E$	0.333	0.283	0.329	0.312	0.311
$W_{A/S}/W_{LE}$	0.170	0.156	0.139	0.152	0.151
W_{PAR}/W_{LE}	0.212	0.085	0.246	0.186	0.184
W_{VS}/W_{LE}	0.312	0.301	0.271	0.301	0.300
$\Sigma W_{DEL}/W_{LE}$	0.694	0.542	0.656	0.639	0.635

TABLE 6.- COMPARISON OF POINT DESIGNS, DIRECT MODE

	Typical VM-7,8 maximum performance	MEM 5/68-min atmosphere			
		Constant $D_{A/S}$ same W_E	Constant $D_{A/S}$ maximum performance	Constant W_E maximum performance	Constant W_{LE} maximum performance
W_E, lb	914	914	1086	914	870
W_{LE}, lb	232	281	356	265	232
$W_{A/S}$, lb	155	155	164	138	131
W_{PAR}, lb	108	35	102	104	99
W_{VS}, lb	131	146	151	130	125
$D_{A/S}$, ft	8.5	8.5	8.5	7.7	7.5
B_E, slug/ft^2	.307	.307	.365	.374	.374
D_{PAR}, ft	52	29	47	46	45
B_{DEC}, slug/ft^2	.02	[a].066	.03	.026	.026
ΔH_{PAR}, ft	6200	8500	4500	3800	3800

[a] B_{DEC} required for aeroshell separation.

Note: $\gamma_E = -26°$, $h_T = 0$, $V_E = 21\ 000$ fps.

TABLE 7.- PERCENTAGE COMPARISON OF DELIVERY SYSTEMS, DIRECT MODE

	Typical VM-7,8 maximum performance	MEM 5/68-min atmosphere			
		Constant $D_{A/S}$ same W_E	Constant $D_{A/S}$ maximum performance	Constant W_E maximum performance	Constant W_{LE} maximum performance
W_{LE}/W_E	0.254	0.307	0.328	0.290	0.267
$W_{A/S}/W_E$	0.170	0.170	0.151	0.151	0.151
W_{PAR}/W_E	0.118	0.038	0.094	0.114	0.114
W_{VS}/W_E	0.144	0.160	0.139	0.142	0.144
$\Sigma W_{DEL}/W_E$	0.432	0.368	0.384	0.407	0.409
$W_{A/S}/W_E$	0.667	0.552	0.461	0.520	0.565
W_{PAR}/W_{LE}	0.465	0.125	0.287	0.393	0.426
W_{VS}/W_{LE}	0.565	0.052	0.424	0.491	0.539
$\Sigma W_{DEL}/W_{LE}$	1.697	0.729	1.172	1.404	1.530

The remaining comparisons shown in tables 5 and 7 are on the basis of percentage of W_E or W_{LE} of the basic delivery systems (i.e., $W_{DEL} = W_{A/S} + W_{PAR} + W_{VS}$). The data illustrate the various system weight improvements for the various point designs compared to the reference. The four comparison configurations cover the gamut from most weight saved in the parachute system (little improvement in the vernier) to most weight saved in the vernier. In all cases, the total delivery system weight ratio is improved over the reference configuration using the VM-7, VM-8 atmospheres.

The basic conclusions derived from this analysis are:

1) The mission mode comparison presented in reference 2 is not basically changed;

2) The new atmospheres do allow greater landed useful weights for a given aeroshell diameter.

LANDING STABILITY ANALYSIS

The stability capability of the Configuration 1B vehicle was determined using the slope probability plot (fig. III-C-4) from reference 1. Figure 64 is a reproduction of these data.

Stability Determination

There were eight steps used to determine the vehicles stability capability:

1) The Martin Marietta Corporation Phase B four-legged lander had an R/H (ratio of leg radius to c.g. height) of 2.2 and a 100% stable landing capability for slopes up to 36° (fig. 3.1-21, ref. 3).

2) The reference configuration for the Mars Mission Mode Study had a R/H of 2.0 and a 100% **stable landing capability of 32° slope.**

3) Applying 10% tolerance to the c.g. of this reference configuration, the minimum R/H is 1.8 and the 100% stable point becomes 28°.

4) Above this angle, a statistical approach was used to determine the landing capability.

5) From figure 3.1-23 of reference 3, it is seen that approximately a 17° difference exists between the 100% stable slope and the 0% stable point. For this analysis, a conservative 6° was used and the 0% stable point of 34°. These two angles 28 and 32° were used in the construction of figure 65.

6) Cummulative probability plots were obtained for the five major parameters involved in landing stability. These parameters are,

   a) Surface slope,

   b) Direction of slope (angle between horizontal velocity and downhill direction),

   c) Vertical velocity,

   d) Horizontal velocity,

   e) Roll attitude (rotation about vertical velocity axis);

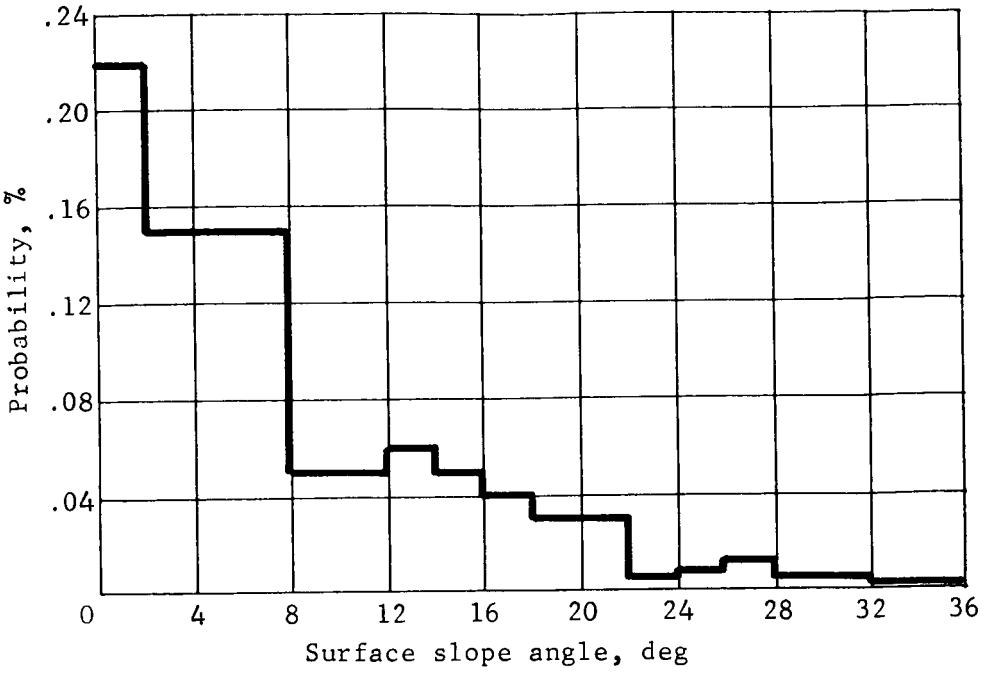

Figure 64.- Probability Density Distribution for Surface Slopes between the -60° to 60° Latitudes on Mars

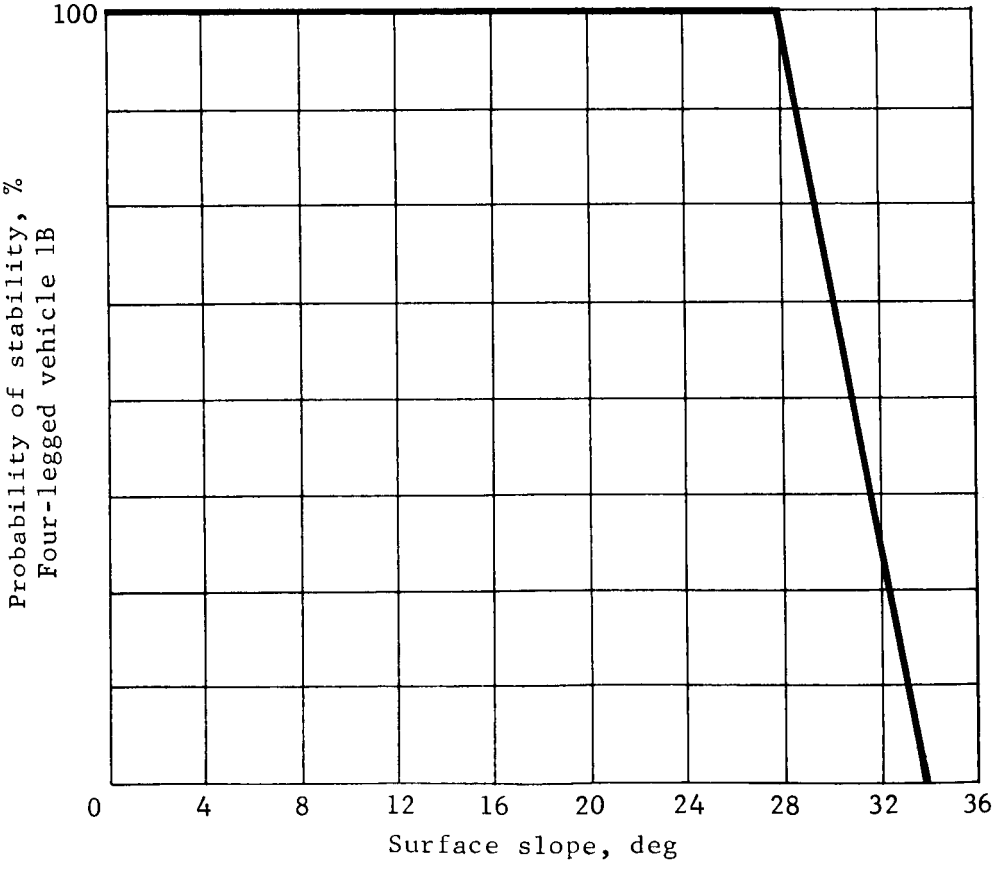

Figure 65.- Probability of Stability vs Surface Slope

These plots are shown as figures 66 thru 70. The surface slope plot (fig. 66) is the integration of figure 64. The velocity data (fig. 68 and 69) were also obtained from reference 3 (Volume II, Section I, table 3.4-4).

7) Tabular representations of these plots were used in a digital computer program incorporating a random number generator to determine the value of the five parameters. The value of each of the five parameters was determined for 5000 "landings" and those that had a surface slope in excess of 28° were printed out.

8) There were 44 "landings" on surface slopes in excess of 28° as presented in table 8. Seven of the "landings" were on a slope in excess of 34° and two others were judged unstable because of the values of the five parameters. The percentage of stable landings is then 4991 out of 5000 or a vehicle stable for 99.82% of the landings.

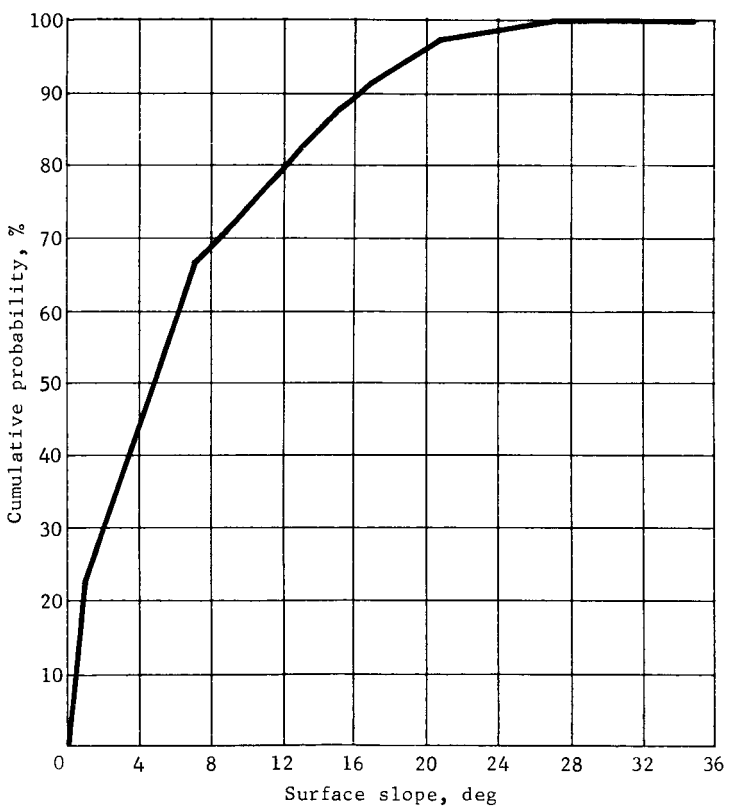

Figure 66.- Cumulative Probability of Surface Slope

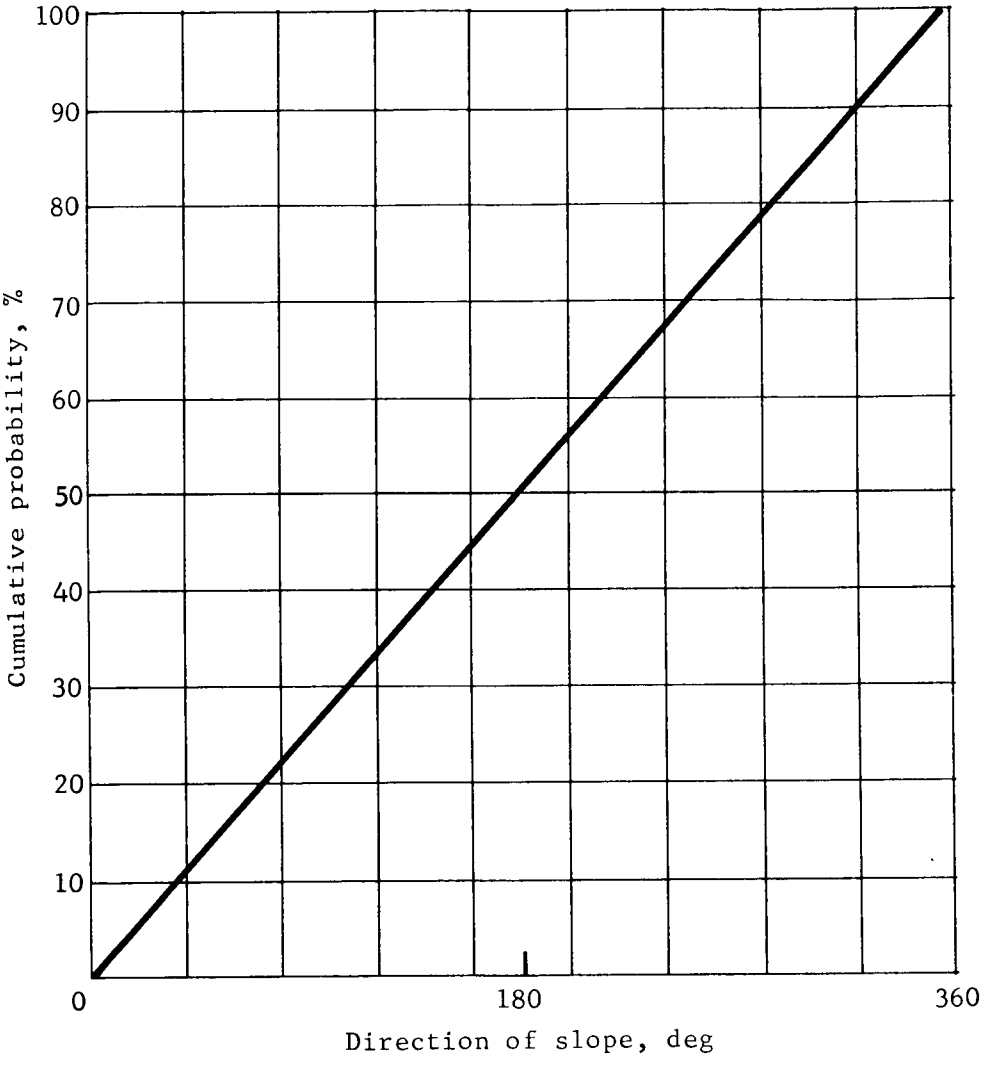

Figure 67.- Cumulative Probability of Direction of Slope

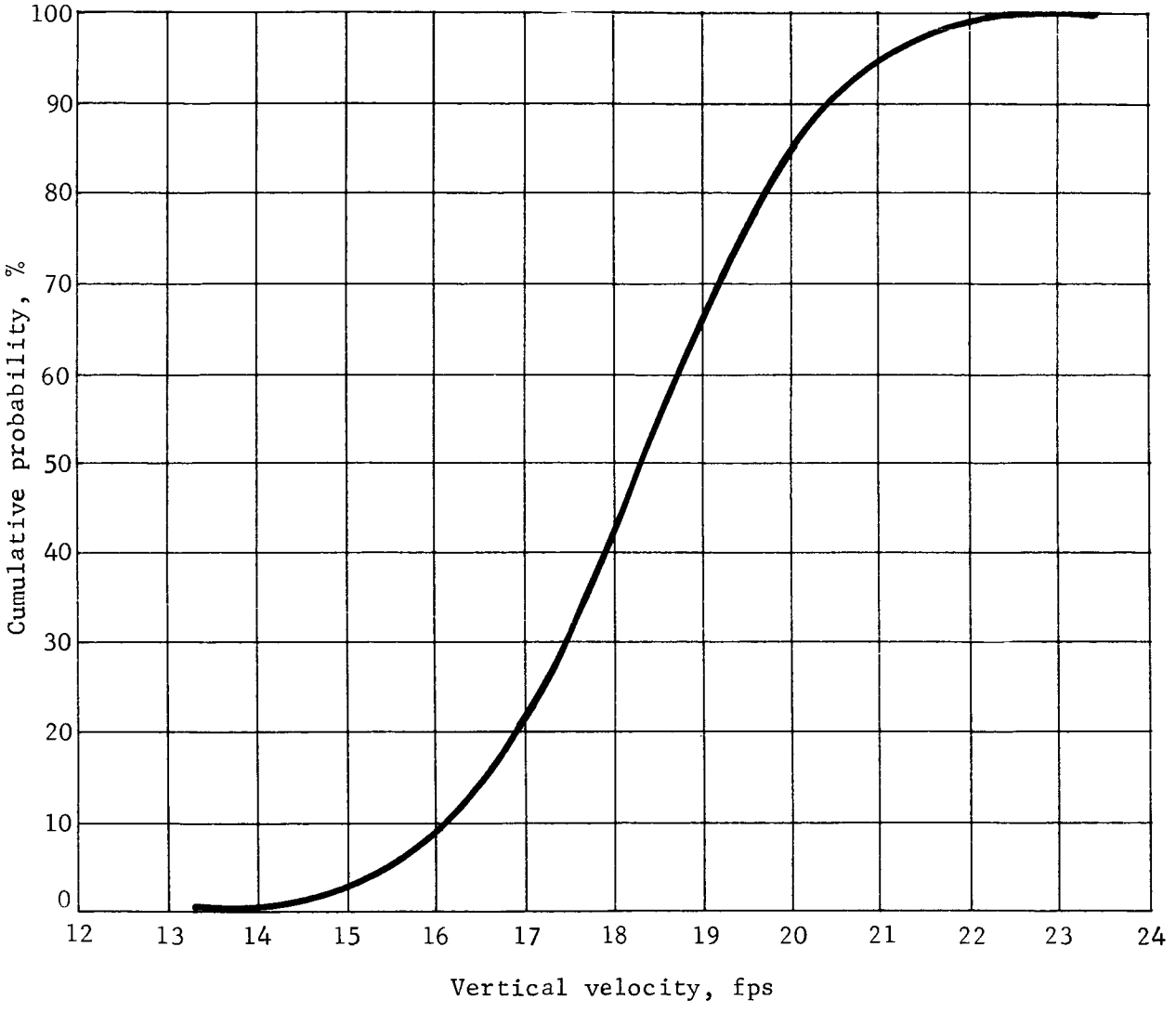

Figure 68.- Cumulative Probability of Vertical Velocity

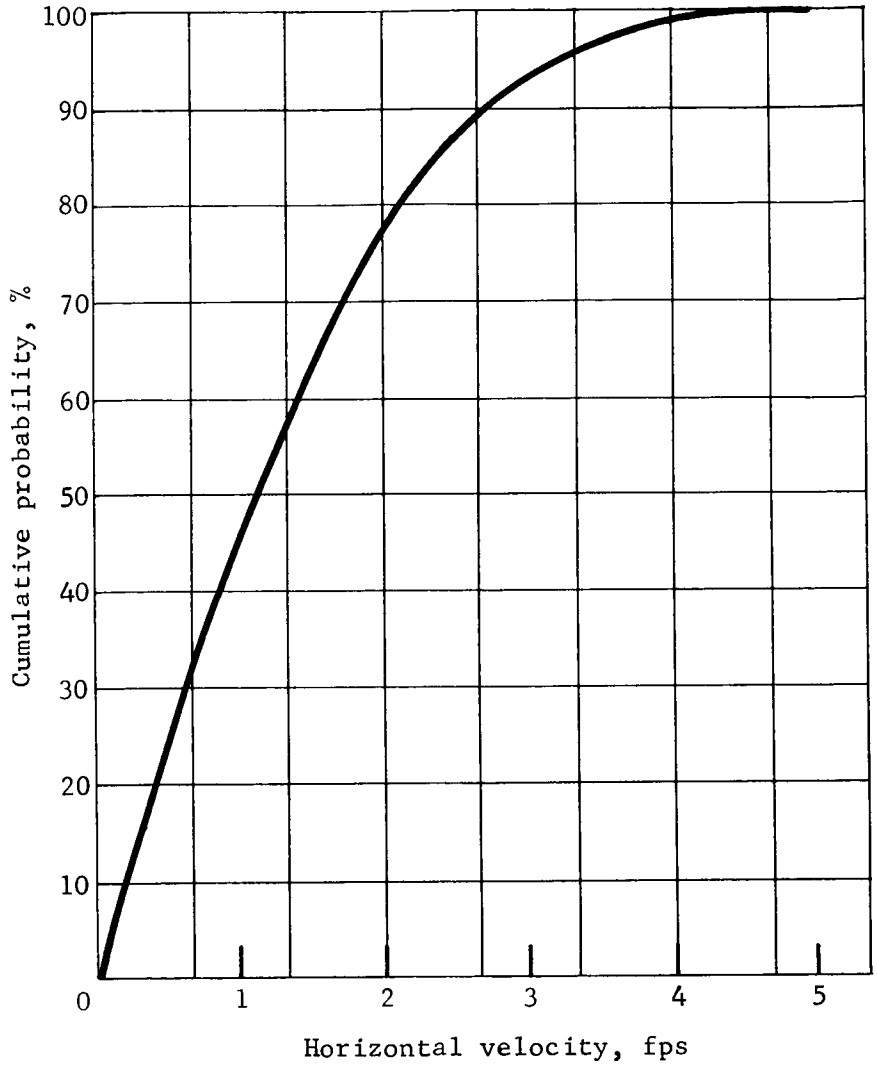

Figure 69.- Cumulative Probability of Horizontal Velocity

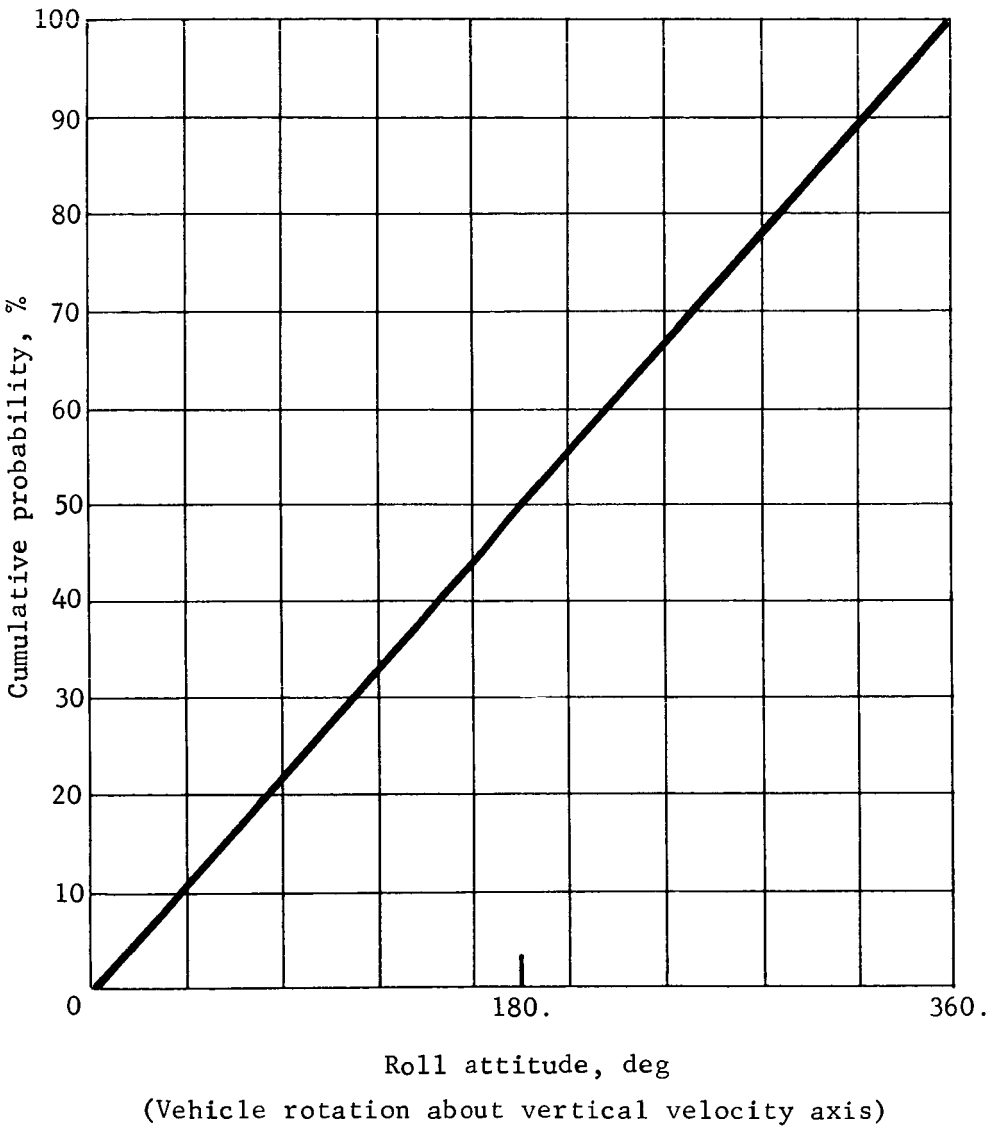

Figure 70.- Cumulative Probability of Roll Attitude

TABLE 8.- "LANDINGS" WITH SLOPES GREATER THAN 28°

LAND NO	SLOPE DEG	D-SLOPE DEG	VERT VEL FPS	HOR VEL FPS	ROLL DEG
176	29.0	166.19	15.00	0.30	155.03
252	31.0	86.91	15.60	1.30	181.22
288	35.0*	133.14	18.30	2.00	251.36
360	31.0	149.67	19.60	3.00	23.19
574	35.0*	164.52	20.30	1.00	172.34
589	35.0*	39.43	18.30	0.30	34.06
651	29.0	275.60	17.30	0.30	332.81
875	33.0	133.56	18.60	0.30	157.03
890	31.0	118.29	18.00	0.70	102.20
968	29.0	291.70	18.30	2.70	198.97
1012	29.0	354.46	17.00	0.70	40.94
1142	29.0	72.06	21.60	0.30	32.07
1153	31.0*	353.21	15.00	3.30	323.94
1176	29.0	40.68	19.00	1.00	111.08
1185	29.0	135.23	19.30	3.00	139.71
1545	31.0	118.71	18.30	1.70	7.87
1621	33.0	164.94	21.00	2.30	78.01
1922	29.0	134.81	19.30	1.30	234.04
2003	29.0	41.10	19.00	2.70	16.75
2798	31.0	55.53	19.30	2.70	260.24
3099	29.0	166.61	16.30	1.70	60.70
3181	31.0	181.46	17.00	0.30	209.85
3189	29.0	306.97	18.60	2.30	253.80
3251	31.0	259.07	21.60	2.70	200.97
3372	31.0	337.93	20.30	0.30	269.11
3397	35.0*	273.93	15.60	1.00	350.13
3524	29.0	103.43	17.60	2.00	313.06
3538	31.0	243.80	20.30	3.70	146.15
3607	29.0	103.85	18.00	0.70	218.73
3697	33.0	102.18	17.00	1.00	236.04
3698	35.0*	101.76	17.00	0.30	330.37
3882	31.0	9.30	17.30	2.00	190.10
3968	31.0	275.18	17.00	1.70	67.13
3998	31.0	306.56	18.60	1.00	348.13
3999	35.0*	305.30	18.00	0.30	271.11
4130	31.0*	352.79	21.60	1.30	58.26
4174	29.0	197.57	18.00	2.30	76.01
4300	35.0*	195.90	17.00	0.30	93.33
4431	29.0	338.35	21.00	1.30	174.78
4550	31.0	181.04	16.30	1.70	304.18
4601	31.0	227.69	19.00	0.70	279.99
4711	33.0	70.80	20.30	2.00	315.06
4902	29.0	323.08	20.30	1.30	119.96
4999	29.0	212.84	18.60	2.00	130.84

*Unstable.

Surface Bearing Strength Effects

The design effects of the bearing strength data presented in the new environmental model is as described below.

Assuming a 1000-lb lander impacting at approximately 24 fps, the maximum kinetic energy on touchdown is 9200 ft-lb.

The bearing strength data from reference 1 (page 63, sections III-C-3-f-2-b and d):

$p = 0.7$ N/cm^2 at 0 penetration;

$p = 5.5$ N/cm^2 at 5 cm penetration.

Assuming these data to be straight line, the bearing strength would be:

$$p(h) = (0.7 + 4.8h) \text{ N/cm}^2$$

where h is in centimeters or

$$p(h) = (146 + 6120h) \text{ lb/ft}^2$$

where h is in feet. The amount of penetration four foot pads would have in expending 9200 ft-lb would be

$$H = 0.978/d$$

where H is in feet and d is the foot pad diameter in feet.

It is therefore recommended that the foot pads for a four-legged lander be at least 1 ft in diameter.

THERMAL CONTROL ANALYSIS

Thermal Control Parameters

The modified Mars thermal environment parameters that conform to the new Mars engineering model are presented in table 9. The greatest change from the previous values is in the surface emissivity, with lesser differences in the surface thermal inertia, wind velocity, atmospheric composition, and solar transmissivity. These parameters have no appreciable effect on the cruise mode or descent mode thermal control subsystem design.

For the lander thermal control design, the hot extreme environment differs significantly in surface emissivity and thermal inertia, while the cold extreme differs only in the atmospheric composition and wind velocity. Because the intermediate and clear-day environmental parameters were somewhat arbitrarily selected from the anticipated range of values, they are not being altered. The modified tabulation of thermal environments showing the changes that were made are presented in table 10.

Parametric Studies

For the parametric studies, the Mars surface and atmospheric temperatures for the hot extreme are increased as shown in figure 71. The corresponding temperatures for the other environments remain unchanged, as do the quantities and rates of heat input required to maintain 40°F internal temperature. The heat input required to maintain the maximum 100°F internal temperature as a function of insulation thickness with the extreme hot environment is decreased as shown in figures 72 and 73 for two different lander surfaces. The thermal control system weight curves are based primarily on the heat input required with cold extreme, intermediate, and clear-day environments. The overheating check for these curves was also based on the clear-day environment conditions, so these system weight curves do not require modification. If the extreme hot day were used for the overheating check, the Mars environmental model environment curves from figures 72 and 73 would apply.

TABLE 9.- MARS MODIFIED THERMAL ENVIRONMENT PARAMETERS

Environmental parameter	Nominal	Range
Solar flux, Btu/hr ft^2	180	160 to 232
Atmospheric solar transmissivity	----	0 to <1.0
Surface solar absorptivity, α_s	.80	.65 to .95
Surface emissivity, ϵ	.80	.60 to 1.0
Surface density, ρ, lb/ft^3	62.4	----
Surface heat capacity, c, Btu/lb °F	.17	----
Surface thermal conductivity, k, Btu/hr ft °F	.145	.0242 to .242
Surface thermal inertia, $\sqrt{k\rho c}$, Btu/ft^2 °R $hr^{\frac{1}{2}}$	1.24	.51 to 1.6
Surface temperature, T_g, °F	----	-190 minimum
Atmospheric temperature, T_a, °F	----	-190 minimum
Atmospheric pressure, mb	9	6 to 20
Wind velocity at 1 meter, fps	----	44 to 148
Atmospheric composition, mol %		
CO_2	68.5	19 to 100
N_2	18.5	60 to 0
A	13.0	21 to 0

TABLE 10.- MODIFIED THERMAL ENVIRONMENTS

	Environmental parameter	Cold extreme	Intermediate	Clear day	Hot extreme
(1)	Solar flux, Btu/hr ft^2	0	160	180	232
(2)	Atmospheric solar transmissivity	0	.5	1.0	[a] 1.0 → <1.0
(3)	Surface solar absorptivity, α_s	----	.80	.80	.95
(4)	Surface emissivity (ϵ)	----	.92	.92	.85 → .60
(5)	Surface thermal inertia, $\sqrt{k\rho c}$ Btu/ft^2 °F $hr^{\frac{1}{2}}$	----	.97	.97	.97 → 1.24
(6)	Surface temperature, T_g, °F	-190°	Calculated using parameters (1) to (5)		
(7)	Wind velocity at 1 meter, fps	74 → 81	105	0	0
(8)	Atmospheric pressure, mb	20	10	10	5 → 6
(9)	Atmospheric temperature, T_a, °F	-190	Estimated based on parameter (6)		
(10)	Atmospheric composition, mol %				
	CO^2	0 → 19			100
	N_2	100 → 60			0
	A	0 → 21			0

[a] Old VM environment → new MEM environment.

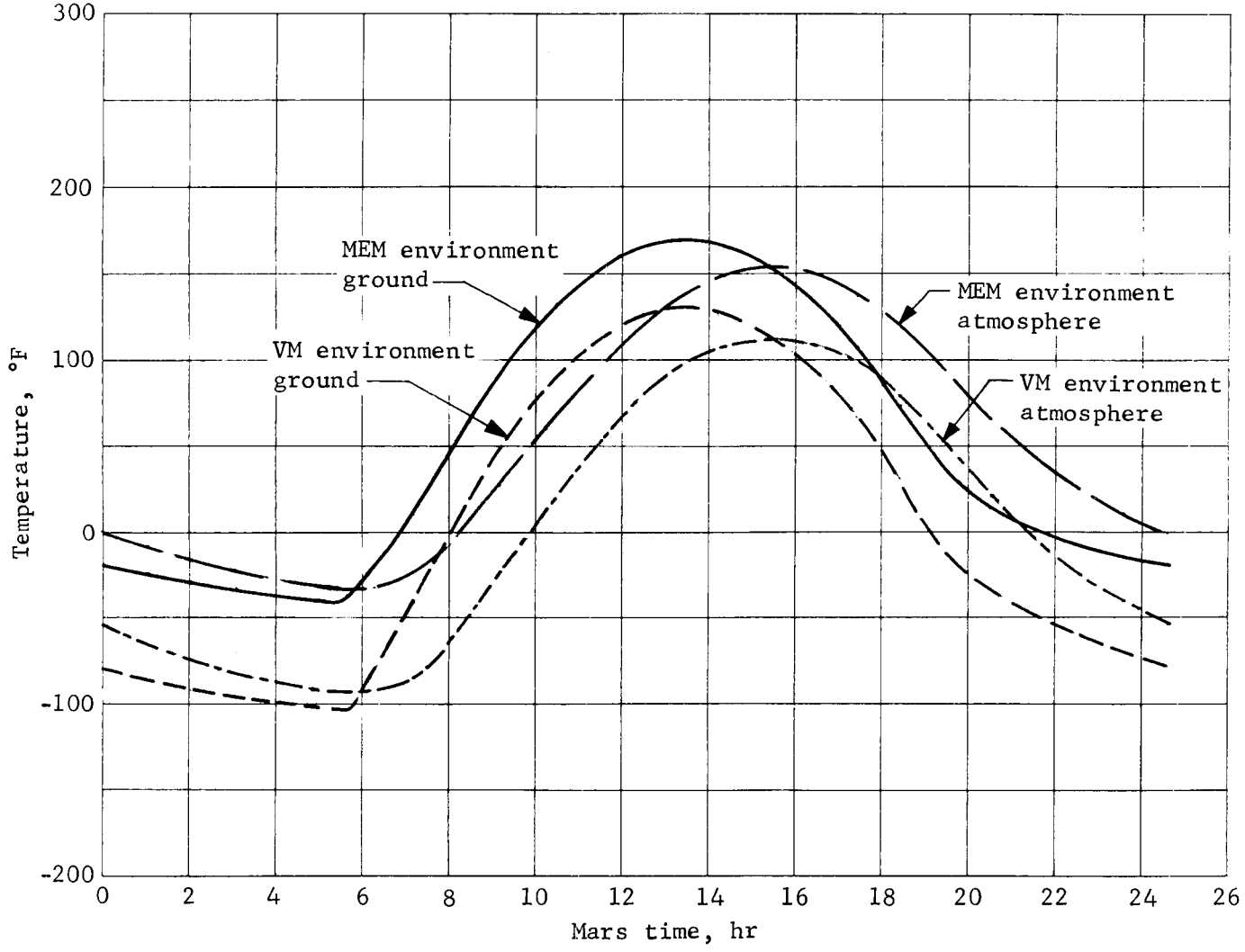

Figure 71.- Mars Surface and Atmospheric Temperatures, Hot Day Environment

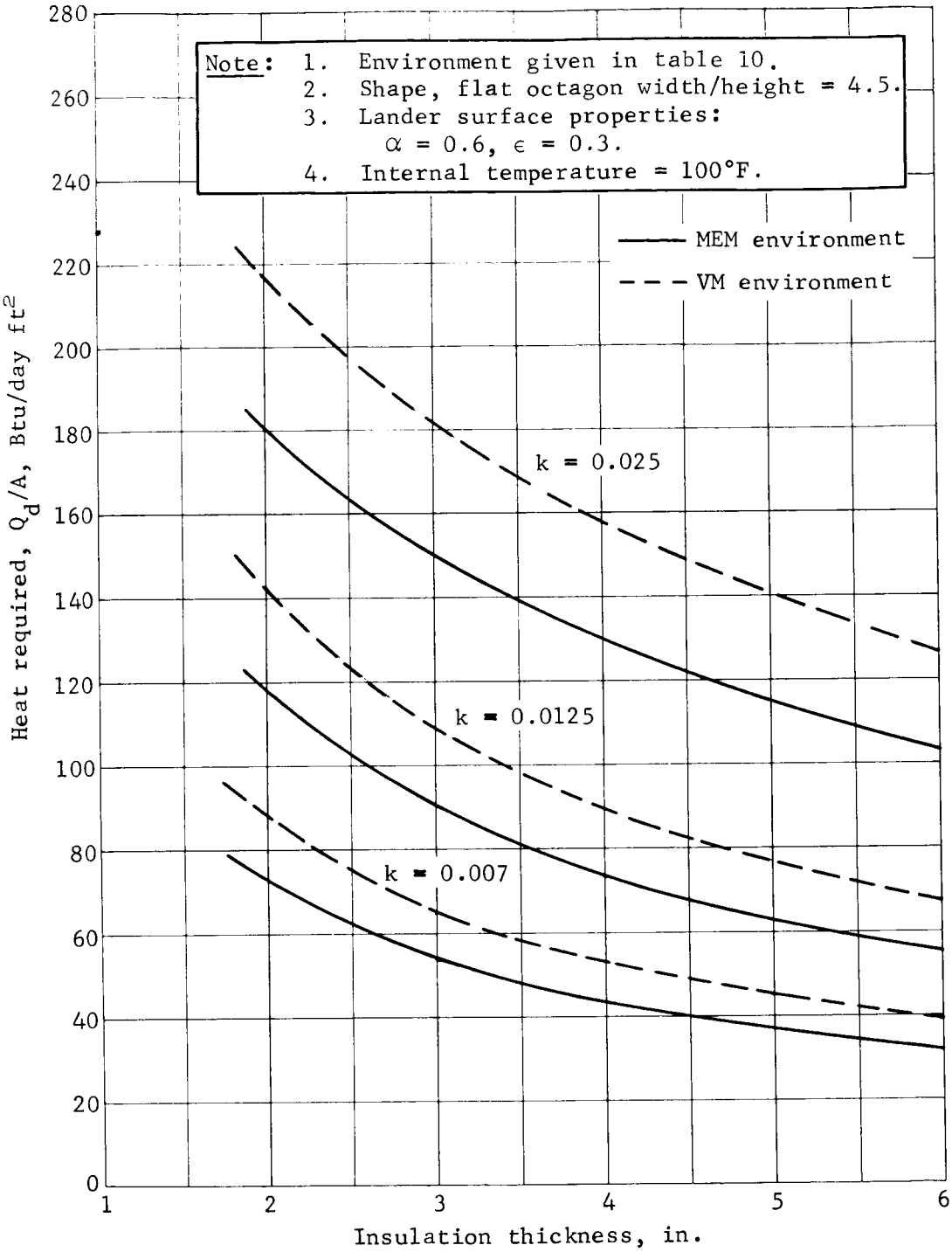

Figure 72.- Heat Required, Hot Environment (α = 0.6, ϵ = 0.3)

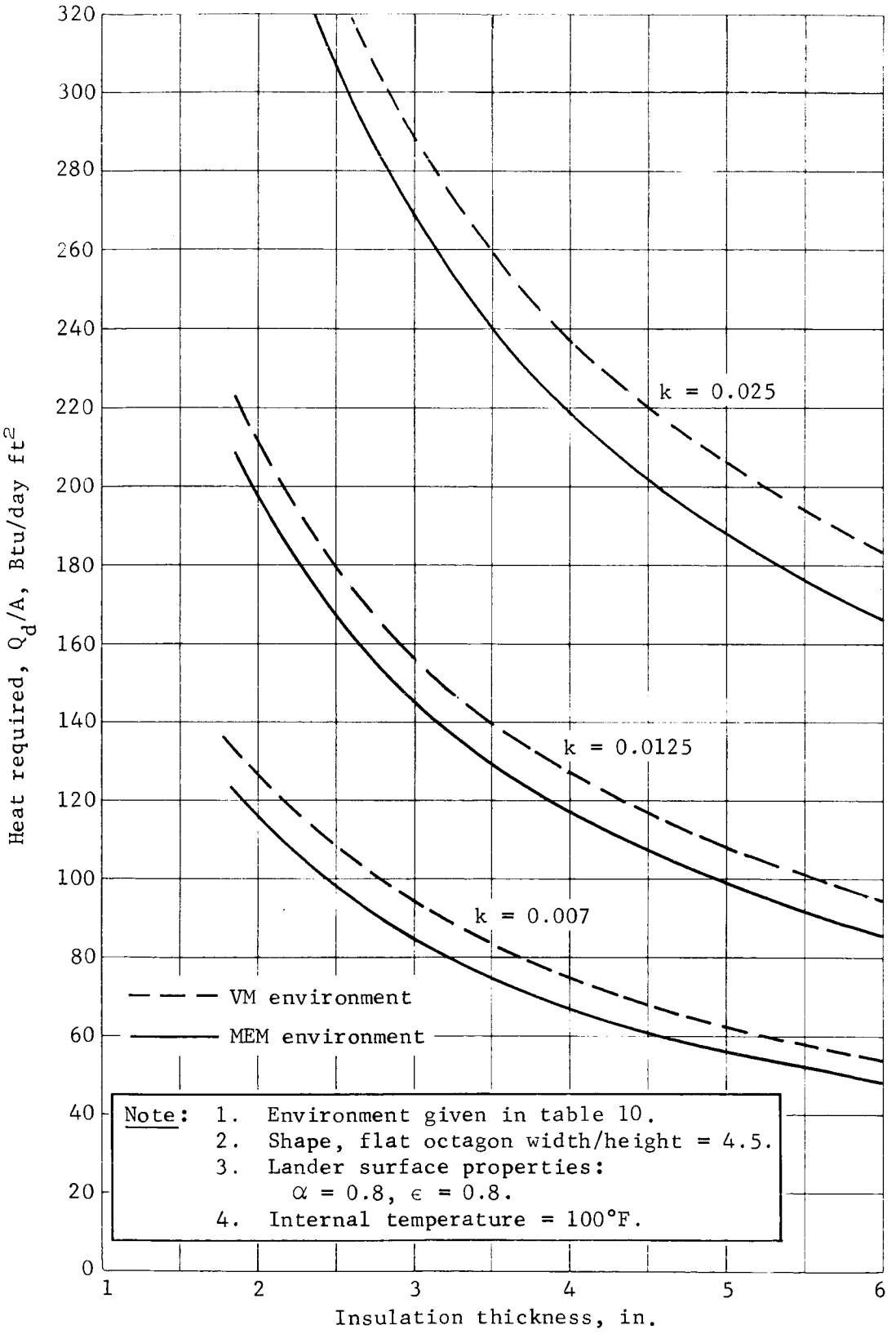

Figure 73.- Heat Required, Hot Environment (α = 0.8, ϵ = 0.8)

Point Designs

A single design was used for the lander thermal control subsystem for Configurations 1A, 2A, 1B, and 2C. This design consists of a 3-in. layer of insulation, radioisotope heaters of 200 W total power, and phase change material for peak power loads. The extreme hot environment did not affect the design, and the extreme cold environment on which the design was based is modified only slightly. The Mars environmental model minimum temperature mixture containing 60% nitrogen has a lower thermal conductivity than pure nitrogen as shown in figure 74, and produces a corresponding lower insulation effective conductivity including penetrations as shown in figure 75. This decrease in thermal conductivity makes a small decrease in the heat loss per inch of insulation. With 3 in. of insulation, the required heater power is decreased from 200 to about 173 W. The corresponding weight decreases are from 28.8 to 24.9 lb for the heater and from 46.8 to 42.9 lb for the total system.

This decrease in conductivity causes a small decrease in the lander cooldown rate with the extreme cold environment, as shown in figure 76. The modified extreme hot environment produces an 8°F increase in the internal temperature peaks as shown in figure 77, but they are still well within the 100°F maximum.

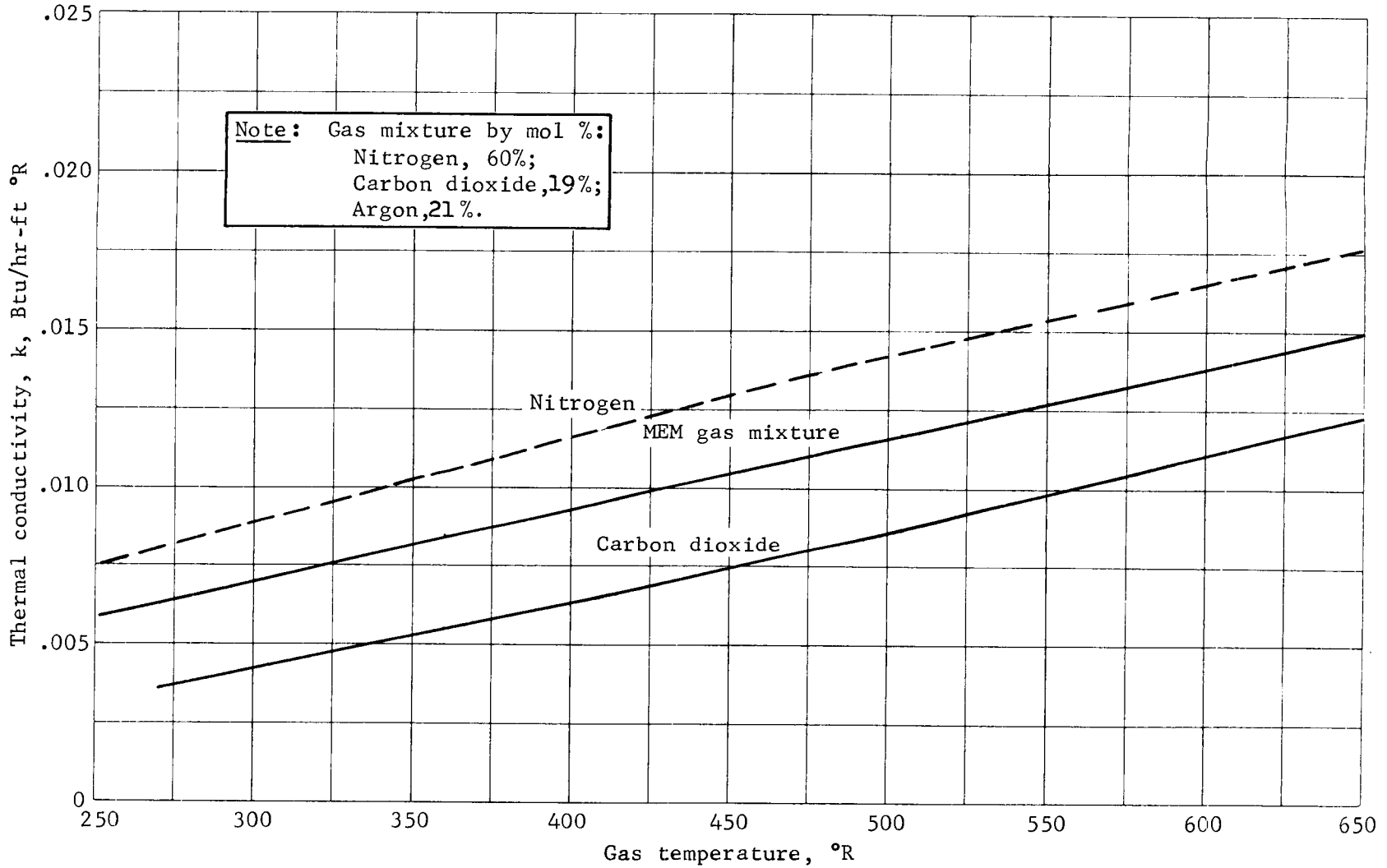

Figure 74.- Gas Thermal Conductivity as a Function of Temperature

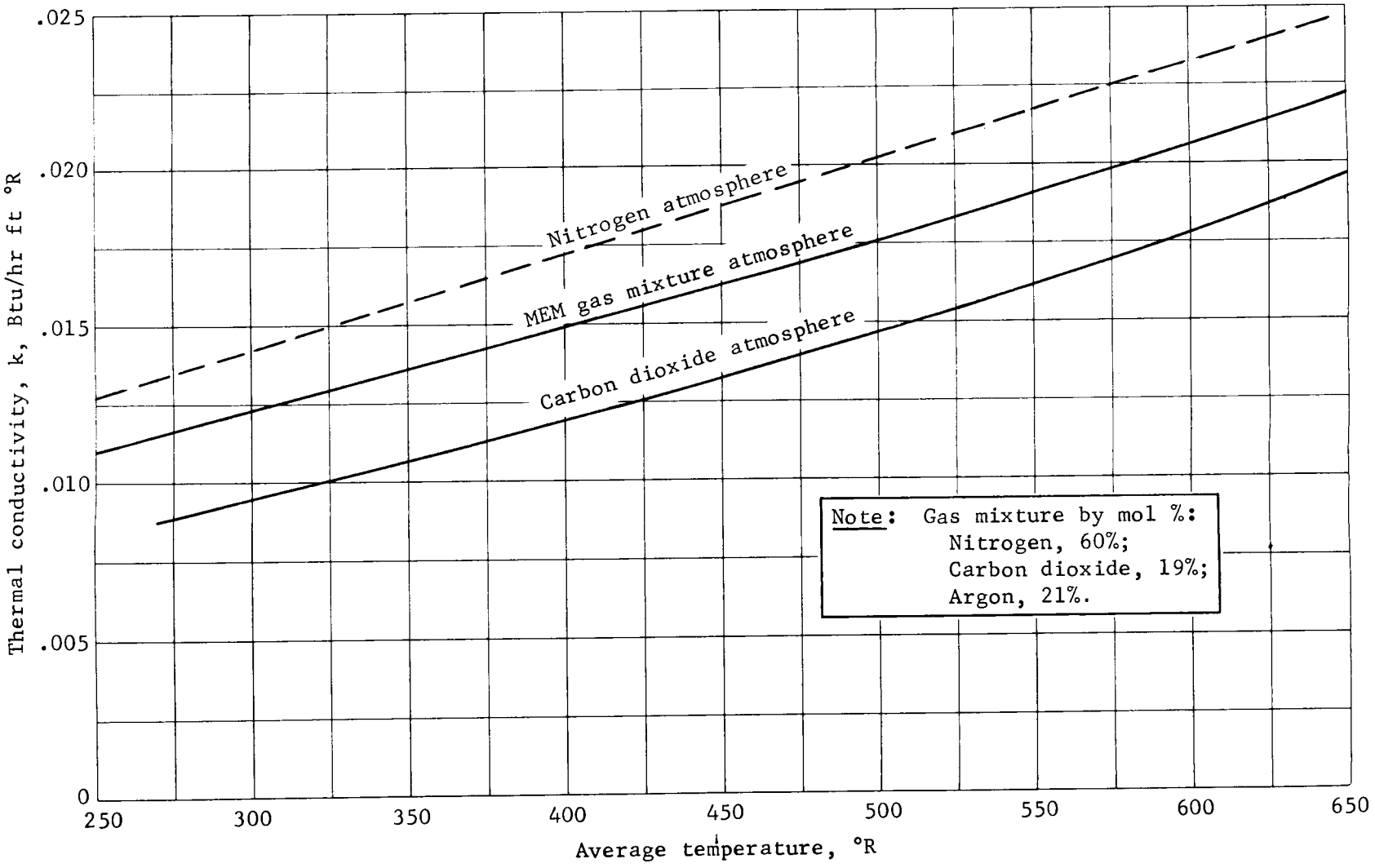

Figure 75.- Effective Conductivity of Insulation plus Penetrations as a Function of Temperature

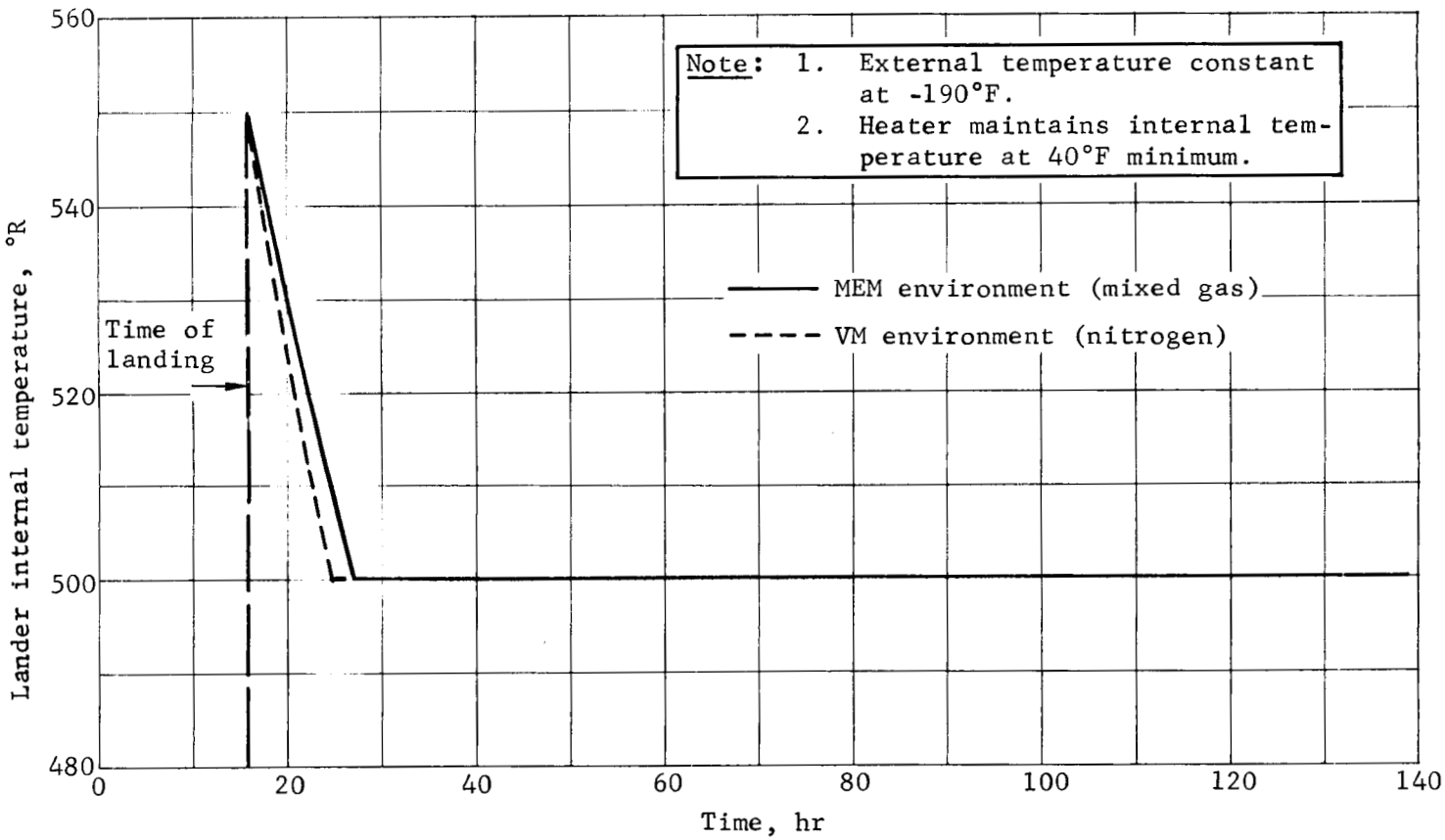

Figure 76.- Lander Temperature as a Function of Time, Cold Environment

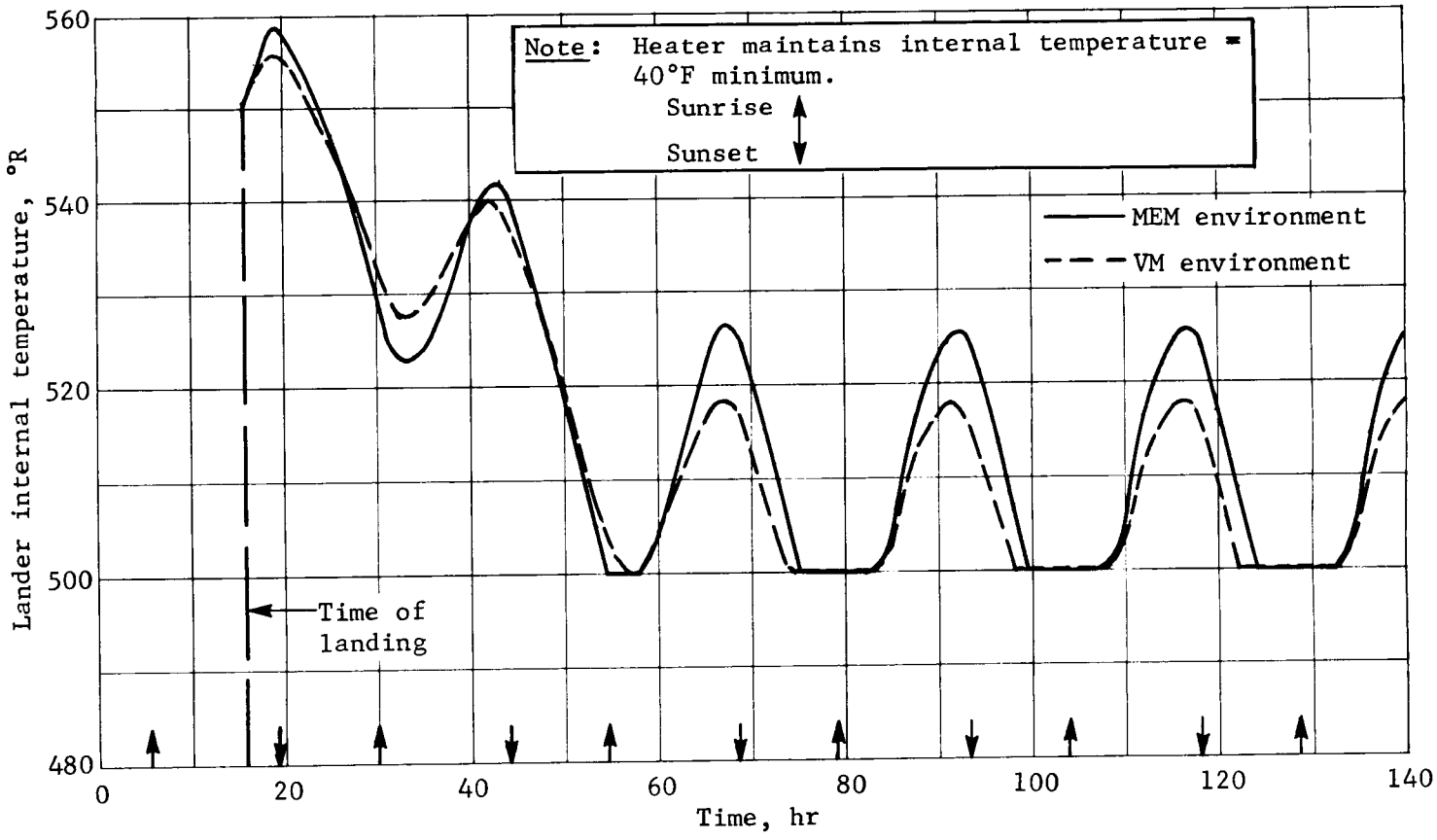

Figure 77.- Lander Temperature as a Function of Time, Hot Environment

SOLAR ARRAY ANALYSIS

The material on clouds, atmospheric characteristics, and surface slopes defined in the new Mars engineering model (ref. 1) was reviewed to determine the effect on the solar array, as defined in reference 2 (Section 8 of Volume VI, and section entitled "Power and Pyrotechnic Subsystem" in Volume II).

The information on clouds is still too limited to permit a determination of the probability of cloud cover or of the attenuation of solar energy due to clouds. Because clouds may be present during the landed mission (some covering very large areas of the surface of Mars), the power system design must still include batteries capable of providing all the required power for the minimum life.

The atmospheric data show that the atmospheric attenuation on a clear day is less than 1% (as compared with 8% used in the original study) with the sun at the zenith and for wavelengths of 0.4 to 1.2 μ. Using 1% instead of 8% for atmospheric attenuation, the energy collected from a solar array at 20°S latitude with a 17°S slope results in a 10 to 12% increase in available energy per day.

The energy available from the solar array is also dependent on the ground slope and slope azimuth at the landing site. The probability density distribution for surface slopes on Mars indicates that 98% of the slopes are 22° or less (ref. 1 fig. III.C-4). Assuming that the probability distribution for the azimuth of the slope is linear, then the probability of landing on a southern slope (135 to 225° azimuth) of greater than 22° is

$$(1.00 - 0.98) \times \frac{(225 - 135)}{360} = 0.5\%$$

Based on this, a south slope of 22° is selected as the worst-case criteria for the design of the solar array.

The solar array energy/output was then recalculated to determine the combined effect of the change in atmospheric attenuation and surface slope. The resulting change in available energy is approximately 2%; therefore, the system design previously presented is not affected.

AEROSHELL DIAMETER ANALYSIS

The objective of this study is to determine the minimum aeroshell diameter required to meet the mission objectives using the new environmental model. Starting with the 570 lb of landed equipment weight required to meet the mission objectives, reference 2 (Volume II), and using the new performance data presented in Entry Trajectory and Terminal Phase Analyses discussion above, aeroshell diameter of 7.3 ft was found to be the minimum usable to meet the performance parameters (see table 11, Configuration 1A′) for a system using the out-of-orbit entry mode. This point design is directly comparable with Configuration 1A of the original study, which required an 8.5-ft aeroshell. As was discussed in reference 2 (Volume II) Configuration 1A included no weight nor performance margin. In addition, packaging the lander in the 8.5-ft aeroshell presented two difficult problems -- stowing the legs during entry, and engine flame impingement on the leg struts. These problems are compounded by the smaller diameter aeroshell of Configuration 1A′.

A similar analysis gives a minimum aeroshell diameter of 9.6 ft for the direct entry case (table 11, Configuration 2A′). This is compared to 10.75 ft required using the VM atmosphere. A second major difference in these two systems is the parachute size required, 56.5-ft-diameter for Configuration 2A′ versus 71 ft for Configuration 2A. Again, these systems have no weight nor performance margin.

TABLE 11.- POINT DESIGN CONFIGURATION SUMMARY

	Configuration		
	1A′	1B′	2A′
Entry mode	Orbit	Orbit	Direct
Weight, lb			
Landed equipment	570	627	570
Useful landed	822	959	905
Landed	935	1083	1022
Verniered	1041	1195	1139
Entry	1340	1450	1545
Separated	1513	1644	1690
Capsule system	1645	1850	1883
Aeroshell diameter, ft	7.3	9.45	9.6
Parachute diameter, ft	63.5	39	56.5
Entry ballistic coefficient, slug/ft^2	.61	.39	.41

To achieve a practical design, a system entering out-of-orbit with 10% weight margin on all hardware elements was generated similar to Configuration 1B of the original study, reference 2 (Volume II). This point design, designated Configuration 1B′ in table 11, requires an aeroshell diameter of just under 9.5 ft compared to 10.5 ft for Configuration 1B. At this diameter, the packaging problems present in the 8.5-ft Configuration 1A′ can be easily resolved. Preliminary analysis also indicates the high probability of integrating this lander system into a standard Surveyor shroud, thus eliminating the need for a new shroud development. For these reasons, Configuration 1B′ is the recommended configuration for the out-of-orbit entry mode.

CONCLUSIONS

With one significant exception, the major conclusions of the original Mars Mission Mode Study are still valid using the new environmental model. The results of this study indicate that an aeroshell diameter of just under 9.5 ft is required to meet the mission objectives using the out-of-orbit entry mode, with weight and performance margin. It is now highly probable that the flight capsule can be integrated into a standard Surveyor 10-ft shroud. The direct entry vehicle still requires a bulbous shroud. Either entry mode is feasible; the out-of-orbit mode is preferred because of mission flexibility. The Titan IIIC/Centaur launch vehicle is still required for either entry mode if orbital science is desired.

Martin Marietta Corporation
Denver, Colorado, August 29, 1968

REFERENCES

1. Anon.: Mars Engineering Model Parameters for Mission and Design Studies 1968. Langley Research Center, May 1968.
2. Wiltshire, Raymond S., et al.: Final Report, Study of Direct Versus Orbital Entry for Mars Missions. Martin Marietta Corporation, Denver, Colorado, August 1968.
   - Vol. I - Summary, NASA CR-66659.
   - Vol. II - Parametric Studies, Final Analyses, and Conceptual Designs, NASA CR-66660.
   - Vol. III - Appendix A - Launch Vehicle Performance and Flight Mechanics, NASA CR-66661.
   - Vol. IV - Appendix B - Entry and Terminal Phase Performance Analysis, NASA CR-66662.
   - Vol. V - Appendix C - Entry Configuration Analysis, NASA CR-66663.
   - Vol. VI - Appendix D - Subsystem Studies and Parametric Data, NASA CR-66664.
3. Anon.: Voyager Capsule Preliminary Design (Phase B) Final Report. FR-22-103 (Vol. I thru VII). Martin Marietta Corporation, Denver, Colorado, Aug. 31, 1967.

NASA CR-66700

National Aeronautics and Space Administration
FINAL REPORT, STUDY OF DIRECT VERSUS ORBITAL ENTRY FOR MARS MISSIONS. Raymond S. Wiltshire, Hugh E. Craig, et al. October 1968

(NASA CONTRACTOR REPORT NASA CR-66700)

This is a supplementary report volume to the final report of the work accomplished by Martin Marietta Corporation for the Langley Research Center under Contract NAS1-7976, Study of Direct Versus Orbital Entry for Mars Mission. The supplemental study based on alternative Mars atmospheres was conducted from June 28 thru September 10, 1968. The study objectives were (1) to obtain the net science payload for the direct entry mode, and (2) to evaluate the direct and out-of-orbit entry modes for soft landing capsules. The three main tasks defined to fulfill these objectives were (1) conduct mission and subsystem parametric analyses, (2) establish mission design for each capsule mode; and (3) provide conceptual design for three capsule systems.

I. Wiltshire, Raymond S.; Craig, Hugh E.; et al.

II. NASA CR-66700 Supplemental Report (Reference Basic Report NASA CR-66659 thru 66664)

NASA

NASA	The total study final report is presented in the following volumes: NASA CR-66659 - Volume I - Summary; NASA CR-66660 - Volume II - Parametric Studies, Final Analyses, and Conceptual Designs; NASA CR-66661 - Volume III - Appendix A - Launch Vehicle Performance and Flight Mechanics; NASA CR-66662 - Volume IV - Appendix B - Entry and Terminal Phase Performance Analysis; NASA CR-66663 - Volume V - Appendix C - Entry Configuration Analysis; NASA CR-66664 - Volume VI - Appendix D - Subsystem Studies and Parametric Data; NASA CR-66700 - Volume VII - Supplementary Report.